Astronomy & Astrophysics

Stellar companions and Jupiter-like planets in young associations

R. Gratton[1] , M. Bonavita[1,2], D. Mesa[1] , S. Desidera[1], A. Zurlo[3,4,5], S. Marino[6], V. D'Orazi[1,7] , E. Rigliaco[1] ,
V. Nascimbeni[1], D. Barbato[1] , G. Columba[1,8] , and V. Squicciarini[1,9]

[1] INAF-Osservatorio Astronomico di Padova, Vicolo dell'Osservatorio 5, 35122 Padova, Italy
e-mail: raffaele.gratton@inaf.it
[2] Institute for Astronomy, University of Edinburgh Royal Observatory, Blackford Hill, EH9 3HJ, Edinburgh, UK
[3] Instituto de Estudios Astrofísicos, Facultad de Ingeniería y Ciencias, Universidad Diego Portales, Av. Ejército 441, Santiago, Chile
[4] Escuela de Ingeniería Industrial, Facultad de Ingeniería y Ciencias, Universidad Diego Portales, Av. Ejército 441, Santiago, Chile
[5] Millennium Nucleus on Young Exoplanets and their Moons (YEMS), Santiago, Chile
[6] Department of Physics and Astronomy, University of Exeter, Stocker Road, Exeter, EX4 4QL, UK
[7] Dipartimento di Fisica, Università di Roma Tor Vergata, via della Ricerca Scientifica 1, 00133 Roma, Italy
[8] Dipartimento di Fisica e Astronomia G. Galilei, Università di Padova, Via Francesco Marzolo, 8, 35121 Padova, Italy
[9] LESIA, Observatoire de Paris, Université PSL, CNRS, Sorbonne Université, Université Paris Cité, 5 place Jules Janssen, 92195 Meudon, France

Received 26 October 2023 / Accepted 31 January 2024

ABSTRACT

Context. The formation mechanisms of stellar, brown dwarf, and planetary companions, their dependencies on the environment and their interactions with each other are still not well established. Recently, combining high-contrast imaging and space astrometry we found that Jupiter-like (JL) planets are frequent in the β Pic moving group (BPMG) around those stars where their orbit can be stable, prompting further analysis and discussion.
Aims. We broaden our previous analysis to other young nearby associations to determine the frequency, mass and separation of companions in general and JL in particular and their dependencies on the mass and age of the associations.
Methods. We collected available data about companions to the stars in the BPMG and seven additional young associations, including those revealed by visual observations, eclipses, spectroscopy and astrometry.
Results. We determined search completeness and found that it is very high for stellar companions, while completeness corrections are still large for JL companions. Once these corrections are included, we found a high frequency of companions, both stellar ($>0.52 \pm 0.03$) and JL (0.57 ± 0.11). The two populations are clearly separated by a gap that corresponds to the well-known brown dwarf desert. Within the population of massive companions, we found clear trends in frequency, separation, and mass ratios with stellar mass. Planetary companions pile up in the region just outside the ice line and we found them to be frequent once completeness was considered. The frequency of JL planets decreases with the overall mass and possibly the age of the association.
Conclusions. We tentatively identify the two populations as due to disk fragmentation and core accretion, respectively. The distributions of stellar companions with a semi-major axis <1000 au is indeed well reproduced by a simple model of formation by disk fragmentation. The observed trends with stellar mass can be explained by a shorter but much more intense phase of accretion onto the disk of massive stars and by a more steady and prolonged accretion on solar-type stars. Possible explanations for the trends in the population of JL planets with association mass and age are briefly discussed.

Key words. planets and satellites: formation – planets and satellites: fundamental parameters – binaries: general –
open clusters and associations: general

1. Introduction

A large fraction of the stars have companions over a wide range of masses: stars (mass $M > 0.075$ $M_\odot$), brown dwarfs (BDs: $0.013 < M < 0.075$ $M_\odot$), or planets ($M < 0.013$ $M_\odot$). The mechanisms for the formation of multiple systems, how they depend on the environment, and how they interact with each other are still not well established. The favoured scenarios for the formation of stellar companions are turbulent fragmentation of clouds for a separation >500 au (Offner et al. 2010, 2016) and disk fragmentation for a separation <500 au (Kratter et al. 2010). However, the details of which are far from being well understood (see e.g. Tohline 2002). Disk fragmentation is expected

to be more efficient around massive stars because of the larger value of the accretion rate from the natal cloud and hence the larger expected disk-to-star mass ratio during early phases of formation, when binaries are likely to form (Machida et al. 2010; Kratter & Lodato 2016; Elbakyan et al. 2023). In disk fragmentation, mass accretion on the secondary may be favoured with respect to accretion on the primary (Clarke 2012); if the disk survives long enough, this would lead to a preference for equal mass binaries (Kratter et al. 2010). Planets and BDs may either form by disk fragmentation (Boss 1997) or more likely by core accretion (Pollack et al. 1996; Mordasini et al. 2012; Bitsch et al. 2015). While disk fragmentation is a fast process (at most a few 10^4 yr), core accretion is a slow process requiring a few million

of years. We then expect that binary formation by disk fragmentation occurs much earlier and sets the stage for the later formation of planets by the core accretion process. Early formation of stellar companions may be an obstacle for the later formation of planets if they reside at a distance from the central star similar to that of planet formation because they may destroy the proto-planetary disk or make planetary orbits unstable (see e.g. Holman & Wiegert 1999).

Related to these issues are basic questions in the study of exoplanets, such as whether the Solar System is an anomaly in the exoplanetary context and where and how it formed. The answers to these questions are uncertain (Martin & Livio 2015; Parker 2020; Gaudi 2022; Raymond et al. 2020; Raymond & Morbidelli 2022) and observations of extrasolar planetary systems may help. Most of the companion mass of our Solar System is represented by the giant planets lying just beyond the ice-line, which is the region of the system where ice can survive the Sun's heat. We can call planets found in this region (semi-major axis of the orbits between 3 and 15 au: Hayashi 1981; Podolak & Zucker 2004; Martin & Livio 2012) in extrasolar systems Jupiter-like (JL) planets if they have a mass equal or larger than that of Jupiter. Apart from transits, an external observer would likely discover JL planets long before detecting smaller inner rocky planets such as the Earth. Furthermore, a correlation is found between the presence of JL planets and inner smaller planets (Bryan et al. 2016; Rosenthal et al. 2022). Therefore, a basic step to answer the above questions is to establish how common JL planets are around Sun-like stars, as it is already known that giant planets are rare amongst stars of a lower mass (see e.g. Laughlin et al. 2004; Alibert et al. 2011; Burn et al. 2021; Johnson et al. 2010). In this respect, it is remarkable that the peak of the distribution of stellar companions is only slightly further out than the ice-line in solar-type stars (see e.g. Raghavan et al. 2010; Gratton et al. 2023b).

Over the last twenty years, surveys based on variations of radial velocities (RVs) have been used to detect planets outside the Solar System (Cumming et al. 2008; Mayor et al. 2011; Wittenmyer et al. 2016; Fernandes et al. 2019; Zhu 2022; Wolthoff et al. 2022). These surveys have found that only about 6% of Sun-like stars host JL planets with a mass >1 $M_{\rm Jup}$[1] and only 2% host a massive JL planet ($M > 3$ $M_{\rm Jup}$). However, planet parameters become highly uncertain when the periods are longer than the time coverage of the RV series (Lagrange et al. 2023), so these results should be taken with care. A similar, though very uncertain, result has been obtained using a single microlensing event involving a massive JL planet (Gould et al. 2010), while a large incidence of wide-orbit planets over a wider range of masses has been found by Poleski et al. (2021). This would indicate that our Solar System is relatively unusual. However, JL planets are difficult to discover through RV, because of the long periods and low amplitudes of RV variations. Typically, these surveys target stars with ages of several billion years, whose sites of formation are essentially unknown. Therefore, they are of limited use to understand where and how our Solar System formed.

A new observation may provide important hints. Using direct imaging, very recently three independent papers (Mesa et al. 2023; De Rosa et al. 2023; Franson et al. 2023) found a third star (AF Lep) hosting a JL planet in the β Pic moving group (BPMG), in addition to β Pic itself and 51 Eri. The BPMG is a sparse group

of 20-million-year-old stars, likely born in a single episode of star formation. The BPMG includes only about 30 Sun-like stars ($M > 0.8$ $M_\odot$). Due to its young age and close proximity to the Sun, the BPMG is the most favourable star ensemble for planet detection by means of direct high contrast imaging (HCI). Even so, the discovery of JL planets with this technique is still difficult, and only JL planets with a mass greater than three times that of Jupiter (i.e., roughly a third of all such planets) can be detected, and that can only occur under favourable conditions. The HCI discovery of three stars hosting JL planets in this small group of stars was therefore rather unexpected.

In a previous paper (Gratton et al. 2023a) we provided a reference framework for these surprising discoveries. We found that there are 17 stars with sufficient data and that can potentially host JL planets with stable orbits in the BPMG. We then estimated various selection effects in HCI as well as information from astrometry and found that seven out of 17 stars in the BPMG are likely hosting massive JL planets ($M > 3$ $M_{\rm Jup}$). If it is then considered that only a third of JL planets are sufficiently massive to be detected by any of the two methods, the conclusion being that nearly all Sun-like stars in the BPMG are likely to host a JL planet. This tells a very different story about how planets form than the result obtained with RV surveys: the frequency of JL planets is overall low, but it is large in the BPMG.

There are several possible explanations for the lack of convergence between RV and imaging methods. The presence of giant planets is known to depend on the metal content and mass of their host stars (Kennedy & Kenyon 2008; Mordasini et al. 2012; Johnson et al. 2010); however, as discussed in Gratton et al. (2023a) this is insufficient to explain the large discrepancy observed across methods. Stars may lose planets due to interactions with other objects that are passing by, whose perturbations may cause long-term instabilities in the systems, especially when several planets are present. A final possibility is that JL planets preferably form in low-density environments, such as the BPMG, while most old stars surveyed through RV formed in larger and higher density environment.

An open question is why it is more likely for JL planets to form in low-density environments. The most widely accepted mechanism for planet formation is the core accretion scenario (Pollack et al. 1996; Mordasini et al. 2012; Bitsch et al. 2015) a process requiring a few million years. Perhaps proto-planetary disks can survive that long only in low-density environments, because in denser ones perturbations or photoionisation by nearby massive stars likely destroy the disks, thus preventing the formation of JL planets (Adams & Myers 2001; Adams et al. 2004; Winter et al. 2018; Parker 2020; Parker et al. 2021; Winter et al. 2022; Wright et al. 2022). We would then predict that the Solar System was likely formed in a low-density environment, that is to say not the commonly accepted scenario (see e.g. Pfalzner 2013; Pfalzner & Vincke 2020).

In this paper we expand this analysis to the remaining young nearby associations. This not only allows us to set this result on a more robust basis, but also to have a first determination of the dependencies on the mass and age of the associations. Young associations are very useful in this context because they had limited, if any, dynamical evolution affecting the properties of their multiple systems (e.g. mass segregation). Star formation is essentially complete in these associations. Stars are young enough (age <200 Myr) and associations are so loose (density <0.1 star/pc^3) that the long-term evolution of multiple systems related to the environment (Heggie 1975; Binney & Tremaine 1987; Kaczmarek et al. 2011) is likely not strongly influencing their properties even for separation as large as a few thousands

---

[1] We adopt here this limit for the JL planets because detection of smaller mass JL planets is very difficult, see e.g. the discussion in Lagrange et al. (2023).

au. We notice that since the density of stars in these associations is lower than that of the solar neighbourhood, the formalism of Binney & Tremaine (1987) indicates that encounters with field stars are more probable than those with other members of the association. This is due to the much larger spread in velocities. Possibly, encounters are more probable in the birthplace of individual stars, but this can be considered as a component of the companion formation mechanisms. On the other hand, to avoid incompleteness that is too large, the analysis must consider only stars close to the Sun. We adopted an upper limit of 100 pc to their distance.

As was done for the case of the BPMG, we combined the search for JL planets with a rather complete census of stellar binary companions. This helps to clarify the relative role of disk fragmentation and core accretion in the formation of companions and to correctly establish what the fraction of stars that host JL planets is over the mother population of the stars that may potentially have them. This paper is organised as follows: in Sect. 2 we present the properties of the associations, the data about the multiplicity of their members, the basic parameters of the stars and of their companions, and discuss the completeness of our search. In Sect. 3 we discuss the main properties of the population of the stellar companions. In Sect. 4 we present the statistics about the JL companions. The trends we observed are discussed in Sect. 5 and conclusions are drawn in Sect. 6. The appendices present a discussion on the jitter in *Gaia* RVs and extensive tables with the relevant data for all stars considered to be a member of the associations and their companions.

2. Data

2.1. Properties of young associations

2.1.1. Choice of associations

We considered known associations and moving groups within 100 pc from the Sun and with ages in the range 10−200 Myr: AB Doradus (Zuckerman et al. 2004), Argus (De Silva et al. 2013), β Pic moving group (BPMG; Shkolnik et al. 2017), Carina (Torres et al. 2008), Carina Near (Zuckerman et al. 2006), Columba (Torres et al. 2008), Tucana-Horologium (Tuc-Hor, Torres et al. 2008), and Volans-Carina (Gagné et al. 2018c).

The case of Volans-Carina should be discussed further. In fact, the membership criteria considered by Gagné et al. (2018c) are very strict and only leave the core members. In a recent study, Moranta et al. (2022) found that a group they considered in their analysis (Crius 221) may be considered as the corona of this association. While membership of some particular star to this group may be questioned, hereinafter we will assume that this is indeed the case, and extended the list of the Volans-Carina association including members of this group. Hereinafter, we will call this extended association Volans/Crius 221.

The main parameters for these associations are given in Table 1. Ages for these associations are an average from a number of literature determinations as given in Sect. 2.1.4. Distances are the median of distances of the individual members with mass >0.8 $M_\odot$ obtained from the parallaxes listed in the Data Release 3 (DR3) of results from European Space Agency astrometric *Gaia* satellite (Gaia Collaboration 2023b). The *Gaia* limit is the mass of a BD with $G = 19$ at the average distance and age of each association. This was obtained using the isochrones by Baraffe et al. (2015) for the age and median distance of the associations. It provides a first estimate of the completeness in the search for wide stellar and BD companions using *Gaia*.

2.1.2. Membership to the associations

We considered members of the various associations from the sources listed in Table 1. Only systems where the primaries have a mass above 0.8 $M_\odot$ were kept. All stars were checked for membership to the respective clusters using the Banyan Σ code (Gagné et al. 2018c)[2], but in the case of Volans/Crius 221 for the reason mentioned above we kept also those objects that have low membership probability. For the case of Argus, whose membership is not well defined, we checked that available information supports a young age for the proposed members. We dropped a few proposed objects because there is evidence they are much older than assumed for the association. In total we considered 296 stars in 280 stellar systems with the primary above the mass limit mentioned above as members of these associations. Some very wide binaries have entries for the individual objects in our list if the mass of each of the component is >0.8 $M_\odot$. The presence of the wide (massive) companion has been considered when estimating multiplicity.

2.1.3. Basic parameters for programme stars

In this paper we considered the *Gaia G* (Gaia Collaboration 2023b) and 2MASS *K* magnitudes (Cutri et al. 2003). Distances were taken from *Gaia* DR3, whenever possible; else from *Gaia* Data Release 2 (DR2) or, as a last resort, from HIPPARCOS (Perryman et al. 1997). Interstellar absorption was neglected, considering the close distance of target stars. We checked that this is appropriate using the 3-d map by Green et al. (2019) for all stars for which they give results.

Masses for the stars are derived from the absolute *Gaia G* magnitudes using the calibration by Pecaut & Mamajek (2013) if $M_G < 3$, else from the isochrone by Baraffe et al. (2015) of appropriate age. In case the star is an unresolved binary in the *Gaia* Catalogue, we corrected the *Gaia G* magnitudes for the contribution by the secondary before extracting the masses. This was done in an iterative way, but convergence was always very fast.

The median mass of the primaries is 1.04 $M_\odot$. The masses of the primary stars in the range 0.8–5 $M_\odot$ distribute close to a Salpeter mass function (Salpeter 1955), with a slope of −2.24 (see Fig. 1).

2.1.4. Age and size of the associations

In our discussion, we wish to link the observed frequency of JL planets to the properties of the environment where they formed. Even selecting young associations and moving groups, they still are tens to hundreds million years old. Their environment has substantially changed within this interval of time and some aspects cannot be recognised any more. We focus here on two of the simplest parameters, that are the age and mass of the star forming region that originated the observed association.

We report in Table 2 a number of literature determination of ages for six of the moving groups considered in this paper. The values we adopted are the straight averages. In this paper, we did not consider the ages by Ujjwal et al. (2020) because they are much lower than and uncorrelated with other estimates. For Carina Near we adopted the age of 200 Myr given by Zuckerman et al. (2006), while for Volans/Crius 221 that of 89 ± 6 Myr given by Gagné et al. (2018a).

---

[2] https://www.exoplanetes.umontreal.ca/banyan/banyansigma.php

Table 1. Main parameters for young nearby associations.

Association	Age (Myr)	Distance (pc)	N. prim. ($M > 0.8\,M_\odot$)	Mass ($M_\odot$)	Size X (pc)	Size Y (pc)	Size Z (pc)	*Gaia* lim ($M_\odot$)	Members source
AB Dor	137 ± 17	50.7 ± 21.1	55	191	33.9 ± 4.6	33.1 ± 4.5	16.5 ± 2.2	0.038	Zuckerman et al. (2004) Torres et al. (2008) Gagné et al. (2018c) Faherty et al. (2018) Gagné et al. (2018d)
Argus	48 ± 10	82.6 ± 34.8	35	118	25.2 ± 34.2	50.8 ± 8.5	20.4 ± 3.4	0.030	Zuckerman (2019) De Silva et al. (2013)
β Pic	21 ± 4	46.6 ± 16.1	27	94	36.4 ± 7.0	16.7 ± 3.2	9.2 ± 1.8	0.013	Shkolnik et al. (2017) Gratton et al. (2023a)
Carina	28 ± 11	79.6 ± 7.7	17	51	11.0 ± 2.7	18.8 ± 4.5	11.7 ± 2.8	0.020	Torres et al. (2008) Booth et al. (2021) Kerr et al. (2022)
Carina Near	200 ± 20	34.3 ± 8.9	12	41	9.3 ± 2.6	23.2 ± 6.4	19.5 ± 5.4	0.045	Zuckerman et al. (2006) Faherty et al. (2018) Stahl et al. (2022)
Columba	36 ± 8	70.2 ± 23.7	52	155	21.5 ± 3.0	32.8 ± 4.6	20.7 ± 2.9	0.030	Torres et al. (2008) Moór et al. (2013) Elliott et al. (2016) Kerr et al. (2022)
Tuc-Hor	37 ± 11	48.8 ± 9.1	41	158	23.9 ± 3.7	14.7 ± 2.3	3.8 ± 0.6	0.023	Torres et al. (2008) Gagné et al. (2018b) Zúñiga-Fernández et al. (2021) Popinchalk et al. (2023)
Volans/Crius 221	89 ± 6	82.1 ± 23.5	41	123	18.5 ± 2.9	28.7 ± 4.4	12.5 ± 1.9	0.040	Gagné et al. (2018a) Moranta et al. (2022)

Notes. In this table N. prim is the number of primaries with a mass >0.8 $M_\odot$. The size X, Y, Z are the quadratic sum of the standard deviation of the X, Y, and Z Cartesian coordinates on the galactic frame (X is towards the centre of the Galaxy), respectively. *Gaia* lim is the mass corresponding to a magnitude of $G = 19$.
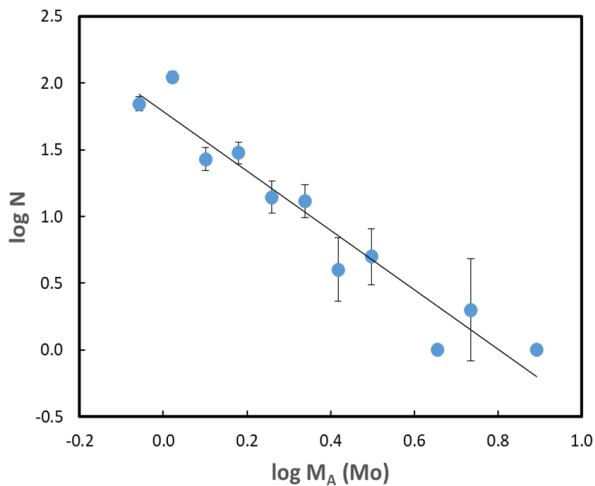
Fig. 1. Mass function for the primaries in the young associations. The slope of the best fitting line (solid line) is −2.24.

The mass of associations was obtained by summing up the mass of all components found and then correcting this value for the mass of the stars with masses lower than 0.8 $M_\odot$. We assumed that the same correction found for the case of the BPMG applies to the other clusters too. A total mass of the BPMG of 94 $M_\odot$ was derived by Gratton et al. (2023a). Masses estimated in this way are given in Table 1. Summing all eight associations, the total mass is 932 $M_\odot$.

The approach we followed – considering known members – likely underestimates the actual values. Furthermore, it might introduce biases, because members may be easier to recognise in the youngest associations. One possible reason is that the older associations are more dispersed. To have a first estimate of the relevance of this effect we determined the actual sizes of the associations and considered if they change systematically with age. We considered separately the size along the three different galactic coordinates because it is expected that they obey different runs with time. In fact the expansion of the associations occurs within the galactic potential (see e.g. Binney & Tremaine 1987; Asiain et al. 1999). If we neglect perturbations due to other stars, molecular clouds and spirals (disk heating), an approximation that is not too bad in view of the very long relaxation time and young ages of these associations, we might expect that after an epicyclic period stars return to a compact configuration in the galactic radial direction X, a focusing effect noticed many years ago by Yuan (1977). Similarly, a compact configuration in the vertical direction Z is obtained twice each vertical period. This argument is similar to that considered by Dinnbier et al. (2022). The run is more complex in the galactic

Table 2. Ages for associations and moving groups (in million years).

Reference	BPMG	Columba	Carina	Tuc-Hor	Argus	AB Doradus
Isochrones						
Bell et al. (2015)	24	42	45	45	58	149
Booth et al. (2021)			13			
Lithium						
Barrado y Navascués et al. (2004)					50	
Mentuch et al. (2008)	21			27		>45
Binks & Jeffries (2014)	21					
Malo et al. (2014)	26					
Shkolnik et al. (2017)	22					
Schneider et al. (2019)	22		22			
Wood & Mann (2023)			40			
Kinematics						
McCarthy & Wilhelm (2014)						125
Miret-Roig et al. (2018)	13	>40	>28	>28	37	
Miret-Roig et al. (2020)	19					
Booth et al. (2021)			20			
Kerr et al. (2022)		26	26	46		
Couture et al. (2023)	20					
Mean	21	36	28	37	48	137
Standard deviation	4	8	11	11	10	17

azimuthal direction Y, where the focusing effect is lower and stars spread over time along an arc that grows almost linearly with time. We use the publicly available code galpy (Bovy 2015)[3] to model the motion of the stars of an association in the Milky Way galactic potential, neglecting self-gravity. We considered the evolution of the position dispersion with time for samples of 100 stars extracted with Gaussian distributions in the original positions and velocities. We run this exercise 200 times, each one with a random extractions of the initial spread along X, Y, and Z axes with uniform distribution between 2 and 15 pc, comparable to the original size of the BPMG as derived by Miret-Roig et al. (2020). In all cases we assumed an initial isotropic velocity dispersion of 0.5 km s^{-1} that is at the lower edge of the typical velocity distribution in nearby low-mass star forming regions (0.5–1.0 km s^{-1}; Hennebelle & Falgarone 2012; Heyer & Dame 2015) and it is similar to the velocity dispersion in the BPMG (Miret-Roig et al. 2020). The galactic potential has epicyclic and vertical periods of 170 and 80 Myr, respectively, at the Sun position; this corresponds to the galactic constants of Kerr & Lynden-Bell (1986). Figure 2 compares the results of this model with the observed association sizes on the three galactic coordinates. We found that indeed the size of the associations should remain limited over time in X and Z direction, as observed. However, we expect that the associations should become very elongated in the Y direction after 50 Myr, only marginally modulated on the epicyclic period. This is not observed: the oldest associations have dispersion in Y similar to the youngest ones. We notice that the larger the initial velocity dispersion (that is $\sigma(V)$ in the usual notation used in galactic dynamics), the highest would be the dispersion along the Y direction, and that the value we assumed is actually at the lower edge of the expected distribution. To eliminate this discrepancy,

---

[3] https://docs.galpy.org/en/v1.9.0/
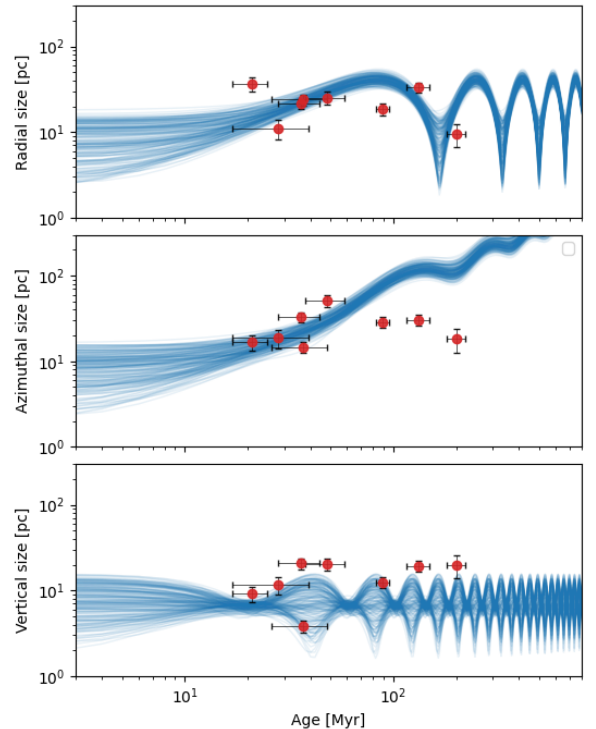
Fig. 2. Run of the size of the young associations considered in this paper with age (red dots). X is the direction of the galactic centre (upper panel); Y is the direction perpendicular to X on the galactic plane (middle panel); Z is the vertical direction (lower panel). For comparison, expectations for a simple model of expansion of an association in the galactic potential is also shown; results for 200 random extractions for the initial sizes along X, Y, and Z axes with uniform distribution between 2 and 15 pc are shown. In all cases we assumed an initial isotropic velocity dispersion of 0.5 km s^{-1}.

we should assume values of $\sigma(V) = 0.1–0.2$ km s^{-1}, while higher values would be needed for the other directions to match observations. While this is perhaps not impossible (for instance, Miret-Roig et al. 2020 found $\sigma(V) = 0.43$ km s^{-1} for the BPMG), such a systematic effect would require an explanation.

Rather, we consider the possibility that while there are not significant selection effects for the associations with ages <50 Myr, the case can be very different for the oldest ones. In fact, the small sizes along Y of the older associations may be an artefact of selection effects: only those stars that are in the region of the association that is closest to the Sun (75 pc for AB Dor, 50 pc for Carina Near) or in one of the two hemispheres (southern one for Carina Near and Volans/Crius 221) are considered as members in the papers from which we extracted membership (and in Banyan Σ). At their age and using the same initial expansion velocity considered for the other associations, we expect them to be more extended than observed along the Y direction, by factors of 2.7, 3,7, and 5.6 for Volans/Crius 221, AB Dor and Carina Near, respectively. The missing stars should be searched in the directions around the galactic coordinates ($l = 90, b = 0$ for Carina Near and Volans/Crius 221) and ($l = 270, b = 0$) at distances of the order of 100 pc or more. They should not be easily separable from field objects because they should have small proper motions and RVs with low errors are required for their selection. We then consider the possibility that these associations were much more massive at birth and that their total mass should be corrected upwards by a factor of at least two.

2.2. Companion detections

We carried out an extensive search for companions to the programme stars. We considered visual, spectroscopic, eclipsing, and astrometric binaries, as well as substellar companions.

2.2.1. Visual binaries

We considered visual binaries companions from several sources. First we considered if there are companions with similar distances and proper motion within 600 arcsec listed as separate entries in the *Gaia* DR3 catalogue (Gaia Collaboration 2023b). The limiting contrast of *Gaia* is discussed in Brandeker & Cataldi (2019). Given the very low surface densities of these associations (typical values are 0.01–0.02 stars per square degree), the probability that physically unbound objects of the same association are projected within this radius from a star is of about 5×10^{-4} and can then be neglected. We then checked if the stars are in the Washington Double Star (WDS) visual binary catalogue (Mason et al. 2001), in the Multiple Star Catalogue by Tokovinin (2018; we found 44 entries), or were detected in HCI (Biller et al. 2007; Brandt et al. 2014; De Rosa et al. 2014; Elliott et al. 2015; Galicher et al. 2016; Bonavita et al. 2016, 2022a; Janson et al. 2017; Stone et al. 2018; Asensio-Torres et al. 2018; Nielsen et al. 2019; Vigan et al. 2021; Zhou et al. 2022; Dahlqvist et al. 2022; Mesa et al. 2022). *Gaia* data are available for all stars in the sample, and HCI is available for 194 stars. Orbital parameters for HIP 3589 were from Cvetković (2011).

2.2.2. Spectroscopic binaries

We checked if the programme stars have entries in the spectroscopic binary catalogue (Pourbaix et al. 2004), in the catalogue obtained from GALactic Archaeology with

HERMES[4] (GALAH) survey data (Traven et al. 2020), and from *Gaia* RVs (*gaiadr3.nss_two_body_orbit*). We also considered data from the catalogues of high precision RV by Butler et al. (2017); Tal-Or et al. (2019); Trifonov et al. (2020); Grandjean et al. (2020, 2021, 2023). Overall, high precision RV are available for 79 stars; lower precision RV are available for 181 additional stars; there is no RV sequence for 37 stars. Whenever data were available, they were used to constrain the orbital parameter of the companion. For the double line spectroscopic binary HIP 89925 (108 Her) data were from Fekel et al. (2009) and for HIP 100751 (α Pav) from Luyten (1936).

A few planets were discovered around stars claimed to be members of young associations using high precision RV: β Pic c (Lacour et al. 2021) in the BPMG; HIP 50786 (Korzennik et al. 2000; Wittenmyer et al. 2019) and HIP 72339 (Udry et al. 2000) in the AB Dor moving group. Most of them are giant planets with $a > 1$ au, but HIP 72339b is a hot-Jupiter. However, HIP 50786 and HIP 72339 are likely old stars, so we will not consider them any more in this paper.

In general, when using RVs of young stars the large value of the stellar jitter related to the high activity level must be considered (see e.g. discussion in Lagrange et al. 2023). The RV jitter from high precision measurements on timescales of decades decreases from over 500 m s^{-1} for 5 Myr-old stars to 2.3 m s^{-1} for stars with ages of around 5 Gyr (Brems et al. 2019; Tran et al. 2021). Special techniques may limit its impact, but this requires extensive observation and thorough discussion, possible only for individual cases such as that of β Pic (Lacour et al. 2021). We also notice that the *Gaia* robust RV amplitude is a less good indicator for young stars because of the higher activity and faster rotation. In particular, it is unreliable for fast rotating K-stars (such as TYC 7100-2112-1 in Columba), likely because of severe blending in the spectra. These stars can be identified as short period (∼1 day) quasi-periodic variable thanks to the TESS light curves. We considered the higher jitter in *Gaia* RVs for young stars as described in Appendix A.

2.2.3. Eclipsing binaries

Obviously, to detect a companion by eclipses/transits the Sun should be close to the orbital plane. Hence only a fraction of the companions can be detected this way. We looked for entries corresponding to the stars in the eclipsing binary (EB) catalogue by Avvakumova et al. (2013) and in the *Kepler* EB catalogue Slawson et al. (2011). In addition, all programme stars but 15 have been observed by the NASA Transiting Exoplanet Survey Satellite (TESS) satellite, though only 260 of them have been observed with a 2-minute cadence. The 21 objects observed but missing the 2-minute cadence data are generally faint, and so of low-mass. We inspected the TESS catalogues of EB (Prša et al. 2022; IJspeert et al. 2021) and found two EBs listed: HIP 57013 in the Argus moving group and HIP 28474 (RT Pic) in the Columba moving group. However, the second star is likely not an EBs, as discussed in Appendix C[5]. A single EB detected would be consistent with the total number of seven detected stellar companions with $a < 0.165$ au and $M_B > 0.075$ $M_\odot$, that roughly corresponds to a period of 20 days where the search for EB should be complete over at least 89% of the targets.

---

[4] HERMES is the High Efficiency and Resolution Multi-Element Spectrograph at the Anglo Australian Telescope.
[5] The TESS light curve shows two periods with an amplitude larger than 0.01 mag and a length of about six days, but no obvious transit.

We also inspected the TESS Target of Interest catalogue where we found a hot Neptune transiting DS Tuc A in the Tuc-Hor moving group (Newton et al. 2019; Benatti et al. 2019) and a mini-Neptune (3 R_{Earth}) transiting HIP 94235 in the AB Dor moving group (Zhou et al. 2022). Since mass is not available for this second planet, it will not be considered in the tables in the Appendix C.

2.2.4. Astrometric binaries

We inspected the *Gaia gaiadr3.nss_two_body_orbit* catalogue (Gaia Collaboration 2023a) and found entries for 12 objects: HIP 12838 and HIP 37855 in AB Dor; TYC 9412-1370-1 in Argus; HIP 76629 in BPMG; HIP 26144 in Carina; HIP 35564 and HIP 37918 in Carina-Near; HIP 2729, HIP 16853, and HIP 108422 in Tuc-Hor; and TYC 8933-327-1 in Volans/Crius 221. An orbit solution is available for these stars. We found five entries in the *gaiadr3.nss_acceleration_astro* catalogue (Gaia Collaboration 2023a): HIP 55746 in AB Dor, CD-58 2194 in Argus, TYC 8602-718-1 in Carina, HIP 37635 in Carina Near, and HIP 18714 in Tuc-Hor. We searched for entries corresponding to the programme stars in the catalogue of astrometric orbit determination with Markov chain Monte Carlo and genetic algorithms by Holl et al. (2023) and found two entries: HIP 16853 and HIP 102626 (BO Mic), both in Tuc-Hor.

We considered the Proper Motion Acceleration (PMa) from Kervella et al. (2022). The PMa is the difference between the proper motion in *Gaia* DR3 (baseline of 34 months) and that determined using the position at HIPPARCOS (1991.25) and *Gaia* DR3 (2016.0) epochs. This quantity is available for 178 stars. The PMa is sensitive to binaries with separation between 1 and 100 au. We considered as an indication for the presence of companions any value of the PMa with a signal-to-noise ratio $S/N > 3$.

We also considered the renormalised unit weight error (RUWE) as an indication of binarity. This parameter is an indication of the goodness of the 5-parameters solution found by *Gaia* (Lindegren et al. 2018). Belokurov et al. (2020) showed that a value >1.4 of this parameter is an indication of binarity, at least for stars that are not too bright ($G > 4$) and saturated in the *Gaia* scans. This method is sensitive to systems with periods from a few months to a decade (Penoyre et al. 2021). The RUWE parameter is available for all but seven stars. Orbital parameters for HIP 21965 were retrieved from Goldin & Makarov (2007). All these data were considered in our analysis.

2.2.5. Substellar companions

We searched for substellar companions in the NASA Exoplanet Archive[6]. For all objects with entries in this catalogue, we looked for the individual references to derive parameters for the substellar companions: HIP 30034: Vigan et al. (2021); HIP 77797: Huélamo et al. (2010); Nielsen et al. (2013); HIP 99770: Currie et al. (2023); HIP 114189 (HR8799): Zurlo et al. (2022); HIP 116805 (κ And): Carson et al. (2013); Uyama et al. (2020); TYC 8047-232-1: Chauvin et al. (2010).

We also checked that none of the free-floating substellar objects listed in Aller et al. (2016); Artigau et al. (2015); Best et al. (2020); Bowler et al. (2012, 2017); Delorme et al. (2013); Desrochers et al. (2018); Gagné et al. (2015); Gizis (2002); Gizis et al. (2015); Liu et al. (2013, 2016); Naud et al. (2014); Patience et al. (2012); Schneider et al. (2014, 2017, 2019, 2023);

---

[6] https://exoplanetarchive.ipac.caltech.edu/applications/Inventory/search.html

Shkolnik et al. (2017) and Zhang et al. (2021) is projected within 600 arcsec of any of the target stars.

2.3. Companion masses and semi-major axis

While other properties of the companions (e.g. the eccentricity of their orbits) are of high interest to determine their origin, in this paper we only considered the semi-major axis of the orbit and the mass of the companion because information about eccentricity could be derived only for a small fraction of the objects. We derived estimates of the mass and semi-major axis for all the companions found. Even though in a significant fraction of the cases they have rather large uncertainties, they are still useful for the statistical discussion done in this paper. In general, whenever these data were available from previous analysis, we used them. When this was not possible, for visual binaries we used the photometry of the individual stars to derive the masses using isochrones by Baraffe et al. (2015) and assumed that the semi-major axis is equal to the projected separation divided by the parallax. On average, this corresponds to the thermal eccentricity distribution considered by Ambartsumian (1937) of $f(e) = 2e$ (see Brandeker et al. 2006). This last paper indicates that this assumption underestimates the semi-major axis by about 25% in the case of circular orbits. This can be compared with the eccentricity distribution for wide binaries by Hwang et al. (2022). These authors found that the eccentricity distribution ranges from uniform (that yields a mean value of $e = 0.5$) for semi-major axis $a < 100$ au, to thermal (that yields a mean value of $e = 0.67$) and even suprathermal for $a > 300$ au.

For a number of objects, indication of binarity comes from PMa, RUWE, or RVs, but the secondary was not observed as a separate object and no period or semi-major axis were determined. These objects have different range of semimajor axis, depending on the technique used to detect them. This is illustrated by Fig. 3 that shows the run of the *Gaia* robust RV amplitude, of RUWE, and of S/N(PMa) with semi-major axis of the orbit for previously known spectroscopic and visual binaries in the young associations and in the Hyades, for which we performed a similar analysis. They are compared with the detection limits, that we set at 10 km s^{-1} (this value is only indicative, however, for the reasons explained in Sect. 2.4 and Appendix A, and was not actually used to claim binarity), Sects. 1.4, and 3 for the robust RV amplitude, RUWE, and S/N(PMa), respectively. We notice that the Hyades are at a distance similar to that of the young associations considered in this paper, so they have a similar sensitivity of the astrometric indicators on the presence of companions. They are particularly useful in this context because thanks to efforts by many investigators in the last decades, they have been intensively studied looking for spectroscopic binaries. These plots indicate that binaries discovered through RVs have semimajor axis that typically are lower than about 1 au, those discovered through RUWE have semimajor axis in the range 1–10 au, while those detected through PMa have a typical semi-major axis of around 10 au (see Appendix B). For the objects detected through astrometry these values are related to the maximum sensitivities achieved that depend on the baseline considered: the length of the *Gaia* DR3 observations (34 months) for the case of RUWE, and the separation between the HIPPARCOS and *Gaia* DR3 epochs (24.75 yr) for S/N(PMa). Of course we should consider the typical total mass of these binaries, that is about 1.5 $M_{\odot}$. The different sensitivities of the various techniques indicate that masses and separation may be better constrained combining the different methods rather than considering only a single technique.
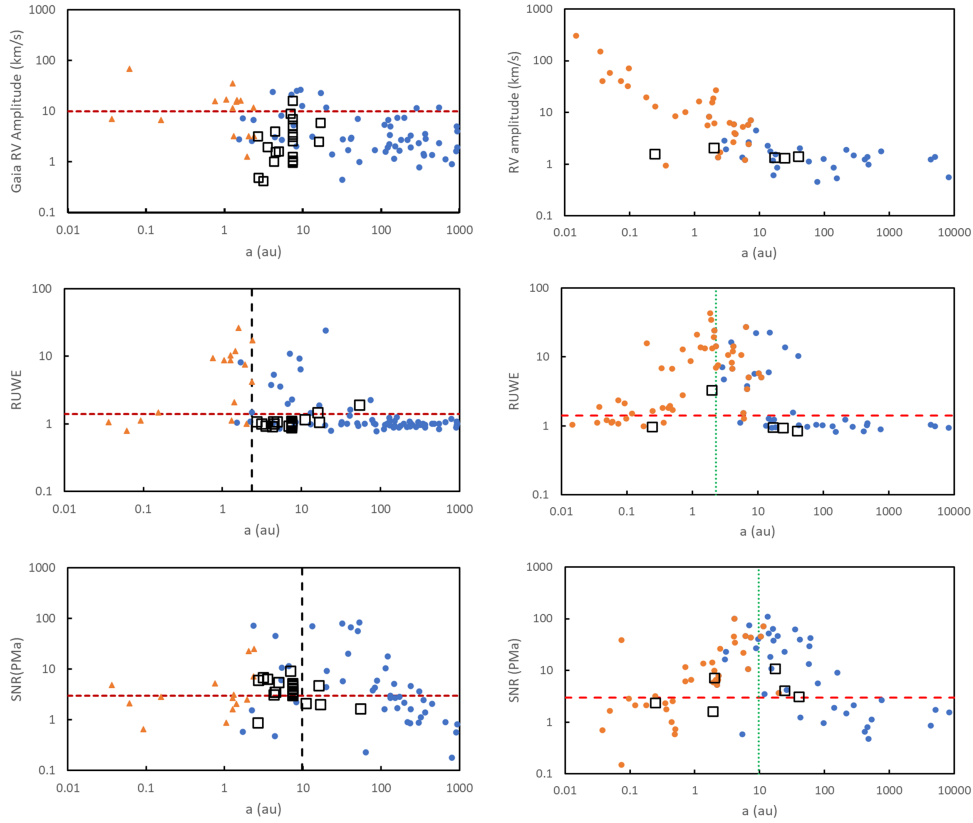
Fig. 3. Relation between the semi-major axis and *Gaia* RV amplitude (upper row), RUWE (middle row), and S/N(PMa; lower row) for previously known binaries in the young association stars (left column) and in the Hyades (right column). Filled blue circles are visual binaries; filled orange triangles are spectroscopic binaries; open squares are substellar companions. Horizontal short dashed horizontal lines are the detection limits for binaries; vertical black long dashed lines mark semi-major axis corresponding to periods of 34 months (for RUWE) and 24.75 yr (for S/N(PMa)) where maximum sensitivity are expected for these two techniques.

We listed in Table 3 the objects for which indication of binarity comes from PMa, RUWE, or RVs. For these objects, we looked for solutions that are compatible with the observed values of the RUWE, of the PMa, the scatter in RV, and the non-detection in HCI as done in Gratton et al. (2023b). This was done exploring the semi-major-axis – mass ratio plane using a Monte Carlo code. We adopted eccentric orbits, with uniform priors between 0 and 1 on eccentricity (in agreement with Hwang et al. 2022 for this range of separation), 0 and 180 degrees in the ascending node angle Ω, and 0 and 360 degrees in the periastron angle ω and left the inclination and phase to assume a random value. In addition, whenever available, period was used to fix the solution.

The adopted final values are the mean of those for solutions compatible with observations within the errors, and the uncertainty is the standard deviation of this population. Data for the derivation of these masses are given in Tables C.17–C.24 in the Appendix C, while the values of the semimajor axis a and of the masses of the stars are given in Table 3. The distribution of the companions in the $a - q$ plane is shown in Fig. 4; they have $0.1 < a < 10$ au, but companions of those stars for which the PMa is available tend to be at slightly larger values of the semi-major axis a. For small mass objects with significant PMa, we considered the masses provided by the table by Kervella et al. (2022) and adopted a semi-major axis of 7.5 au.

We expect that in most cases close binaries unresolved by both *Gaia* and 2MASS should appear brighter in the colour-magnitude diagram than single stars of similar colour because of the contribution by the secondary. This happens when the secondary is also a main sequence star or a substellar object; the case is more complicate if the secondary is a stellar remnant, an occurrence that should be rare but that cannot be completely excluded. In addition, the secondary might itself be a close binary: this would cause it to be under-luminous with respect a single star with the same total mass. The magnitude offset dG in the *Gaia* G – magnitude between single stars and binaries should depend on the mass ratio between the two components, the maximum offset being expected for equal mass systems. The actual run with the mass ratio depends also on the colour that is considered (here the $G - K$ colour), on the age, and on the mass of the components. Although this relation is rather complex, we may use this offset as a check on the dynamical mass ratios indicated by the combination of PMa, RUWE, and RVs. This comparison is done in Fig. 5. The agreement between the photometric and dynamical masses is not perfect. The most discrepant cases are 2MASS J05301907-1916318 (AG Lep) in Columba and 2MASS J08264964-6346369 in Volans/Crius 221. In the first case, the magnitude offset is d$G = 0.714 \pm 0.075$ mag, that would be consistent with a value of $q > 0.6$, that is a mass of $M_B > 0.5\ M_\odot$, while the value we obtained from dynamical arguments is only $M_B = 0.228 \pm 0.050\ M_\odot$. The second case is an SB according to Steinmetz et al. (2020); the magnitude off-set d$G = -0.052 \pm 0.056$ mag is negligible while the dynamical mass ratio ($q = 0.70 \pm 0.24$) indicates the presence of a rather massive companion ($M_B = 0.557 \pm 0.192\ M_\odot$). In this case a small mass ratio $q \sim 0.2$ (that is only 2-σ off the preferred value

Table 3. Companion masses and semi-major axis from dynamical data (RVs, RUWE, and PMa).

HIP	2MASS	RUWE	RV Ampl. (km s^{-1})	S/N(PMa)	dG (mag)	M_A ($M_\odot$)	M_B ($M_\odot$)	a (au)	Association
					Selected for RUWE > 1.4				
12635	J02422094+3837212	26.545	2.36	12.39	−0.031 ± 0.038	0.756	0.267 ± 0.014	2.159 ± 0.125	AB Dor
14551	J03075083-2749520	4.176	11.76	7.18	−0.176 ± 0.041	1.608	0.091 ± 0.019	2.346 ± 0.114	Columba
	J05044132+4024003	2.245	25.32		−0.009 ± 0.034	0.725	0.203 ± 0.168	2.726 ± 4.043	AB Dor
	J05301907-1916318	1.575	8.67		0.714 ± 0.075	0.838	0.228 ± 0.050	0.299 ± 0.236	Columba
	J05345923-2954041	1.912	5.91		0.106 ± 0.034	0.756	0.144 ± 0.035	0.369 ± 0.309	Argus
35564	J06582764+2215067	8.691	16.96	0.88		1.386	0.683 ± 0.200	0.365 ± 0.109	Carina-Near
37635	J07432149-5209508	17.534	2.91	45.54	−0.087 ± 0.075	1.127	0.180 ± 0.064	3.842 ± 0.850	Carina-Near
37855	J07453559-7940080	7.633	1.28	2.49	0.039 ± 0.075	1.138	0.205 ± 0.031	1.802 ± 0.160	AB Dor
	J08134777-5837139	1.661	5.08		−0.082 ± 0.066	1.388	0.275 ± 0.144	1.582 ± 3.491	Volans
	J08264964-6346369	11.879	16.58		−0.052 ± 0.056	0.792	0.557 ± 0.192	1.800 ± 1.736	Volans
	J08391155-5834281	2.527	29.38		0.520 ± 0.050	1.003	0.658 ± 0.113	0.253 ± 0.092	Argus
43783	J08550282-6038406	3.731	7.25	9.86	0.481 ± 0.212	4.822	0.911	3.387	Volans/Crius 221
46460	J09283051-6642067	3.192	72.03	1.69	0.681 ± 0.057	2.227	0.851 ± 0.627	0.818 ± 0.625	Volans/Crius 221
	J09534760-5453540	4.861	6.41		0.230 ± 0.047	0.911	0.237	2.530	Carina
50191	J10144416-4207189	2.873		0.97	0.428 ± 0.066	2.110	0.559 ± 0.360	0.285 ± 0.179	Argus
50567	J10194613-7133173	44.080	5.07	12.73	0.216 ± 0.067	1.024	0.488 ± 0.047	2.453 ± 0.146	Volans/Crius 221
	J12063292-4247508	4.253	22.38		0.432 ± 0.039	0.910	0.635 ± 0.113	0.471 ± 0.473	Argus
	J12203437-7539286	26.350	16.39		0.340 ± 0.035	0.754	0.564 ± 0.161	1.805 ± 1.080	Argus
108422	J21575146-6812501	10.369	35.72	2.72	0.633 ± 0.039	0.948	0.421	0.746	Tuc-Hor
					Selected for S/N(PMa) > 3				
560	J00065008-2306271	0.933	3.02	3.42	−0.069 ± 0.065	1.413	0.0017 ± 0.0009	16.57 ± 15.78	BPMG
8233	J01460105-2720556	1.071	5.15	3.01	−0.037 ± 0.065	1.431	0.0052 ± 0.0060	22.07 ± 18.26	Tuc-Hor
11696	J02305064+5532543	1.061	16.12	4.18	0.093 ± 0.070	1.326	0.0048 ± 0.0030	7.68 ± 7.08	AB Dor
15201	J03155768-7723184	1.000	0.42	6.74	0.167 ± 0.068	1.418	0.0135 ± 0.0114	17.78 ± 12.87	Carina
16449	J03315364-2536509	1.079	3.94	3.48	0.007 ± 0.046	1.762	0.0056 ± 0.0052	12.54 ± 10.06	Columba
17675	J03471061+5142230	0.995	2.56	3.15	−0.193 ± 0.063	1.445	0.0097 ± 0.0099	24.09 ± 19.02	Columba
22152	J04460056+7636399	0.900	3.10	3.09	−0.169 ± 0.072	1.221	0.0012 ± 0.0006	17.11 ± 15.72	Columba
30034	J06191291-5803156	0.923	1.96	6.26	0.208 ± 0.033	0.913	0.008 ± 0.004	3.571 ± 1.167	Carina
45585	J09172755-7444045	1.070	1.59	5.37	0.041 ± 0.088	2.072	0.0176 ± 0.0084	6.85 ± 2.46	Carina
47391	J09392101-6119410		11.61	45.80	0.508 ± 0.134	3.011	1.287 ± 0.687	34.622 ± 26.864	Carina
60831	J12280445+4447394	0.905	1.02	3.12	−0.065 ± 0.074	1.166	0.0034 ± 0.0020	9.47 ± 3.90	Carina-Near
60832	J12280480+4447305	1.067	0.48	5.94	0.176 ± 0.066	1.042	0.0074 ± 0.0029	9.27 ± 3.84	Carina-Near
					Selected for RV Ampl. > 100 km s^{-1}				
47017	J09345645-6459579	0.971	122.40	1.46	0.487 ± 0.073	1.376	0.322 ± 0.242	2.925 ± 24.901	Volans/Crius 221
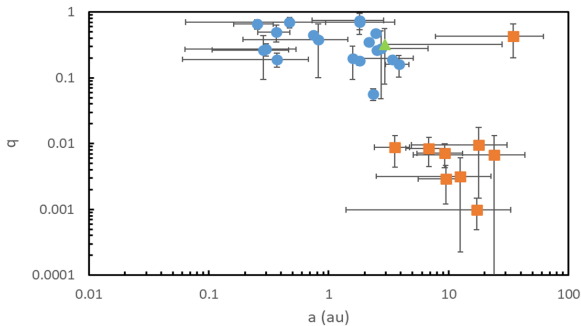
Fig. 4. Relation between the semi-major axis and mass ratio for the companions of the young association stars discovered through *Gaia* PMa, RUWE, or a variation in RVs that are not visual binaries or do not have an orbit determination. Filled blue circles are companions selected on the basis of the value of RUWE > 1.4; filled red squares are those selected from S/N(PMa) > 3; filled green triangles are those selected from RVs.
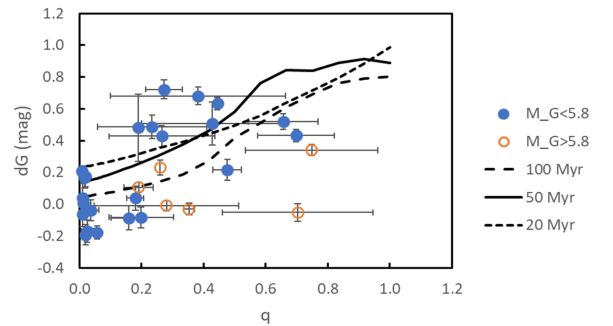
Fig. 5. Run of the offset in *Gaia G* magnitude dG with respect to the single star main sequence as a function of the mass ratio q for the stars with masses determined from a combination of 4PMa, RUWE, or a variation in RVs. Filled blue symbols are stars with $M_G < 5.8$, open red symbols are for fainter stars. The lines are the expected runs of the magnitude offset as a function of q for binaries with primaries of 1.3 $M_\odot$ and different ages.
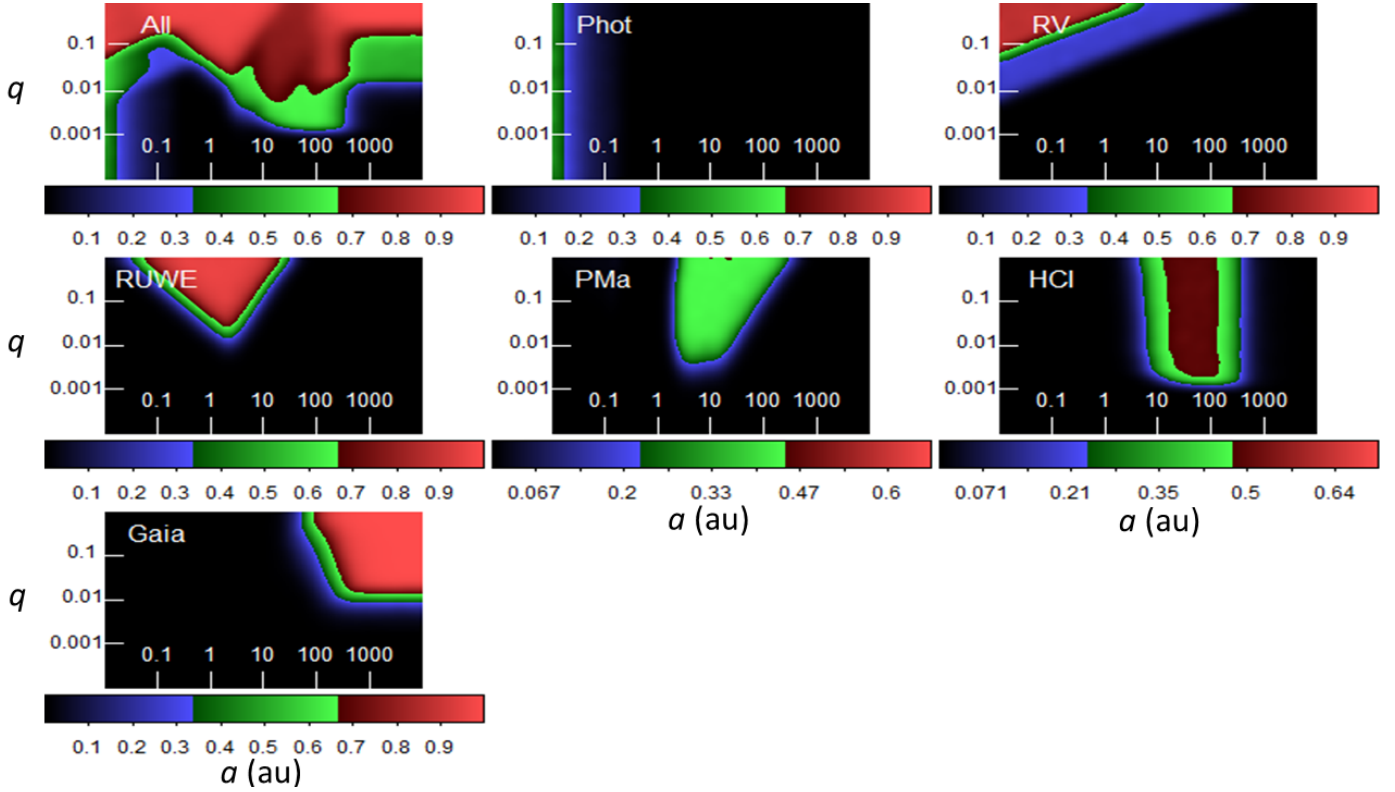
Fig. 6. Completeness map of the search of companions in the semi-major axis a (in au) – mass ratio q plane. The upper left panel is the result obtained using all the techniques considered in this paper; the remaining panels are results for the individual techniques: Phot = Eclipsing binaries; RV = spectroscopic binaries; RUWE = *Gaia* goodness of fit RUWE parameter; PMa = Proper Motion Anomaly; HCI = high contrast imaging; *Gaia* = separate entry in the *Gaia* catalogue. Different level of completeness are shown as different colours; the colour scale used is shown on bottom of each panel.

and would correspond to a 0.15 $M_\odot$ star) would make dynamical and photometric results in fair agreement with each other. Given the fair agreement existing between dynamical and photometric masses for most cases, we however think that the adopted masses may be considered acceptable for the statistical purposes of this paper.

2.4. Detection completeness

Figure 6 illustrates the completeness of our survey in the semi-major axis a vs. mass ratio q plane. This is shown for the individual techniques as well as for the combination of them. These completeness maps were obtained through simulations of 10 000 companions (stellar and planetary) for each of the stars in our sample (with appropriate values of the magnitude, mass, parallax and age) with random values of the orbital parameters. For each target and methodology we considered if the appropriate data sets were available. We then determined the signal expected for each simulated companion according to the various methods considered and compared them with the detection limits appropriate for each method. This method was already considered in Gratton et al. (2023b), where a full description is reported, save for errors and limits in RV; this procedure is actually similar to that proposed by Wood et al. (2021). While the detection limits are possibly questionable, they were used consistently in the simulation and on the real data. This is of course not properly an injection/recovery process, in the sense that we did not start from real raw data adding a companion signal and recovering it. This full injection/recovery process was done to determine the

detection limits in HCI; however, it was not possible to use it in other data sets, in particular for those provided by *Gaia* that are the most useful for the present purposes, because the raw data are not available. In these cases we simply considered the signal on the time series of *Gaia* positions and RVs relevant to each simulated companion, added a random Gaussian noise, extracted from these noisy simulated series the relevant signal (RUWE, RV variation, proper motion anomaly), and compared it with the observed values (both above and below threshold for detection). We notice that also signals below threshold can be useful to constrain the range of parameters where acceptable solutions can be found. For eclipses/transits the detection procedure is much more complicated and there is no simple threshold value available in the literature. For what concerns stellar companions, we simply assumed that all EBs with periods <28 days are recovered by TESS. TESS is in principle also able to recover some EB with longer periods depending on the number of sectors where the target was observed. However, the EB catalogues we used only refers to the early observations with TESS and very few stars were observed on a large number of sectors. For transiting planets the situation is much more complex and TESS is of course less efficient in discovering young transiting planets; we then discussed the case of transiting planets separately in Sect. 4.3, where we make explicit reference to literature papers that used an injection/recovery procedure (Fernandes et al. 2022, 2023).

For what concerns RVs, the precision achievable for solar-type stars is in principle much higher than for early-type stars, due to the slower rotation and much higher number of spectral lines available. On the other hand, we should take into account
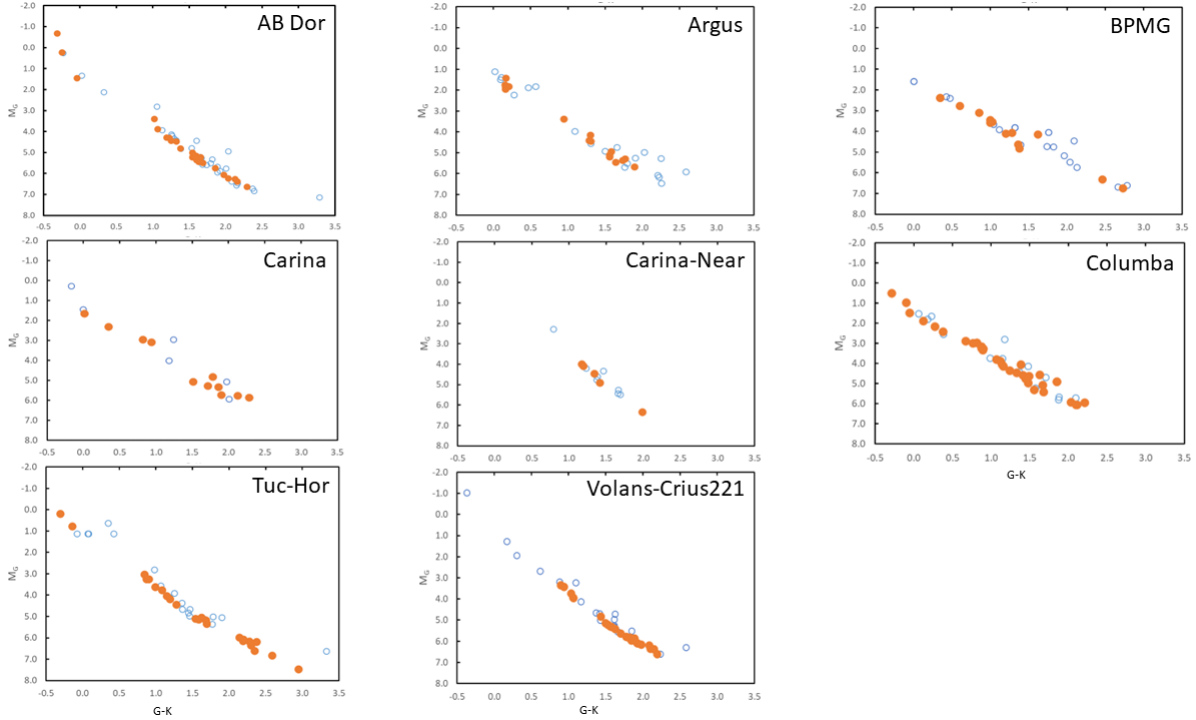
Fig. 7. $M_G - G - K$ colour-magnitude diagram for stars in the young associations considered in this paper. Orange filled circles are bona fide single stars; blue empty circles are multiple stars.

the concern related to the jitter due to the stellar activity. To evaluate the appropriate RV jitter, we considered in Appendix A the value of the robust RV amplitude in those stars that do not have any other clear signs of being close binaries (separation <100 au). We found that as expected for these objects, the robust RV amplitude is a function of both star absolute magnitude (a proxy for spectral type) and age. In addition, there are a number of young late-type stars that are very fast rotators (as indicated by the short period that can be derived by the TESS light curves) and for them the robust RV amplitude is not a reliable indicator of real RV variations, probably because of severe line blending not properly taken into account by the *Gaia* RV pipeline. This indicates that the *Gaia* RVs are sometime poor indicators of variation of the centre-of-mass RVs. In our procedure, we then considered the maximum between the internal error and the median RV jitter expected for the age and absolute magnitude of each star as an appropriate indicator of the errors in individual RVs and we did not consider as binaries young late-type star whose only indication of binarity is a high value of the *Gaia* robust RV amplitude, save for the case of HIP 47017 that has a *Gaia* robust RV amplitude of 122.4 km s^{-1}. For the statistical purposes of this paper, we then considered detection thresholds of 1 km s^{-1} for those cases where there are high precision RV series, and of 10 km s^{-1} for those when only the *Gaia* RV sequence is available, respectively. These values are much larger than the typical internal errors, that are a few m s^{-1} from high precision RVs and ~0.3 km s^{-1} for those from *Gaia*. With these thresholds, the completeness level for separation in the range 0.1–1 au is however higher than obtained for B-stars in Gratton et al. (2023b). We notice that for what concerns eclipses, the detection efficiency considered preparing this figure includes the probability that the transit occurs.

For what concerns stellar companions, thanks to *Gaia*, the search for visual companions should be complete down to a

projected separation of about 100 au. A fraction of the substellar companions is not detected by *Gaia*. The masses corresponding to a magnitude of $G = 19$ (roughly the detection limit to be considered here in order to have reasonably accurate astrometry) for the age and average distance of each association are listed in Table 1. They are all in the BD regime, ranging from 0.013 $M_\odot$ for the BPMG to 0.040 $M_\odot$ for Volans/Crius 221. HCI imaging, available for (at least) 194 stars, should reveal all stellar companions with semi-major axis in the range 20–150 au.

For the programme stars, the PMa (available for 178 stars) should have $S/N > 3$ for all systems having a stellar companion in the range 3–100 au. There are 61 stars for which neither PMa nor HCI is available. Though additional data is available (for instance visual observations or speckle interferometry), for these stars (21% of the total) there may be incompleteness in the 10-100 au region. Stellar companions with separation in the range 0.2–10 au would produce a value of RUWE > 1.4 and should be detected. RUWE is available for all but seven stars in the sample. RV variations with clearly significant amplitude would be detected for semi-major axis <1 au and for many others with larger radii. High precision RV sequences are available for 79 stars, while RV series from *Gaia* are available for 181 additional stars in the sample. Finally, TESS data about photometric variations are available for 269 stars. The search for eclipsing binaries with $a < 0.2$ au (roughly a period of 27 days) should be then almost complete. However, we expect that only about 1/10 of the close binary systems should be eclipsing/transiting. We conclude that while some massive companions may still be missed, we think our search is almost complete for stellar companions and that few BDs are missing at separation greater than 10 au.

While completeness in the binary search is on average high, we find indications that a few binaries may still be missed. Figure 7 shows the $M_G - G - K$ colour-magnitude diagram for
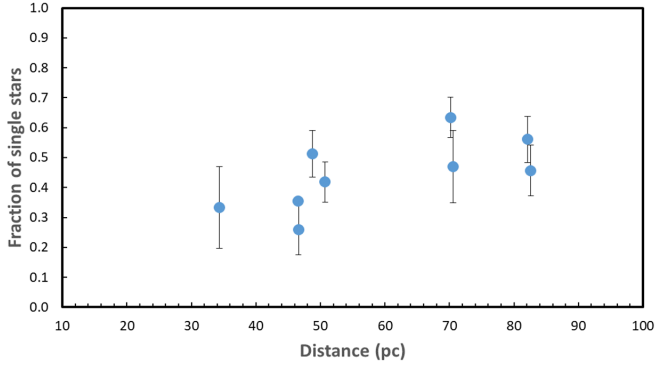
Fig. 8. Fraction of single stars in individual associations as a function of the distance.

Table 4. Frequency of single stars for young nearby associations.

Association	Primaries	Single stars	Frequency
AB Dor	55	23	0.42 ± 0.07
Argus	35	16	0.46 ± 0.08
β Pic	27	7	0.26 ± 0.08
Carina	17	8	0.47 ± 0.12
Carina Near	12	4	0.33 ± 0.14
Columba	52	33	0.63 ± 0.07
Tuc-Hor	41	21	0.51 ± 0.08
Volans/Crius 221	41	23	0.56 ± 0.08

stars in the young associations considered in this paper. Different symbols are used for bona fide single stars and multiple stars. The single star sequences are generally very narrow. However, a few binaries may still be present among the sample of bona fide single stars. Furthermore, the search is likely less complete around stars that are more distant from the Sun. This is shown in Fig. 8, where a trend for the fraction of single stars with distance of the individual associations is apparent. These data yield a Persson linear coefficient $r = 0.63$ that is significant at 2.5% level of confidence. This trend is due to the lack of PMa data for stars not included in the HIPPARCOS catalogue; in fact, the fraction of stars that have PMa data changes systematically with distance of the association, from about 100% for the closest association (Carina Near) to about 40% for the furthest ones (Argus and Volans/Crius 221). This highlights the importance of the distance limit in our analysis.

2.5. All companions in the semi-major axis vs. mass ratio plane

Figure 9 shows the correlation between semi-major axis a and mass ratio q for all companions considered in this paper. The distribution of the detected companions in this plane is the result of both the real distribution and of the selection effects due to completeness of the search, as shown in Fig. 10. As expected, detection efficiency of small mass companions ($q < 0.01$) is rather low. After consideration of the selection effects, this diagram shows two main groups of objects: a wide distribution of companions with mass ratio q from 0.015 to 1, and a second group of objects with semimajor axis from 1 up to about 100 au at $q < 0.01$. This second group covers a region of the plane that is more extended in semi-major axis than that corresponding to the definition of JL planets. We should note that the buildup of dynamical companions at 7.5 au is simply a consequence of the fact that lacking better information, we assumed this value to estimate their masses from the tables by Kervella et al. (2022). Uncertainties in the semi-major axis are of at least a factor of three, so this value should only be taken as an approximation of the real value. We remind that our paper is only aimed to a statistical discussion of the frequency of companions of different masses and semi-major axis. This only requires order of magnitude estimates these quantities. Given this consideration, we will consider all members of this group as JL planets. Incompleteness is high in this region. If we strictly consider the area corresponding to the definition of JL-planets, the average completeness factor is 36%. However, even within this restricted area

there is a strong gradient with mass ratio and less extreme in semi-major axis, so more massive and further out planets are more easily detected than the close-by and smaller mass ones. Detection efficiency is as low as 0.5% at the lower left corner of this range. If the mass function of JL-planets favours smaller mass object, as it is very likely, the completeness factor for the detection of JL-planets is well below the number given above.

Finally, around the stars considered in this paper there is a hot-Neptune transiting DS Tuc A ($5.6 \pm 0.2\ R_{\rm Earth}$: Newton et al. 2019; Benatti et al. 2019) in the Tuc-Hor moving group, to which we have to add the mini-Neptune around HIP 94235 ($3.00^{+0.32}_{-0.28}\ R_{\rm Earth}$: Zhou et al. 2022) for which no mass is available.

In the next two sections we consider first the properties of stellar companions and then those of the planetary companions, with emphasis on the JL ones.

3. Stellar companions

3.1. Statistics of stellar companions

Table 4 lists the total number of stars and the number of single stars in each association. The total number of single stars (we do not consider planetary companions here) is 135 over 280 systems surveyed[7], that is a fraction equal to 0.48 ± 0.03[8]. The value is likely overestimated by a few per cent because our search for companions is not complete. This fraction is lower than the value of 0.54 ± 0.02 obtained for field solar-type stars by Raghavan et al. (2010; see upper panel of Fig. 12). This is not an effect of a different mass distribution. In fact, the median mass of the primaries considered in this paper is 1.04 $M_\odot$, that is only marginally different from the solar value. A high frequency of multiple stars in nearby young association was already noticed (CrA: Köhler et al. 2008; Taurus-Auriga: Leinert et al. 1993; Köhler & Leinert 1998; Sco-Cen: Gratton et al. 2023b).

The upper region of Figs. 9 and 10 contains stars and BDs (objects with $\log q > -1.8$). Our search is reasonably complete for these objects: the mean detection efficiency over the whole area is 74%. The lowest efficiency is obtained for the search of BD companions with separation of the order of a few tenths au. These companions would be easily detected through high precision RVs, that are however available for only 79 stars, that is 28% of the sample. Anyhow, the lack of any BD at small

---

[7] The total number of entries in our lists is 296 stars because there are several wide binaries with separate entries for the individual components.

[8] Throughout this paper, uncertainties in the fractions were computed as $\sqrt{qp/n}/n$, where p, q, and $n = q + p$ are the number of positive, negative, and total cases considered.
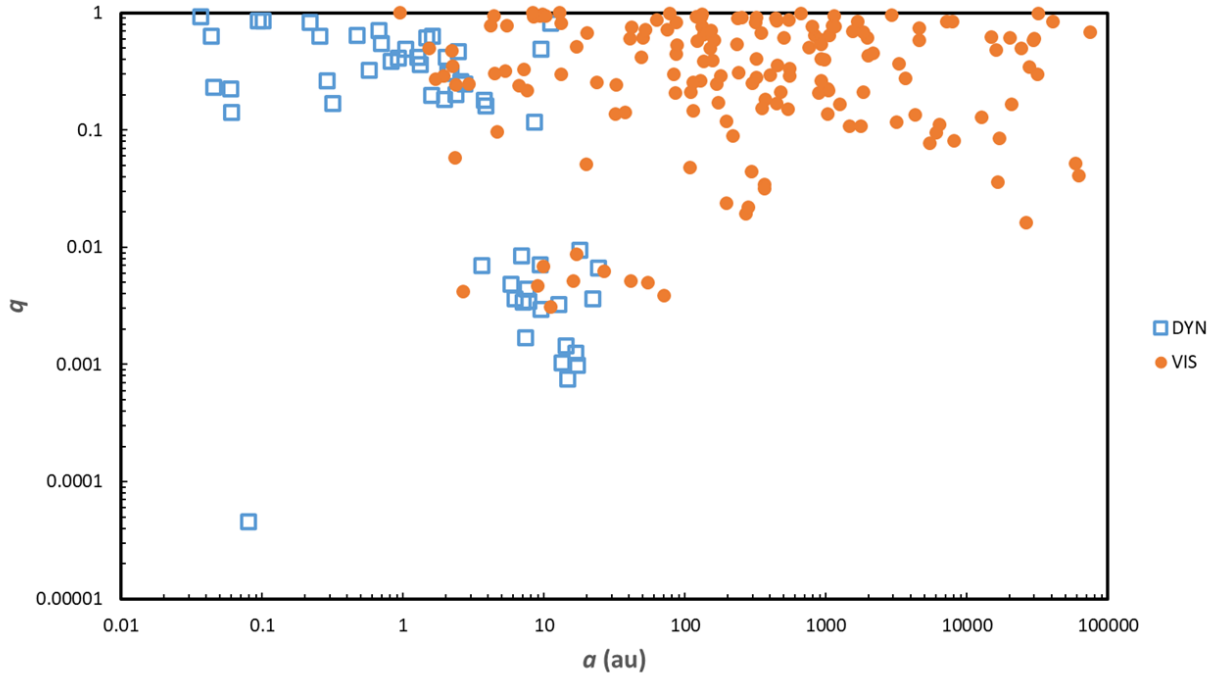
Fig. 9. Relation between semi-major axis *a* (in au) and mass ratio *q* between components for all companions found so far around stars that are member of the young associations considered in this paper. Filled orange circles are companions detected in imaging; open blue squares are those detected using dynamical methods or eclipses/transits.
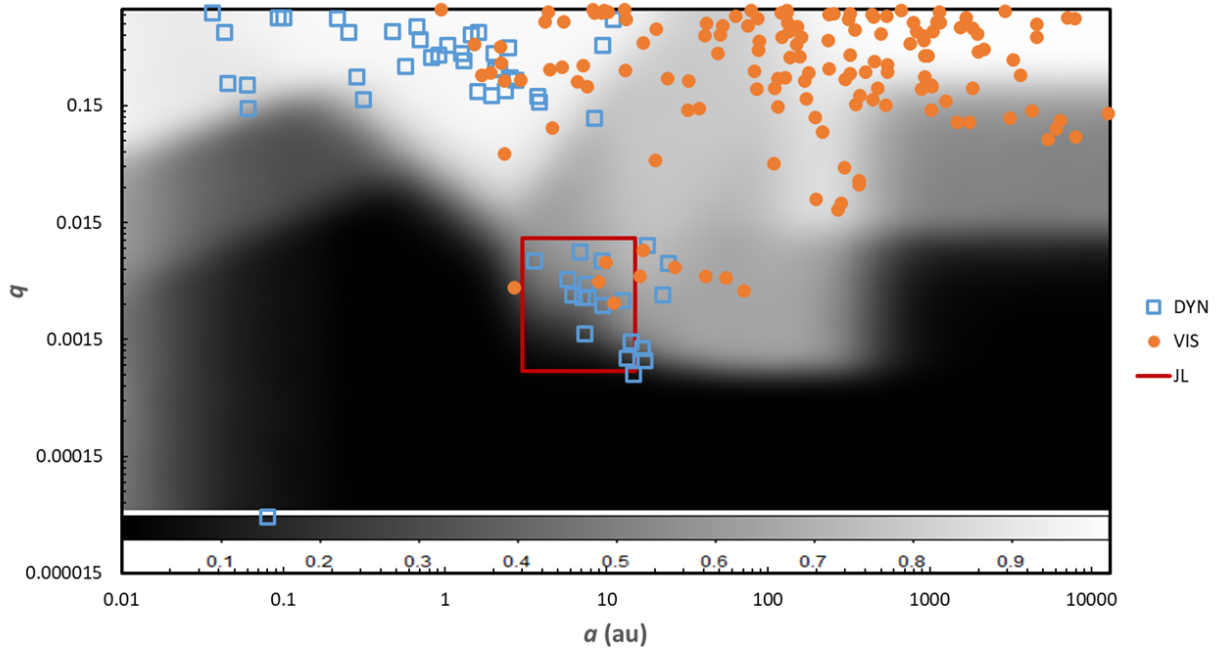
Fig. 10. Same as Fig. 9 but with the detection completeness in the background. The grey scale on the bottom of the figure indicates the level of completeness achieved in different region of the $a - q$ plane. The red rectangle marks the area covered by JL planets.

separation around these 79 stars shows that this region of the diagram is at most scarcely populated. On the other hand, the discovery efficiency for stellar companions (objects with $\log q > -1.15$) is 84% and the minimum value is 31%. This indicates that our sample is fairly complete so far stellar companions are considered. Overall, our lists include 182 stellar companions

(mass > 0.075 $M_\odot$) and nine BDs (here objects with a mass $0.02 < M < 0.075\ M_\odot$) around 145 stars. We will consider here stellar and BD companions together. A log-normal fit to their semi-major axis *a* yields an average value of $\log a/au = 1.94$ (that is 88 au), with a sigma of 1.50. The companions with separation wider than 1000 au are 44, that is $23.0 \pm 3.5\%$ of the total.
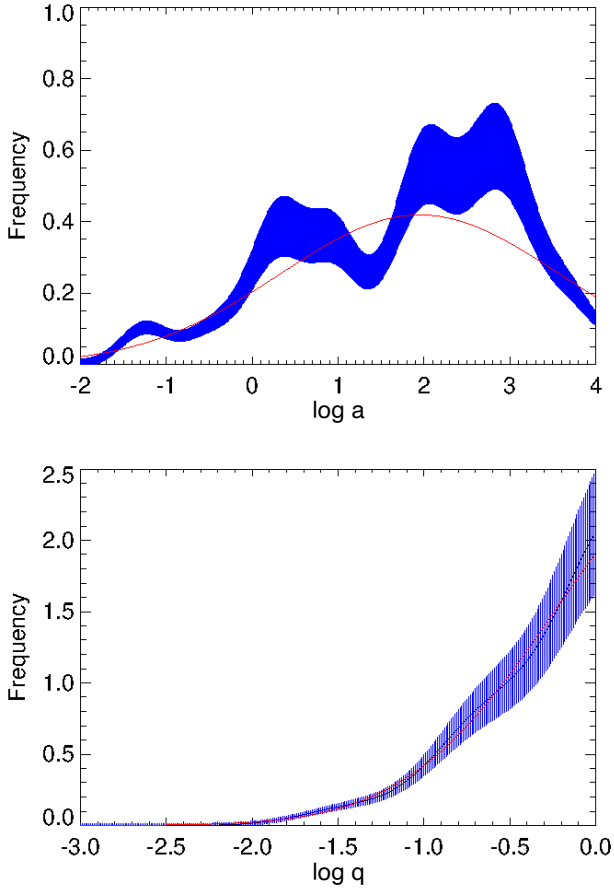
Fig. 11. Distribution of companions with mass ratio and semi-major axis. Upper panel: v with $\log q > -1.08$ as a function of the logarithm of the semi-major axis a in au. Lower panel: distribution of companions with $0.5 < \log a < 3$ as a function of the logarithm of the mass ratio q. The red lines are best fit log-normal through the observed distributions. The shaded area in both panels corresponds to 1σ uncertainty.

Within the upper strip we can still discern trends in the values of q with separation. Namely, there is an empty region with $a < 200$ au and $0.01 < q < 0.05$. As mentioned above we are not fully complete over this region, however, the lack of objects in this region is clearly significant. This is the well-known BD desert (Marcy & Butler 2000; Raghavan et al. 2010; Stevenson et al. 2023; Unger et al. 2023). However, at separation $a > 200$ au this region is populated by a number of objects, similarly to what found previously by Metchev & Hillenbrand (2009). We notice in fact that four out of ten of the BDs are at separation wider than 1000 au. This feature should be reproduced by mechanisms of formation of companions.

3.2. Distribution with mass and semimajor axis of stellar companions

Figure 11 shows the distribution of stellar companions with semi-major axis a and with the mass ratio q corrected for completeness. The semi-major axis $\xi(\log a/\text{au})$ distribution can be described by a log-normal as:

$$\xi(\log a/\text{au}) = 0.418 \exp\left[\frac{-0.5\,(\log a/\text{au} - 1.95)^2}{1.62^2}\right]. \tag{1}$$

The mean value made on the logarithm of a yields a value of $a = 89^{+28}_{-21}$ au. This value is close to that obtained for early-B
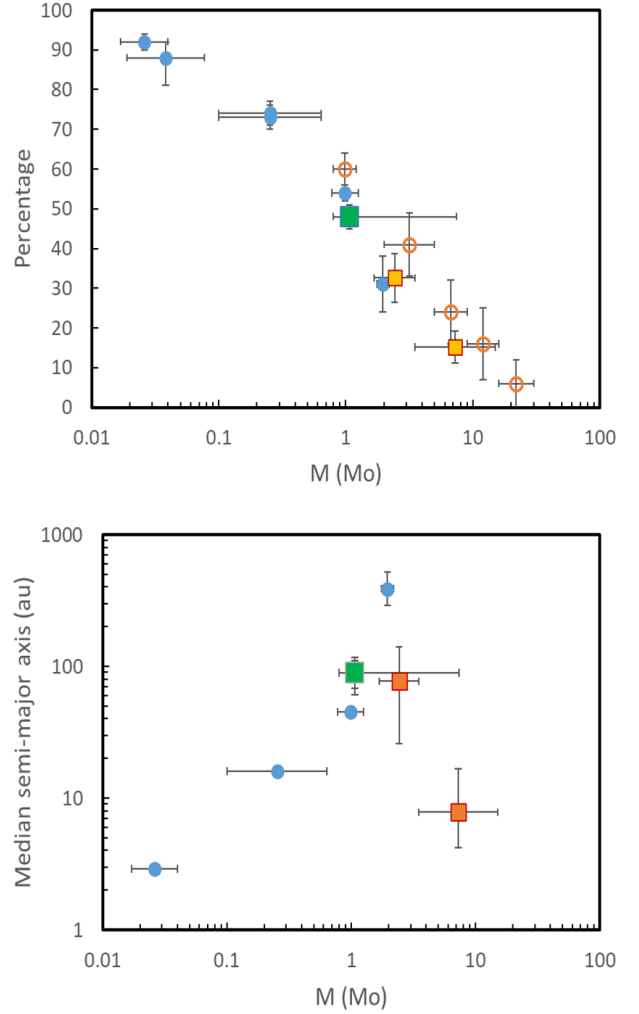
Fig. 12. Runs of statistical properties of binaries with the stellar mass. Upper panel: Run of the frequency of single stars from our data (green squares), the samples in Table 4 (filled circles), from Moe & Di Stefano (2017) (opens circles), and the B stars in Sco-Cen (Gratton et al. 2023b). Lower panel: run of the median semi-major axis. Horizontal error bars reproduce the mass range of the different samples

stars in Sco-Cen by Gratton et al. (2023b) and the peak of the run with stellar mass (see lower panel of Fig. 12).

The distribution with $\xi(\log q)$ of companions in the range 3–1000 au for $0.003 < q < 1$, again corrected for completeness, is reproduced by the tail of a log-normal law of the form:

$$\xi(\log q) = 2.453 \exp\left[\frac{-0.5\,(\log q - 0.61)^2}{0.86^2}\right]. \tag{2}$$

Figure 13 compares the median semi-major axis of the orbits of stellar companions with the location of the water ice-line (solid line) and five times this distance as a function of the mass of the primary star. Formation of JL planets by core-accretion mechanism is expected in this range of separation from the star. We notice that the peak of the distribution with semi-major axis for stellar companions is very close to the region where formation of JL planets is expected. Hence, such a formation will be prevented in a rather large fraction of the systems. This should be considered when estimating the frequency of JL planets in the context of the mechanisms for their formation. Also, this figure shows that for solar-type stars (as well for stars of lower mass),
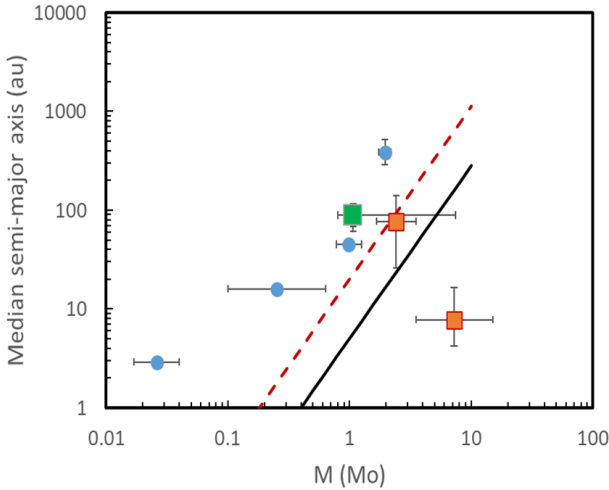
Fig. 13. Same as the lower panel of Fig. 12 but with added the location of the water-ice line (solid black line) and five times this distance (dashed red line) as a function of the mass of the primary star. Formation of JL planets by core accretion is expected in this range of separation from the star.

planets in binary systems are most likely to be found closer to the star than the companions (S-type planets), while the opposite should hold in the case of planets around B-stars (P-type planets).

4. Planetary companions

4.1. Detections and candidates JL planets

Overall, we considered 24 stars hosting JL or candidates in the eight associations considered. JL planets have been already observed through HCI around seven stars. They are 51 Eri (Macintosh et al. 2015; De Rosa et al. 2020; Samland et al. 2017), AF Lep (Mesa et al. 2023; De Rosa et al. 2023; Franson et al. 2023), and β Pic (Lagrange et al. 2009; Lacour et al. 2021) in the BPMG; HIP 30034 (AB Pic) in Carina (Chauvin et al. 2005; Vigan et al. 2021); HR8799 (Marois et al. 2008, 2010; Zurlo et al. 2022) and κ And (Carson et al. 2013; Uyama et al. 2020) in the Columba moving group; and b03 Cyg in the Argus moving group (Currie et al. 2023).

In addition to these seven stars (with a total of 11 planets), indications for the presence of JL planets are obtained from PMa for 18 additional stars. The strong cases for JL companions being responsible of the observed PMa are already discussed for HIP 30314 in AB Dor (Mesa et al. 2022); HIP 560, HIP 10679, HIP 84586, and HIP 88399 in the BPMG (Mesa et al. 2022 and Gratton et al. 2023b), for HIP 1481 in Tuc-Hor (Mesa et al. 2022), and for HIP 52462 (Mesa et al. 2021) and HIP 96334 (Mesa et al. 2022) in Volans/Crius 221 and will not be repeated here. We will now discuss the remaining ten cases.

HIP 8233 (HR 517). Member of Tuc-Hor with a mass of 1.42 $M_\odot$. There is no HCI in the ESO archive and no high precision RV in the literature. The star has no infrared excess (Pawellek et al. 2021). The value of the PMa is consistent with the not significant RUWE and the non-detection of companions from *Gaia* over a wide range of semi-major axis (3–100 au) and mass (4–120 M_{Jup}: see Fig. 14). Waiting confirmation from HCI data (an upper limit would also be adequate), we will assume here that the companion is a JL planet.

HIP 11696. Member of AB Dor with a mass of 1.39 $M_\odot$. High contrast imaging has been obtained by Mesa et al. (in prep.)

with LBT-SHARK with no detection. The observed PMa, the lack of significant RUWE and of a detection in HCI strongly suggest the presence of a JL companion.

HIP 15201 (iot Hyi, 2MASS J03155768-7723184). Member of Carina with a mass of 1.41 $M_\odot$. There is unpublished Spectro-Polarimetric High-contrast Exoplanet REsearch instrument (SPHERE) observation in the ESO archive by De Rosa & Nielsen, that is still not public. There is no indication of binarity in the literature and no high precision RV data. The value of the PMa is consistent with RUWE and the non-detection of companions from *Gaia* over a wide range of semi-major axis (3–55 au) and mass (10–100 M_{Jup}: see Fig. 14). Waiting confirmation from the SPHERE data (an upper limit would also be adequate), we will assume here that the companion is a JL planet.

HIP 16449 (HR 1082). Member of Columba with a mass of 1.72 $M_\odot$. High contrast imaging was obtained by Esposito et al. (2020); Dahlqvist et al. (2022); Pearce et al. (2022) with no detection. A debris disk was detected by ALMA with inner radius of 68 au and outer radius of 120 au Higuchi et al. (2020); Pearce et al. (2022). The value of the PMa, the lack of a significant RUWE and of a HCI detection, and the location of the debris disk strongly suggest that the companion is a JL planet.

HIP 17675 (2MASS J03471061+5142230). Northern member of Columba with a mass of 1.44 $M_\odot$. There is no high precision RV data. The value of the PMa is consistent with the not significant RUWE and the non-detection of companions from *Gaia* over a wide range of semi-major axis (3–100 au) and mass (4–180 M_{Jup}: see Fig. 14). Waiting confirmation from HCI data (an upper limit would also be adequate), we will assume here that the companion is a JL planet.

HIP 22152 (2MASS J04460056+7636399). Northern member of Columba with a mass of 1.21 $M_\odot$. HCI has been obtained within the International Deep Planet Survey (Galicher et al. 2016) and there is *Hubble* Space Telescope imaging from Song et al. unpublished, reported in Vigan et al. (2017), with no detection. Within the constraints given by the lack of detection in HCI and the lack of a significant RUWE signal, the PMa is only compatible with a planetary companion, over a range of separation from 3 to 40 au. We will assume here that the companion is a JL planet.

HIP 45585 (2MASS J09172755-7444045). Member of Carina with a mass of 2.07 $M_\odot$. The object was observed with SPHERE by Dahlqvist et al. (2022) with no detection of a companion and an upper limit of about 30–100 M_{Jup} over the separation range 3–300 au. There are HARPS High precision RV data available (Trifonov et al. 2020) over about 74 d that show a rather large scatter and a possible trend of 23 m s^{-1}/day. However, since RUWE is not significant, this trend in RV (if real) can only be attributed to a small mass companion very close to the star and is certainly unrelated to the PMa. The star hosts a debris disk whose spectral energy distribution suggests two belts with $T_{eff} \sim 290$ and 140 K (Chen et al. 2014; Kennedy & Wyatt 2014). These temperatures correspond to semimajor axes of about 5 and 17 au. If these disks signal the presence of a planet, this should be at about 8–10 au from the star; this value corresponds to where the observed value of the PMa is consistent with the upper limits set by RUWE and imaging. The mass of the candidate companion (20–25 M_{Jup}) corresponds to a small BD. However, given the high mass of the star and hence the low value of the mass ratio q, we may consider this object as a JL planet.

HIP 47115 (2MASS J09360518-6457011). Wide binary with the HIP 47017 system in Volans/Crius 221; the far companion
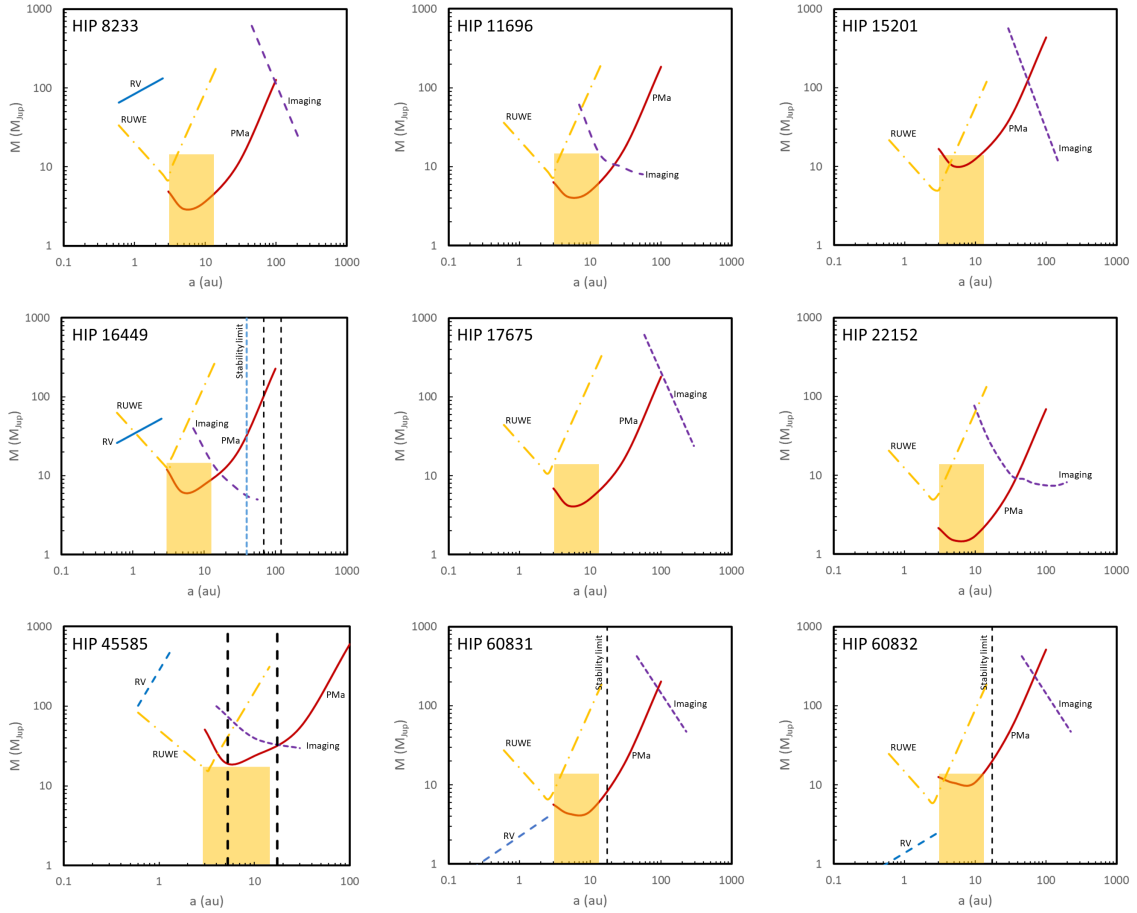
Fig. 14. Diagrams showing the mass of companions (in $M_{\rm Jup}$) that may be responsible for the observed proper motion anomaly (PMA) Kervella et al. (2022) as a function of semi-major axis a in au (solid red line) for the stars discussed individually in Sect. 4.1. They are compared with the upper limits from imaging (short dashed violet line), RUWE (dash-dotted orange line) and RVs (dashed blue line). The area marked in orange is that occupied by JL-planets. When the star has debris disks, the vertical black dashed lines mark their position, and the vertical blue dashed line the stability limit. First row, from left to right: HIP 8233 in Tuc-Hor, HIP 11696 in AB Dor, HIP 15201 in Carina; second row; HIP 16449, HIP 17675 and HIP 22152 in Columba; third row: HIP 45585 in Carina Near, and HIP 60831 and HIP 60832 in Carina Near

(itself a ternary system) is at a projected separation of about 40 000 au. HIP 47115 was observed with NACO[9] in the L'-band (Program 091.C-0154) on April 14, 2013. Since data are unpublished, we downloaded them from the ESO archive and found that they show the presence of a stellar companion with $\Delta L' = 2.18 \pm 0.04$ mag at 1.053 ± 0.006 arcsec (projected separation of 89 au) and PA = 169.3 ± 0.3 degree. This companion should then be a G6V star with a mass of 0.97 $M_\odot$. This object is very likely responsible for the observed PMa. In fact its PA agrees very well with that of the PMa (172.2 ± 9.6 degree), as expected for long periods, and its mass is larger by only a factor of two than that expected for an object responsible for the PMa at the observed separation, that is a reasonable agreement given the approximations considered by Kervella et al. (2022). The star also has a debris disk with $T_{\rm eff} = 190$ K (Cotten & Song 2016) that corresponds to a distance of about 7 au from the star. This is at the limit of the stability region due to the stellar companion (that however can be further from the star than its projected separation). We conclude that our analysis rejects a JL planet as responsible for the PMa for this star.

HIP 60831 (HD 108574, 2MASS J12280445+4447394). Northern member of Carina Near with a mass of 1.15 $M_\odot$. It is a wide companion of HIP 60832, with a projected separation of 440 au. High precision RV data obtained with the SARG high resolution spectrograph at the Italian Telescopio Nazionale *Galileo* (TNG) by our group are available (Carolo et al. 2011). They do not show any significant periodicity or trend over four years time span and have an r.m.s. of about 20 m s^{-1} compatible with the expected jitter. The stellar companion cannot be responsible for the PMa because this is much larger than expected for the large separation and directed towards a different direction – in fact we expect that for very long periods, the PMa be directed towards the object responsible for it. The stability limit leaves only a JL solution for the companion responsible of the PMa.

HIP 60832 (HD 108575, 2MASS J12280480+4447305). Northern member of Carina Near with a mass of 1.04 $M_\odot$. It is a wide companion of HIP 60831. The stellar companion cannot be responsible for the PMa because this is much larger than expected for the large separation and directed towards a different direction - in fact we expect that for very long periods, the PMa be directed towards the object responsible for it. High precision RV data from SARG (Carolo et al. 2011) and Elodie are available. They do not show any any significant periodicity or trend over four years time span and have an r.m.s. of about 20 m s^{-1}

---

[9] Nasmyth Adaptive Optics System (NAOS) – Near-Infrared Imager and Spectrograph (CONICA) at the ESO Very Large Telescope.

Table 5. Masses and semi-major axis for candidate planets from PMa.

HIP	M_A ($M_\odot$)	M_B ($M_\odot$)	a (au)	Frac(JL)
11696	1.326	0.0048 ± 0.0030	7.68 ± 7.08	0.928
30314	1.067	0.0011 ± 0.0004	13.28 ± 13.93	0.507
560	1.413	0.0017 ± 0.0009	16.57 ± 15.78	0.596
10679	1.036	0.0054 ± 0.0030	5.74 ± 2.96	0.998
84586	2.234	0.0038 ± 0.0012	7.28 ± 4.28	0.984
88399	1.309	0.0043 ± 0.0026	7.02 ± 3.39	0.954
15201	1.391	0.0135 ± 0.0114	17.78 ± 12.87	0.634
45585	2.124	0.0176 ± 0.0084	6.85 ± 2.46	0.687
60831	1.166	0.0034 ± 0.0020	9.47 ± 3.90	0.940
60832	1.042	0.0074 ± 0.0029	9.27 ± 3.84	1.000
16449	1.762	0.0056 ± 0.0052	12.54 ± 10.06	0.780
17675	1.445	0.0097 ± 0.0099	24.09 ± 19.02	0.467
22152	1.221	0.0012 ± 0.0006	17.11 ± 15.72	0.452
1481	1.129	0.0016 ± 0.0011	14.17 ± 14.98	0.585
8233	1.431	0.0052 ± 0.0060	22.07 ± 18.26	0.444
52462	0.833	0.0007 ± 0.0003	14.64 ± 14.98	0.187
96334	1.000	0.0037 ± 0.0023	6.15 ± 3.77	0.935

compatible with the expected jitter. The stability limit leaves only a JL solution for the companion responsible of the PMa.

Summarising, among these ten stars there is clear indication for the presence of a JL companion in six and a weak one (the object may either be a planet or a small mass star) for three, while our reduction of unpublished data revealed that for the last object the companion is stellar. Nine candidates are then remaining.

In Table 5 we give masses and semimajor axis derived in a uniform way for all the candidate JL planets suggested by PMa. The procedure we followed is similar to the Monte Carlo one described in Sect. 4.2; however we considered here that stars with significant PMa but not significant RUWE and RV variation (as it is the case for all the ones considered here) should have semimajor axis $1 < a < 300$ au. We also considered the upper limits due to HCI, whenever available, as well as stability limits indicated by other companions and the presence of debris disks. The best values and the error bars are the mean and standard deviation of the solutions compatible with the observational data. In the last column of this table we report the fraction of the solutions compatible with observational data that correspond to JL planets. Here we assumed that JL planets are those planets that have $3 < a < 20$ au and a mass $< 20 \, M_{\rm Jup}$. This fraction actually depends on the assumed distributions of a and q in the Monte Carlo approach. Here we assumed uniform distributions in the logarithm of a and q. In 13 out of 17 cases this fraction is higher than 0.5, and for three others higher than 0.4. The lower fraction is for HIP 52462, where however most of the solutions are at masses below 1 $M_{\rm Jup}$, that is, they are still giant planets not far from the snow line.

On the other hand, we notice that in addition to false positive (objects with significant PMa but no real JL planet) we should also consider the presence of false negatives (stars hosting planets but that do not have a significant PMa, such as 51 Eri and β Pic). We do not know how many false negatives are present in our sample. Our approach is to consider that all the seventeen PMa candidates considered here are indeed JL planets. Overall, the fraction of stars hosting only uncertain planet over the total of 24 is limited (~12%) and should not change much the discussion. We further notice that in total our list includes

29 companions with mass $M \leq 0.020 \, M_\odot$ and separation larger than 1 au because more than one planet has been detected around some stars.

4.2. Statistics of JL planets

Table 6 gives the frequency of JL planets around the various associations. To derive this number we first considered the stars that have values of the PMa in the catalogue of Kervella et al. (2022). This is a subset of the stars that are in the HIPPARCOS catalogue because for a few of them there is no astrometric solution in the *Gaia* DR3 catalogue. These few stars are likely binaries with large residuals in the astrometric solution. Likely most of these objects cannot have a JL planet in stable orbit because of the presence of massive nearby companions. We considered a total of 175 stars with this PMa available.

We then used the information about companions more massive than JL planets collected in the previous section to examine the possible stability of the orbits of JL planets. To this purpose we first estimated the inner and outer radii of the instability regions around these companions using the formulation by Holman & Wiegert (1999). We assumed here an orbit eccentricity given by Eq. (1) in Gratton et al. (2023a). Driven by the results obtained this way, we assumed that the orbit of a JL planets would be unstable around any star for which $a_{\rm max} > 1.5$ au or $a_{\rm min} < 20$ au. Here, $a_{\rm min}$ and $a_{\rm max}$ are the inner and outer edges of the region where orbits are unstable due to the perturbations by a companion. We found a total of 121 stars (that is 69% of the total) with PMa values that passed this criterion.

We found in the literature detection of JL planets through HCI around seven of these stars. In addition, we found additional systems where there is dynamical indication for the presence of a JL planet, in most cases from PMa (we considered meaningful those cases where $S/N({\rm PMA}) > 3$). After culling cases in which the PMa can be attributed to other known companions, we finally have a total of 17 additional objects that likely are JL companions. So, in total there is indication of the presence of JL companions around 24 stars, that is $20 \pm 4\%$ of the stars that might potentially have a JL planet.

Most of the JL planets are detected using the PMa, with a few additional ones coming from HCI. However, only a fraction of the JL planets can be detected using existing data. This is clearly shown in Fig. 15 that shows the stars found hosting with JL planets and those where there was no detection in the distance vs age and distance vs mass of the primary planes. Only stars with PMA measures are plotted; data for the remaining stars are too incomplete, and in fact there was no detection around them. In both panels, crosses mark stars that have stellar/BD companions that make the orbits of JL planets unstable. Detected planets are mainly around the closest, youngest, and most massive primaries. Distance is the most relevant parameter: while JL planets are found around 19 out of the 66 stars with distance lower than 50 pc where their orbits are stable, the similar fraction for stars beyond 50 pc is five out of 55. In addition, detected planets are generally massive, in most cases with a mass larger than 3 $M_{\rm Jup}$; only a fraction of the JL planets is expected to be so massive. The fraction of planets that can be detected this way depends on the limiting mass $M_{\rm min,i}$ for this technique, that on turn depends on many factors, mainly distance from the Sun. An approximate value for this limiting mass for each star is given by the mass corresponding to a $S/N({\rm PMa}) = 3$ at a separation in the range of JL planets given in the tables by Kervella et al. (2022). We considered here an average of the values at 5 and 10 au, that should

Table 6. Frequency of JL planets.

Association	Stars PMA	Stable	Fraction stable	Detected JL comp	Dyn	Total JL comp	$N_{\rm eff}$	Freq.
AB Dor	35	21	0.60	1	1	2	8.41	0.24 ± 0.16
Argus	15	15	1.00	1		1	2.65	0.38 ± 0.38
BPMG	22	15	0.68	3	4	7	5.18	1.35 ± 0.37
Carina	12	9	0.75	1	2	3	2.03	1.48 ± 0.70
Carina Near	15	10	0.67		2	2	3.42	0.58 ± 0.37
Columba	30	21	0.70	2	3	5	6.11	0.82 ± 0.32
Tuc-Hor	30	18	0.60		2	2	7.36	0.27 ± 0.18
Volans/Crius 221	20	10	0.50		2	2	6.61	0.30 ± 0.19
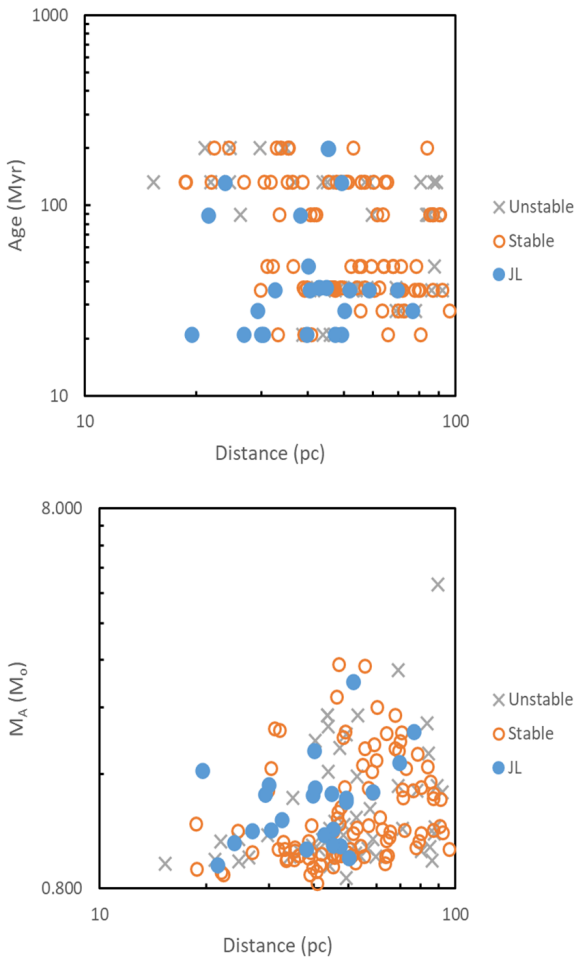
Fig. 15. Diagrams showing the stars found hosting with JL planets (blue filled circles) and those where there was no detection (open orange circles) in the distance vs. age (upper panel) and distance vs. mass of the primary (lower panel) planes. Only stars with PMA measures are plotted. In both panels, crosses mark stars that have stellar/BD companions that make the orbits of JL planets unstable.

Fig. 16. Frequency of stars hosting JL planets (corrected for completeness) in individual associations as a function of age. Blue dots are associations with a total mass <100 $M_\odot$; orange squares are associations with a total mass >100 $M_\odot$. The open square represents the frequency of stars hosting JL planets from the RV surveys. We arbitrarily assumed an age of 4 Gyr as typical for the stars in these surveys.

the quantity:

$$N_{\rm eff} = \sum \frac{\int_{M_{\rm min,i}}^{13} f(m)\,{\rm d}m}{\int_{1}^{13} f(m)\,{\rm d}m}, \tag{3}$$

where the index i refers to each star and m is in units of $M_{\rm Jup}$. $N_{\rm eff}$ represents the effective number of stars around which JL planets could be found with the PMa technique for each association. We assumed this is also the number of stars where we could detect JL planets including HCI too.

Summing all associations, in total we have $N_{\rm eff} = 41.77$. So our estimate of the frequency of stars hosting JL planets in these association is $24/N_{\rm eff} = 0.57 \pm 0.11$. This frequency is much higher than that obtained from RV surveys. It is however lower than that obtained for the case of the BPMG by Gratton et al. (2023a). We also notice that for some of the associations, the nominal value of the frequency of JL planets is >1, though never in a statistically significant way. This may happen because in the actual realisation of the extraction of companions from the mass distribution, they may have randomly masses larger than the average value when the sample is small.

In order to better explore this point, we plotted in Figs. 16 and 17 the runs of the frequency of JL planets for each individual associations as a function of age and mass.

We obtain trends for decreasing frequency of JL planets with increasing age and mass. These trends are suggestive of

be representative for JL planets. We then considered the fraction of JL planets around each star that are expected to be above this limiting mass. This depends on the assumed mass function $f(m)$ for JL planets. We adopted a mass function that is a power law with a slope of -1.3 as proposed by Adams et al. (2021), the same considered in Gratton et al. (2023a). We then call $N_{\rm eff}$
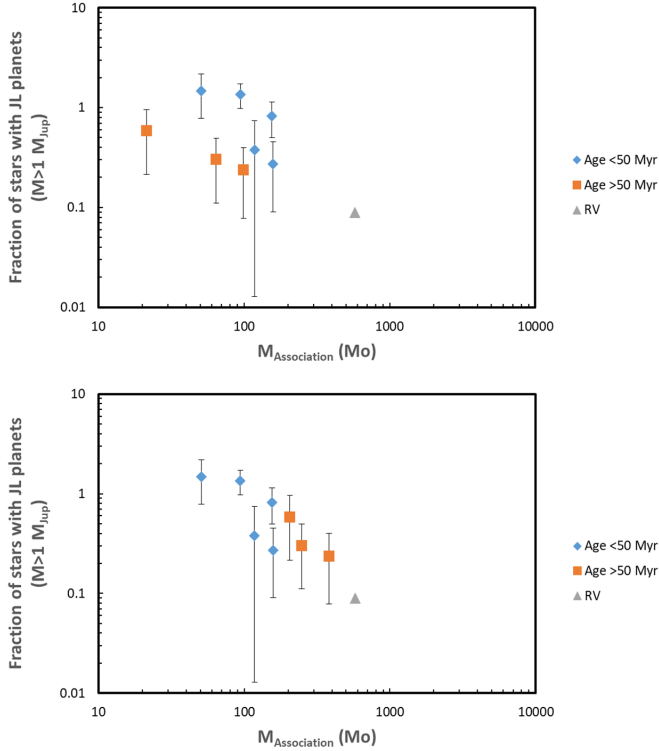
Fig. 17. Frequency of stars hosting JL planets (corrected for completeness) in individual associations as a function of association mass. Upper panel: masses as obtained by summing the mass of the member stars. Bottom panel: masses corrected for the selection along the galactic Y coordinate. Blue dots are associations with an age <50 Myr; orange squares are associations with a total mass >50 Myr. The open triangle represents the frequency of stars hosting JL planets from the RV surveys. We arbitrarily assumed a mass of 1000 $M_\odot$ for the typical birthplace of stars in these surveys.

real physical effects, that are even more obvious when compared to the results from RV surveys that refers to stars several Gyr old (we assumed an age of 4 Gyr in the plot) and likely mostly formed in rich groups with thousands of stars or more (we assumed a typical value of 1000 $M_\odot$ in the plot).

To quantify these hints, we obtained the best relation through the observed points in the frequency f of JL planets vs. mass m (in $M_\odot$) plane. We did not consider the results obtained from RV surveys, because of their very different meaning. The best fit is:

$$\log f = -(0.05 \pm 0.05) - (0.70 \pm 0.27)(\log m - 2.0) \quad (4)$$

The trend with mass is then significant at about 2.6σ. The reduced χ^2 value is 1.69. If we assume higher masses by a factor of two for the associations with ages > 50 Myr (AB Dor, Carina Near, and Volans/Crius 221) as proposed in Sect. 2.1.4 we obtain the equation:

$$\log f = (0.02 \pm 0.03) - (1.01 \pm 0.14)(\log m - 2.0). \quad (5)$$

The trend is now highly significant at 7.5σ and the reduced χ^2 value is 2.78.

The best relation through the observed points in the frequency f vs. age t (in Myr) plane is:

$$\log f = -(0.69 \pm 0.13) - (0.37 \pm 0.07)(\log t - 2.0). \quad (6)$$

The trend with age is then significant at about 5.1σ and the reduced χ^2 value is 0.87. However, the dependence of the frequency of JL planets on age may be in part an artefact of

observational biases because detection with direct imaging is easier for very young system. We then repeated the analysis but only considering those detections obtained through dynamics, that are insensitive to age. The planets around β Pic, 51 Eri, and κ And are only detected in imaging, the S/N of the PMa being <3 and should then be dropped from the analysis. In this case, the best fit when higher masses are considered for the older association is:

$$\log f = -(0.54 \pm 0.14) - (0.38 \pm 0.07)(\log t - 2.0). \quad (7)$$

The trend in age would still be significant (at 4.0σ) and the reduced χ^2 value is 0.86.

However, it is possible that there is some correlation between age and mass and that the trend with age is an artefact of this. We then further explored a possible linear combination of the dependencies on age and mass. In this case, the best relation is:

$$\log f = -(0.10 \pm 0.14) - (0.78 \pm 0.30)(\log m - 2.0)$$
$$-(0.21 \pm 0.27)(\log t - 2.0). \quad (8)$$

The reduced χ^2 value is now 0.62. We notice that the trend with mass is still significant at more than 2.5σ, while that on age is not larger than its error bar.

We conclude that the frequency of JL planets in young associations is much higher than obtained from RV surveys and that it depends on the total mass and possibly the age of the association. However data are not enough to precisely determine these dependencies.

4.3. Hot planets

As mentioned in Sect. 2.5, around the stars considered in this paper there is no known hot-Jupiter, a hot-Neptune transiting DS Tuc A (5.6 ± 0.2 $R_{\rm Earth}$, period 8.1 d, and mass <0.0453 $M_{\rm Jup}$, that is <14 $M_{\rm Earth}$: Newton et al. 2019; Benatti et al. 2019) in the Tuc-Hor moving group, and a mini-Neptune around HIP 94235 ($3.00^{+0.32}_{-0.28}$ $R_{\rm Earth}$, period 7.7 d: Zhou et al. 2022) in the AB Dor moving group. The mass is not available for this last planet. It is not possible to draw firm conclusions about the frequency of these classes of objects in the sample from such sparse detections. However, we may add a few comments here.

We first have to discuss the detection efficiency. Mayor et al. (2011) estimated that there is a 70–80% probability that any hot-Jupiter would have been detected if present with high-precision RV series (available for 79 stars, 28% of the stars surveyed). According to Fernandes et al. (2023) they would almost certainly be detected by TESS if transiting (2-minute cadence data available for 248 stars, 91% of the stars surveyed), though transits are expected for about 1/10 of the hot Jupiters or less (depending on the period distribution). No detection over this sample is then not inconsistent with the overall frequency of hot Jupiters. In fact, Wright et al. (2012) estimated an overall frequency of $1.20 \pm 0.38\%$ for solar-type stars. More recently, Zhou et al. (2019) found lower occurrence rates of $0.26 \pm 0.11\%$ for A stars, $0.43 \pm 0.15\%$ for F-stars, and $0.71 \pm 0.31\%$ for G-stars.

For what concerns the hot-Neptunes, they are very difficult to detect using RV in very active stars such as those considered here; even the TESS search is likely incomplete for this reason. The frequency of hot planets in 31 young clusters and associations with a median age of 45–50 Myr (including some of those considered in this paper) is discussed in Fernandes et al. (2022, 2023) who found a frequency of $90 \pm 37\%$ of sub-Neptunes/Neptunes (1.8–6 $R_{\rm Earth}$) with orbital periods less than

12.5 days for the stars for which they could compute stellar properties. This frequency is higher than *Kepler*'s Gyr old occurrence rate of $6.8 \pm 0.3\%$ even when accounting for evaporated sub-Neptunes (Bergsten et al. 2022).

When comparing this occurrence rates with those for older populations, we should consider that young hot planets are likely inflated (Benatti et al. 2019) and then of smaller mass than indicated by their radius when using standard relations such as that by Otegi et al. (2020). For instance, in the case of DS Tuc b the radius corresponding to the upper limit of the mass ($<14\ M_{\rm Earth}$) is 3.7 $R_{\rm Earth}$ using the appropriate relation by Otegi et al. (2020), while the observed radius is $5.6 \pm 0.2\ R_{\rm Earth}$. The mass of the mini-Neptune around HIP 94235 is not known, but it may well be below 10 $M_{\rm Earth}$.

We may then notice that Kunimoto & Bryson (2021) obtained an analytic form for the distribution of (mainly old) planets with mass and periods combining *Kepler* transits and results from RV surveys. Using their equations, we derive an expected occurrence frequency of 24% for planets with mass between 10 and 60 $M_{\rm Earth}$ and period less than 20 days. Considering the caveat given above, this value is well consistent with the current determination for young associations.

5. Discussion

5.1. Understanding the properties of stellar binaries in young associations

5.1.1. Comparison with binary formation model

In order to discuss the properties of the stellar companions found around the stars in young associations, we considered the same toy model considered by Gratton et al. (2023b) for the binaries around B-stars in the Sco-Cen associations. As in that case, we may assume that this distribution mainly reflects the characteristics of binary systems at birth. The toy model considered by Gratton et al. (2023b) is essentially similar to that formulated by Tokovinin & Moe (2020) and it is appropriate to describe the formation of binaries by disk fragmentation. In this toy model the complex physics of binary formation is described by several distribution function whose parameters may be determined by matching the observed binary distribution with predictions by the models. Gratton et al. (2023b) considered six different parameters: the total number $n_{\rm max}$ of accretion events onto the disk; the exponent α of the power-law of the mass of accreting events on the disk; the minimum $d_{\rm min}$ and maximum $d_{\rm max}$ radii of the disk; the exponent μ giving the relevance of outward migration; and the parameter β of the relative accretion of secondary and primary. A Monte Carlo procedure was devised to select which values of the parameters allows a good fit between computed and observed distributions. The comparison was done only considering the closest companion to the star that have $a < 1000$ au, because widest binaries likely formed by other mechanism (cloud fragmentation). Gratton et al. (2023b) found that only two of the model parameters really constrain the observed distributions: the exponent μ of the power-law of the mass of accreting events on the disk; and the parameter β giving the relevance of outward migration. These parameters have been found to be systematically different for early and late-B stars in Sco-Cen.

The comparison (see Fig. 18) is made using maps of the smoothed distribution of companions in the $a - q$ plane; these maps were obtained replacing the point relative to each companion with a Gaussian distribution with a sigma equal to

Table 7. Best parameters for the toy model.

Parameter	Prior range	All
$n_{\rm max}$	[20, 60]	37 ± 10
α	[−1.0, 1.0]	-0.01 ± 0.19
$d_{\rm min}$ (au)	[30, 100]	62 ± 18
$d_{\rm max}$ (au)	[200, 1200]	750 ± 297
μ	[0.5, 2.0]	1.40 ± 0.13
β	[0.0, 1.0]	0.61 ± 0.27

0.2 dex. The upper panels of Fig. 18 show the maps we obtained in this way considering only the closest companions for our sample of 141 binary systems. This smoothed distribution is then compared with analogue distributions obtained using the model. For each set of parameters $n_{\rm max}$, μ, α, $d_{\rm min}$, $d_{\rm max}$, and β, we run the model 2000 times, each time simulating the evolution of 10 000 systems, to define with a reasonable accuracy the distribution of companions. With these data we constructed maps of distributions in the $\log a - \log q$ plane, after applying the same smoothing to observing data. Once normalised to the total populations, we may compare these model maps with the observed ones and define a suitable goodness of fit parameter; in practice, we considered the mean quadratic residual between models and observation r. We considered acceptable those cases giving the best 1% of the values of r. We assumed that the average values for each parameter over the acceptable solutions is its best guess and the σ is its uncertainty.

Table 7 gives the result of our analysis. Notice that this model produces a fraction of single stars of 41%, close to the observed value of $<48 \pm 3\%$. When compared to the results obtained by Gratton et al. (2023b) for the B-stars in the Sco-Cen association, it should be considered that the typical mass of the stars considered in this paper is much lower than that of the B-stars, with a typical value of 1.04 $M_{\odot}$. This is to be compared with typical values of about 2.43 $M_{\odot}$ for the late-B stars and about 7.25 $M_{\odot}$ for the early ones. We found that the properties of the companions of the solar-type stars in young associations yield higher values of α and μ than those of the B-stars (see Fig. 19). The trend of α with mass implies that many episodes with similar accreted mass are needed for lower mass stars. This is illustrated by Fig. 20 that shows the run of the mass accreted from the interstellar matter to the disk with episode of accretion for the best fit parameters of the toy model for the formation of binaries by disk instability appropriate for early-B ($M_A = 7.25\ M_{\odot}$), late-B ($M_A = 2.43\ M_{\odot}$), and solar-type stars ($M_A = 1.04\ M_{\odot}$). This run of the accretion onto the disk makes the probability of secondary formation in the early events for massive stars very high, which explains the very high frequency of binaries observed. This agrees very well with the concept that disk fragmentation is more efficient around massive stars because of the larger value of the accretion rate from the natal cloud and the larger expected disk-to-star mass ratio during early phases of formation, when binaries are likely to form (Machida et al. 2010; Kratter & Lodato 2016; Elbakyan et al. 2023). Binary that formed so early are much more likely to become close binaries due to migration and nearly equal mass binaries due to selective accretion than those formed later. The trend of μ with mass implies that inward migration is more pronounced in most massive binaries; this again can be due to the very large initial disk mass. On the other hand, less massive binaries should have only a small prevalence of inward with respect to outward migration. This agrees with the rather large value for the median semi-major axis of the binaries.
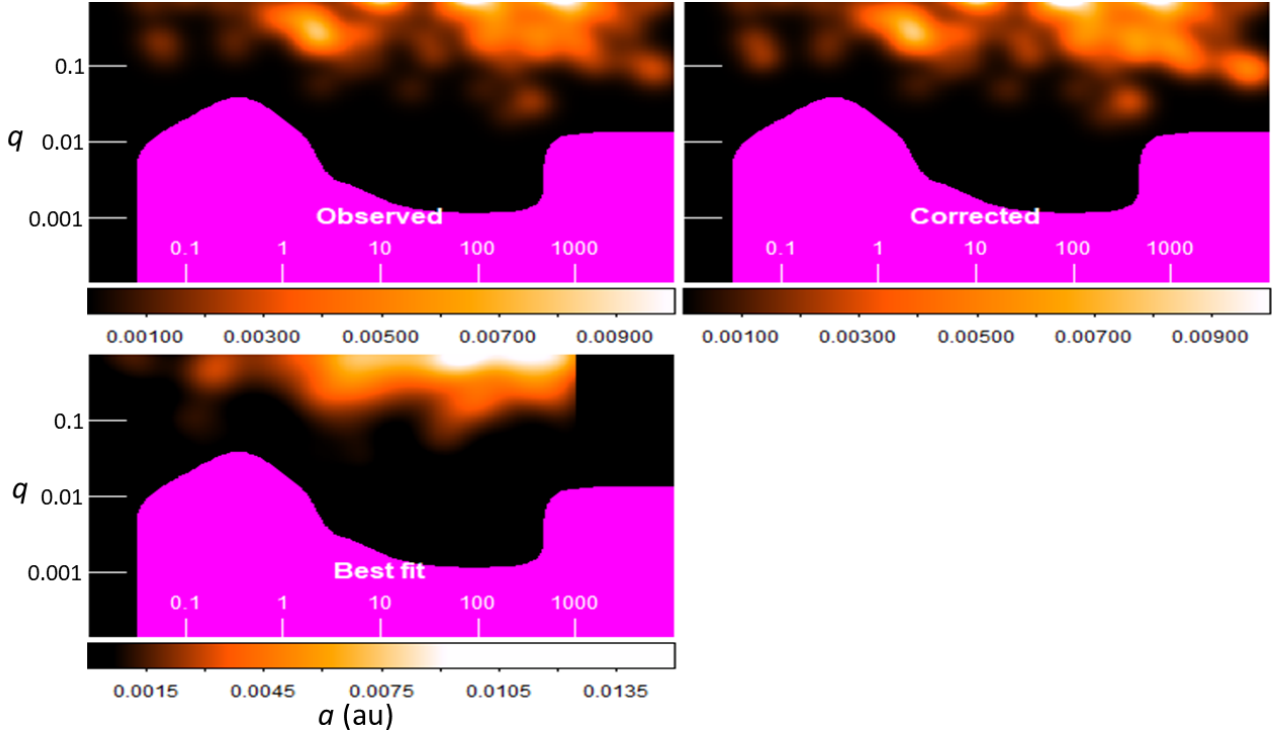
Fig. 18. Comparison between observed (upper left panel), corrected for completeness (upper right panel) and model (bottom panel) maps of the smoothed distribution of companions in the separation (in au) vs. mass ratio plane. We consider here the maps obtained considering only the closest companion, for consistency between the models and the observations. The magenta area marks the region with completeness <0.2, not used in the analysis.

In this picture, low-mass companions (BDs) may originate due to a disk instability occurring in the very late episodes of accretion from the interstellar matter onto the disk, and then have no chance to further accrete mass and become a stellar companion. This is clearly shown in Fig. 21 that shows the run of the final mass ratio q of a binary with episode of accretion for the best fit parameters of the toy model for the formation of binaries by disk instability appropriate for solar-type stars. BDs should be rare because the disk-to-star mass ratio and hence the probability of the onset of the instability is typically low in these late phases. In the model example shown above that produces a fraction of 59% of multiples stars, only 1.2% of the stars have a BD companion ($M_B < 0.075\ M_\odot$), at a median separation of 90 au from the star. The fraction of BD companions expected to be detected by RV surveys is even lower; those with semi-major axis $a < 10$ au is only 0.27%. This agrees with the upper limit of 0.6% for the frequency of BD companions around Sun-like stars obtained by Sahlmann et al. (2011).

We conclude that a simple model of disk fragmentation such as the one we are considering allows to describe the main statistical properties of the observed distribution of those systems within 1000 au from the star. This model generally produces stellar companions, though in rare case massive BDs can be produced.

5.1.2. Comparison between the distribution at large separations with that for free floating objects

Companions at separation farther than 500–1000 au are expected to form through instabilities in star-forming clouds. It is then expected that they have a different mass distribution from companions forming in the disk around primaries because in the last case the onset of the instability requires a larger minimum mass that is proportional to the stellar mass. Rather, it is expected that the mass function of these far companions resembles that of objects formed in isolation. We may test if this occurs for our sample.

The median mass of the 62 stellar and BD companions with semi-major axis $a > 500$ au is 0.528 $M_\odot$, that is very close to the value of 0.512 $M_\odot$ obtained for the 124 closer companions. The same result is obtained if we only consider companions with separation larger than 1000 au or even 10 000 au. That is, in our sample there is no obvious trend of the mass of the stellar companions with separation.

For comparison, using data by Luhman (2022) we estimate that approximately 4750/6000 ~ 79% of the stars of Sco-Cen are in the mass range $0.072 < M < 0.5\ M_\odot$. This last result agrees with the expectation for the Chabrier (2003, 2005) IMF's. If we then use this IMF and the detection efficiency of *Gaia* for these companions (see Fig. 10), we find that the frequency of objects in this mass range should be 70% in our sample, much more than the $50 \pm 6\%$ observed. This indicates that there are less low-mass objects among far companions to the solar-type stars in these young associations than expected with the Chabrier (2003, 2005) IMF's and observed for free-floating objects in Sco-Cen.

This result is quite unexpected and might signal that a large fraction of the far stellar companions of stars in young associations formed within the disk and were lately ejected towards larger separations. Alternatively, it might indicate that a large fraction of the substellar and low mass objects found in the field originated in multiple systems and it was later lost to the general field (see Miret-Roig 2023; Miret-Roig et al. 2022 for similar conclusions). This is indeed a more palatable choice, given the higher typical density of the environments where most of the

Fig. 20. Run of the mass accreted from the interstellar matter to the disk with the episode of accretion for the best-fit parameters of the toy model for the formation of binaries by disk instability appropriate for early-B ($M_A = 7.25\ M_\odot$), late-B ($M_A = 2.43\ M_\odot$), and solar-type stars ($M_A = 1.04\ M_\odot$).

Fig. 21. Run of the final mass ratio q of a binary with the episode of accretion where they formed for the best-fit parameters of the toy model for the formation of binaries by disk instability appropriate for solar-type stars ($M_A = 1.04\ M_\odot$).

Fig. 19. Upper panel: run of the toy-model parameter α (exponent of the power-law of the mass of accreting events on the disk) as a function of the mass of the primaries M_A from this paper and Gratton et al. (2023b). A lower value means that early episodes are more powerful. Lower panel: same for the toy-model parameter μ (relevance of outward migration). A lower value means that outward migration is more relevant

field stars likely formed. As for the case of the JL frequency discussed below, the young associations would then have characteristics that are more similar to those reproduced in model computations than the general field.

5.2. Dependence of JL planet frequency on the mass and age of the association

As discussed in Gratton et al. (2023a), the higher frequency of JL planets in young associations with respect to that obtained from RV surveys may have different explanations. The frequency of giant planets is known to depend on stellar mass and metallicity (see e.g. Sozzetti et al. 2009; Johnson et al. 2010; Santos et al. 2011; Mortier et al. 2012; Barbato et al. 2019). However, the metallicity of the young associations is roughly solar (Viana Almeida et al. 2009; Biazzo et al. 2012; Barenfeld et al. 2013; Baratella et al. 2020) and the average mass of the stars considered within young associations (1.04 $M_\odot$) is only mildly larger than that of the Sun. Hence the mass and metallicity dependencies are not likely to be the main reason of the observed difference. Rather, the dependencies on mass of the associations

and on their age suggests that more JL form in smaller star forming regions, likely because of the presence of less disturbing neighbours, and that perhaps they are lost from the stars as the associations age.

This suggests that in absence of disturbance by other stars, the natural outcome of the evolution of a protoplanetary disk is the formation of JL planets. They are not very frequent as given by this prediction because most stars do not form in isolation. As reviewed by Parker (2020), there are essentially three density regimes that pose a threat to planetary system formation and evolution. In the presence of massive stars (and then, depending on the overall mass of the association), far ultraviolet (FUV) and extreme ultraviolet (EUV) radiation can affect protoplanetary disks at stellar densities as low as 10 $M_\odot$ pc^{-3}. At stellar densities greater than 100 $M_\odot$ pc^{-3}, planetary orbits can be altered (which can include changes to the orbital eccentricity, inclination and semimajor axis of individual planets). At higher densities still (greater than 1000 $M_\odot$ pc^{-3}) protoplanetary disks can be physically truncated by encounters.

In addition, the associations considered in this paper are also young while the RV surveys target old stars with ages of billions of years. In the long run (hundreds of million to billions of years) a fraction of the planetary systems may be destabilised by close passage of other stars. In the following subsections we will consider separately these two mechanisms.

5.2.1. Impact of nearby massive stars on the formation of JL planets

In the core accretion scenario (Pollack et al. 1996; Ida & Lin 2004; Mordasini et al. 2009), the disk must survive for at least a few million of years in order to form giant planets. According to the planet formation simulations by Mordasini et al. (2012) there should be virtually no giant planet around solar mass stars if the disk lifetime is shorter than 1.5 Myr, while they may be present around 30–40% of the stars for lifetimes of 5 Myr.

Environment has likely a big impact for disk survival through various mechanism. The lifetime of disks is limited by encounters (around more massive stars) and photo-evaporation (around low-mass stars, $M < 0.5$ $M_\odot$) by nearby massive stars. Various authors considered the impact of these effects (Adams & Myers 2001; Adams et al. 2004; Winter et al. 2018, 2022; Parker et al. 2021; Concha-Ramírez et al. 2021; Wright et al. 2022). Adams & Myers (2001) proposed that encounters potentially disruptive of Solar Systems are frequent for very young clusters with an initial population larger than 1000 stars, while there should be virtually no effect if the population is as low as 100 stars. Winter et al. (2018) found a canonical threshold for the local stellar density ($n \geq 10^4$ pc^{-3}, that is however much larger than typical of associations, Wright et al. 2022) for which encounters can play a significant role in shaping the distribution of protoplanetary disk radii over a time-scale of about 3 Myr. Concha-Ramírez et al. (2021) simulated the effects of photo-evaporation and estimated that a local stellar density lower than 100 stars pc^{-2} is necessary for disks massive enough to form planets to survive for 2.0 Myr. In their simulations there is an order of magnitude difference in the disk masses in regions of projected density 100 versus 10^4 stars pc^{-2}. This agrees with observations. In fact, surveys of protoplanetary disks in star-forming regions show that disks closer to bright stars are less massive and more compact than their counterparts in sparser regions (Mann & Williams 2009; Fang et al. 2012; Mann et al. 2014; Ansdell et al. 2017; van Terwisga et al. 2020).

We now briefly investigate how many massive disk-enemy stars exists in these associations. The mass function of the primaries for mass higher than 0.8 $M_\odot$ is well reproduced by a Salpeter mass function (slope of -2.24). However, there are few massive stars. In total there are 16 B-stars with a mass $M >$ 2.4 $M_\odot$; this is to be compared with a total of about 1300 stars and an overall mass of about 1000 $M_\odot$ summing all the associations considered in this paper together. According to data available, the maximum mass of a star in these associations (the precursor of the massive WD GD50 in the AB Dor moving group, Gagné et al. 2018b) is 7.8 $M_\odot$ and there are only three additional stars above 5 $M_\odot$. The frequency of B-stars (mass >2.4 $M_\odot$: $1.2 \pm 0.3\%$) is lower than that observed in the Sco-Cen association, where there are 182 B-stars over about 6000 stars (about $3.0 \pm 0.2\%$) and 54 of them (about 30%) with a primary more massive than 5 $M_\odot$ (Gratton et al. 2023b). The most massive star in Sco-Cen might have been the precursor of PSR J1932+1059 with a mass of possibly 50 $M_\odot$ (Hoogerwerf et al. 2001).

As a typical high density environment, we may consider the Orion Nebula Cluster. The total mass in stars is about 1800 $M_\odot$ (Hillenbrand & Hartmann 1998) and there are some 1750 members (Da Rio et al. 2012). Hillenbrand & Hartmann (1998) estimated that the core radius of the cluster is 0.16-0.21 pc and that the central stellar density approaches 2×10^4 stars pc^{-3}. There are 40 stars more massive than 5 $M_\odot$ (Pflamm-Altenburg & Kroupa 2006) and the maximum stellar mass is of 45.7 $M_\odot$.

There is a large difference in the high-mass content of the nearby young moving groups and the Orion Nebula Cluster. While the total mass is comparable to the sum of all nearby young associations, the number of massive stars and the mass of the most massive star are an order of magnitude larger. B-stars are about 1% of the stars in the young moving groups, 3% in Sco-Cen, and about 7% in the Orion Nebula Cluster.

We may obtain a rough estimate of the relative impact of B-stars on disks around other stars in the same forming region considering the frequency of B-stars over the total number of stars and the density of stars in each environment. Initial density of the associations is not known. For very young systems, Parker (2014) used the presence of structures to estimate this quantity, and gave values of 10 000 $M_\odot$ pc^{-3} for the Orion Nebula Cluster and 1000 $M_\odot$ pc^{-3} for Upper Scorpius (that we may assume to be representative of the whole Sco-Cen association). No value is available for the associations considered in this paper because they are too old for the application of this method. However, the low frequency of B-stars may suggests that at birth these associations looked similar to Tau or CrA, that according to Parker (2014) have densities of a few tens $M_\odot$ pc^{-3}. We further assume that the impact scales down with the square of the typical distance from a B-star. We then obtain that the impact of the B-stars is 340 times higher in the Orion Nebula Cluster with respect that in nearby young moving groups, with the Sco-Cen association in between (a factor of about 30 higher). While this estimate is very rough, we may conclude that the nearby young moving groups are quiet environments where disk evolution can proceed rather undisturbed by nearby stars while the Orion Nebula Cluster is an hostile environment where extended disks are rapidly destroyed (see also the discussion in Parker 2020 and references therein). Interestingly, in star-forming regions where massive stars are present, there are very few detections of gas in protoplanetary disks (Ansdell et al. 2017; Mann et al. 2014, 2015) suggesting that they were subject to intense photoevaporation.

On the other hand, RV surveys average over a wide range of environments. Most stars in the disk of our Galaxy likely formed in regions similar to the Sco-Cen association or the Orion Nebula Cluster. Miller & Scalo (1978) estimated that about 20% of the stars should form in T-associations (that evolve into the young moving groups such as those considered in this paper), about 60% in more massive OB-associations (most massive stars with a mass >10 $M_\odot$), 10% in R-associations (most massive stars in the range 3–10 $M_\odot$), and the remaining 10% in open clusters (see also Lamers & Gieles 2006). Lada & Lada (2003) spell that the vast majority (90%) of stars that form in embedded clusters form in rich clusters of 100 or more members with masses in excess of 50 $M_\odot$, and embedded clusters account for a significant (70–90%) fraction of all stars formed in giant molecular clouds.

Most of these environments are hostile to long-term survival of disks. Depending on the actual fraction of stars that formed in such hostile environments, the fraction of stars hosting JL planets in RV surveys may well be much lower than observed in the nearby young moving groups.

5.2.2. Loss of JL planets

The possible dependence of the frequency of JL planets on age suggests that solar-like system may be disrupted on a typical timescale of the order of several hundred million years even in the low density environments of associations. Taken at face value, Eq. (8) indicates that about 50% of the JL companions are lost in the first 200 Myr, that is the range covered by our sample, but this value is highly uncertain and it is not yet sure that this

dependence on age really exists. In this section we considered various mechanisms that may cause disruption of these systems.

The associations considered here probably had densities of the order of a few tens star/pc^3 at birth but the density rapidly drops due to expansion. Using formulas by Maraboli et al. (2023) we found that close encounters with single stars are by far too rare for these young associations to produce ejection of single planets. Even considering close encounters with binaries, that have much larger cross sections, only a tiny fraction of single JL planets are lost in such low density environments as the young associations considered here (Li et al. 2020a). However, even a passage at moderate separation can perturb enough the orbits in a multiple packed planetary system to produce ejection of some planet though in general we do not expect ejection of a strict Jupiter analogue unless the passage is very close (a few tens au, see Cai et al. 2017; Flammini Dotti et al. 2019; Li et al. 2019, 2020b). If we limit ourselves to the stars with imaging detections, two out of seven of the planetary systems are rather packed (β Pic and especially HR 8799) and can possibly become unstable as a consequence of a close passage (Götberg et al. 2016; Zurlo et al. 2022). This data is likely incomplete and suggests that this evolution is possible for a fraction of systems.

Alternatively, we can consider the effect of wide stellar companions. We already considered as unstable all solar-like systems for which the inner radius of the unstable region due to a stellar companion is $a_{max} < 20$ au. This practically means that orbits of all JL planets in systems where there is a stellar companion with $a < 185$ au are considered unstable. This roughly corresponds to the separation where the characteristics of the planet population in binary systems begins to be statistically different from that of single stars (Desidera & Barbieri 2007). In addition, we should consider the disruptive effect of long-term instability that may be induced by the presence of far stellar companions. Kaib et al. (2013) considered the disruptive effect of the galactic tidal field on solar-like systems residing in wide binaries (separations greater than 1000 au). They found that between a third to a half of the solar-like systems residing in wide binaries are disrupted over a timescale of a few hundred million of years, that is indeed the timescale we are interested in. In our sample, about 25% of the stars have a similar wide companion. We then expect that about 10% of the original JL planets can be lost due to the presence of far stellar companions.

We conclude that the combination of the perturbations induced by wide binaries whose orbits are modified by the galactic tidal field and of close encounters of packed planetary systems with multiple stars may possibly produce an age dependence of the frequency of JL planets, but that the expected depletion is only some 10–20% over the age range 20–200 Myr covered by the associations considered in this paper.

6. Conclusions

To discuss the mechanisms of formation of companions (both stellar and substellar) to solar-type stars ($M > 0.8\ M_\odot$), we have presented an analysis of the existing data for eight nearby (distance < 100 pc) young (age < 200 Myr) associations. The limits in distance and age are important because completeness rapidly declines for further and older associations. In total the sample includes 296 stars in 280 systems. Data clearly indicate two separate populations of companions; a massive sequence (stellar binaries, but also massive BDs) with mass ratios $q > 0.05$ covering the whole range of separation surveyed here, and a low-mass sequence ($q < 0.015$) that is concentrated at the semi-major axis $1 < a < 100$ au (JL planets). There is an empty region

separating these two groups: this region is the BD desert (Marcy & Butler 2000). We tentatively identified the first sequence as the product of disk fragmentation, mainly in the very early phases of disk evolution, and the second one as the product of the core accretion mechanism that requires long-living disks.

Once survey completeness was considered, we found that both groups of companions are very frequent around solar-type stars in these young associations. The survey for stellar companions is almost complete. Only 48 ± 4% of the stars are single in our analysis; this value is likely overestimated by a few per cent because our search is not complete. The distribution of the companions in the separation mass ratio plane can be reproduced well within the framework of disk fragmentation. To explain the observations, the parameters used in the model have a trend with stellar mass corresponding to a few, massive episodes of accretion from the interstellar matter onto the disk in B stars, and a more uniform and prolonged accretion over time for solar-type stars. This agrees with expectations. In addition, inward migration is much more efficient in early B stars, a fact that can be explained by the higher mass of the disks in the early phases.

Again, once detection limits are considered, we found that also JL companions are very frequent around stars in young associations, being present in 0.57 ± 0.11 of the stars that do not have stellar companions that make their orbit unstable. The frequency of JL seems to depend on the mass and possibly the age of the associations. This can be explained by a combination of lower formation rate in environments richer in early-type stars – that might photoionise the proto-planetary disk before formation of the JL planets – and of the destruction of planetary systems related to long-term dynamical instabilities – that more easily occur in systems with several giant planets.

Confirmation of this result might possibly be obtained in the near future both by exploiting the next release of *Gaia* data (foreseen in a couple of years from now) and with HCI with the Extremely Large Telescope (ELT, in a few more years). The longer high precision astrometric series provided by *Gaia* DR4 and the smaller inner working angle possible with ELT should allow for a much higher fraction of the JL planets to be discovered in young associations. Progress is also expected thanks to longer time series of high-precision RV.

Modelling the disk and multiple planetary system destruction by nearby stars may also provide a better understanding of the relevant processes. For what concerns disks, a systematic investigation of disk survival in different environments with, for example, ALMA is also very important. Some studies already exist (Ansdell et al. 2017; Mann et al. 2014, 2015). We then anticipate significant progress in the next few years.

References

Adams, F. C., & Myers, P. C. 2001, ApJ, 553, 744
Adams, F. C., Hollenbach, D., Laughlin, G., & Gorti, U. 2004, ApJ, 611, 360
Adams, F. C., Meyer, M. R., & Adams, A. D. 2021, ApJ, 909, 1
Alibert, Y., Mordasini, C., & Benz, W. 2011, A&A, 526, A63
Aller, K. M., Liu, M. C., Magnier, E. A., et al. 2016, ApJ, 821, 120
Ambartsumian, V. A. 1937, AZh, 14, 207
Ansdell, M., Williams, J. P., Manara, C. F., et al. 2017, AJ, 153, 240
Artigau, É., Gagné, J., Faherty, J., et al. 2015, ApJ, 806, 254
Asensio-Torres, R., Janson, M., Bonavita, M., et al. 2018, A&A, 619, A43
Asiain, R., Figueras, F., & Torra, J. 1999, A&A, 350, 434
Avvakumova, E. A., Malkov, O. Y., & Kniazev, A. Y. 2013, Astron. Nachr., 334, 860
Baraffe, I., Homeier, D., Allard, F., & Chabrier, G. 2015, A&A, 577, A42
Baratella, M., D'Orazi, V., Carraro, G., et al. 2020, A&A, 634, A34
Barbato, D., Sozzetti, A., Biazzo, K., et al. 2019, A&A, 621, A110
Barenfeld, S. A., Bubar, E. J., Mamajek, E. E., & Young, P. A. 2013, ApJ, 766, 6
Barrado y Navascués, D., Stauffer, J. R., & Jayawardhana, R. 2004, ApJ, 614, 386
Bell, C. P. M., Mamajek, E. E., & Naylor, T. 2015, MNRAS, 454, 593
Belokurov, V., Penoyre, Z., Oh, S., et al. 2020, MNRAS, 496, 1922
Benatti, S., Nardiello, D., Malavolta, L., et al. 2019, A&A, 630, A81
Bergsten, G. J., Pascucci, I., Mulders, G. D., Fernandes, R. B., & Koskinen, T. T. 2022, AJ, 164, 190
Best, W. M. J., Liu, M. C., Magnier, E. A., & Dupuy, T. J. 2020, AJ, 159, 257
Biazzo, K., D'Orazi, V., Desidera, S., et al. 2012, MNRAS, 427, 2905
Biller, B. A., Close, L. M., Masciadri, E., et al. 2007, ApJS, 173, 143
Binks, A. S., & Jeffries, R. D. 2014, MNRAS, 438, L11
Binney, J., & Tremaine, S. 1987, Galactic Dynamics (Princeton, NJ: Princeton University Press)
Bitsch, B., Lambrechts, M., & Johansen, A. 2015, A&A, 582, A112
Bonavita, M., Desidera, S., Thalmann, C., et al. 2016, A&A, 593, A38
Bonavita, M., Gratton, R., Desidera, S., et al. 2022a, A&A, 663, A144
Bonavita, M., Fontanive, C., Gratton, R., et al. 2022b, MNRAS, 513, 5588
Booth, M., del Burgo, C., & Hambaryan, V. V. 2021, MNRAS, 500, 5552
Boss, A. P. 1997, Science, 276, 1836
Bovy, J. 2015, ApJS, 216, 29
Bowler, B. P., Liu, M. C., Shkolnik, E. L., et al. 2012, ApJ, 753, 142
Bowler, B. P., Liu, M. C., Mawet, D., et al. 2017, AJ, 153, 18
Brandeker, A., & Cataldi, G. 2019, A&A, 621, A86
Brandeker, A., Jayawardhana, R., Khavari, P., Haisch, Karl E., J., & Mardones, D. 2006, ApJ, 652, 1572
Brandt, T. D., McElwain, M. W., Turner, E. L., et al. 2014, ApJ, 794, 159
Brems, S. S., Kürster, M., Trifonov, T., Reffert, S., & Quirrenbach, A. 2019, A&A, 632, A37
Bryan, M. L., Knutson, H. A., Howard, A. W., et al. 2016, ApJ, 821, 89
Burn, R., Schlecker, M., Mordasini, C., et al. 2021, A&A, 656, A72
Butler, R. P., Vogt, S. S., Laughlin, G., et al. 2017, AJ, 153, 208
Cai, M. X., Kouwenhoven, M. B. N., Portegies Zwart, S. F., & Spurzem, R. 2017, MNRAS, 470, 4337
Carolo, E., Desidera, S., Gratton, R., et al. 2011, IAU Symp., 276, 403
Carson, J., Thalmann, C., Janson, M., et al. 2013, ApJ, 763, L32
Chabrier, G. 2003, PASP, 115, 763
Chabrier, G. 2005, Astrophys. Space Sci. Lib., 327, 41
Chauvin, G., Lagrange, A. M., Zuckerman, B., et al. 2005, A&A, 438, L29
Chauvin, G., Lagrange, A. M., Bonavita, M., et al. 2010, A&A, 509, A52
Chen, C. H., Mittal, T., Kuchner, M., et al. 2014, ApJS, 211, 25
Clarke, C. J. 2012, IAU Symp., 282, 409
Concha-Ramírez, F., Wilhelm, M. J. C., Portegies Zwart, S., van Terwisga, S. E., & Hacar, A. 2021, MNRAS, 501, 1782
Cotten, T. H., & Song, I. 2016, ApJS, 225, 15
Couture, D., Gagné, J., & Doyon, R. 2023, ApJ, 946, 6
Cumming, A., Butler, R. P., Marcy, G. W., et al. 2008, PASP, 120, 531
Currie, T., Brandt, G. M., Brandt, T. D., et al. 2023, Science, 380, 198
Cutri, R. M., Skrutskie, M. F., van Dyk, S., et al. 2003, VizieR Online Data Catalog: II/246
Cvetković, Z. 2011, AJ, 141, 116
Dahlqvist, C. H., Milli, J., Absil, O., et al. 2022, A&A, 666, A33
Da Rio, N., Robberto, M., Hillenbrand, L. A., Henning, T., & Stassun, K. G. 2012, ApJ, 748, 14
Delorme, P., Gagné, J., Girard, J. H., et al. 2013, A&A, 553, L5
De Rosa, R. J., Patience, J., Wilson, P. A., et al. 2014, MNRAS, 437, 1216
De Rosa, R. J., Nielsen, E. L., Wang, J. J., et al. 2020, AJ, 159, 1
De Rosa, R. J., Nielsen, E. L., Wahhaj, Z., et al. 2023, A&A, 672, A94

De Silva, G. M., D'Orazi, V., Melo, C., et al. 2013, MNRAS, 431, 1005
Desidera, S., & Barbieri, M. 2007, A&A, 462, 345
Desrochers, M.-E., Artigau, É., Gagné, J., et al. 2018, ApJ, 852, 55
Dinnbier, F., Kroupa, P., Šubr, L., & Jeřábková, T. 2022, ApJ, 925, 214
Elbakyan, V. G., Nayakshin, S., Meyer, D. M. A., & Vorobyov, E. I. 2023, MNRAS, 518, 791
Elliott, P., Huélamo, N., Bouy, H., et al. 2015, A&A, 580, A88
Elliott, P., Bayo, A., Melo, C. H. F., et al. 2016, A&A, 590, A13
ESA 1997, The HIPPARCOS and Tycho Catalogues. Astrometric and Photometric Star Catalogues Derived from the ESA HIPPARCOS Space Astrometry Mission (Noordwijk, Netherlands: ESA Publications Division) ESA Special Publication, 1200
Esposito, T. M., Kalas, P., Fitzgerald, M. P., et al. 2020, AJ, 160, 24
Faherty, J. K., Bochanski, J. J., Gagné, J., et al. 2018, ApJ, 863, 91
Fang, M., van Boekel, R., King, R. R., et al. 2012, A&A, 539, A119
Fekel, F. C., Tomkin, J., & Williamson, M. H. 2009, AJ, 137, 3900
Fernandes, R. B., Mulders, G. D., Pascucci, I., Mordasini, C., & Emsenhuber, A. 2019, ApJ, 874, 81
Fernandes, R. B., Mulders, G. D., Pascucci, I., et al. 2022, AJ, 164, 78
Fernandes, R. B., Hardegree-Ullman, K. K., Pascucci, I., et al. 2023, AJ, 166, 175
Flammini Dotti, F., Kouwenhoven, M. B. N., Cai, M. X., & Spurzem, R. 2019, MNRAS, 489, 2280
Franson, K., Bowler, B. P., Zhou, Y., et al. 2023, ApJ, 950, L19
Gagné, J., Faherty, J. K., Cruz, K. L., et al. 2015, ApJS, 219, 33
Gagné, J., Faherty, J. K., & Mamajek, E. E. 2018a, ApJ, 865, 136
Gagné, J., Fontaine, G., Simon, A., & Faherty, J. K. 2018b, ApJ, 861, L13
Gagné, J., Mamajek, E. E., Malo, L., et al. 2018c, ApJ, 856, 23
Gagné, J., Roy-Loubier, O., Faherty, J. K., Doyon, R., & Malo, L. 2018d, ApJ, 860, 43
Gaia Collaboration (Arenou, F., et al.) 2023a, A&A, 674, A34
Gaia Collaboration (Vallenari, A., et al.) 2023b, A&A, 674, A1
Galicher, R., Marois, C., Macintosh, B., et al. 2016, A&A, 594, A63
Gaposchkin, S. 1932, Die Bedeckungsveränderlichen (Berlin: Ferd. Dummlers verlagsbuchhandlung)
Gaudi, B. S. 2022, Astrophys. Space Sci. Lib., 466, 237
Gizis, J. E. 2002, ApJ, 575, 484
Gizis, J. E., Allers, K. N., Liu, M. C., et al. 2015, ApJ, 799, 203
Goldin, A., & Makarov, V. V. 2007, ApJS, 173, 137
Götberg, Y., Davies, M. B., Mustill, A. J., Johansen, A., & Church, R. P. 2016, A&A, 592, A147
Gould, A., Dong, S., Gaudi, B. S., et al. 2010, ApJ, 720, 1073
Grandjean, A., Lagrange, A. M., Keppler, M., et al. 2020, A&A, 633, A44
Grandjean, A., Lagrange, A. M., Meunier, N., et al. 2021, A&A, 650, A39
Grandjean, A., Lagrange, A. M., Meunier, N., et al. 2023, A&A, 669, A12
Gratton, R., Mesa, D., Bonavita, M., et al. 2023a, Nat. Commun., 14, 6232
Gratton, R., Squicciarini, V., Nascimbeni, V., et al. 2023b, A&A, 678, A93
Gratton, R., Bonavita, M., Mesa, D., et al. 2023c, A&A, submitted
Green, G. M., Schlafly, E., Zucker, C., Speagle, J. S., & Finkbeiner, D. 2019, ApJ, 887, 93
Hagelberg, J., Engler, N., Fontanive, C., et al. 2020, A&A, 643, A98
Hayashi, C. 1981, Prog. Theor. Phys. Suppl., 70, 35
Heggie, D. C. 1975, MNRAS, 173, 729
Hennebelle, P., & Falgarone, E. 2012, A&ARv, 20, 55
Heyer, M., & Dame, T. M. 2015, ARA&A, 53, 583
Higuchi, A. E., Kóspál, Á., Moór, A., Nomura, H., & Yamamoto, S. 2020, ApJ, 905, 122
Hillenbrand, L. A., & Hartmann, L. W. 1998, ApJ, 492, 540
Hirsch, L. A., Rosenthal, L., Fulton, B. J., et al. 2021, AJ, 161, 134
Holl, B., Sozzetti, A., Sahlmann, J., et al. 2023, A&A, 674, A10
Holman, M. J., & Wiegert, P. A. 1999, AJ, 117, 621
Hoogerwerf, R., de Bruijne, J. H. J., & de Zeeuw, P. T. 2001, A&A, 365, 49
Huélamo, N., Nürnberger, D. E. A., Ivanov, V. D., et al. 2010, A&A, 521, L54
Hwang, H.-C., Ting, Y.-S., & Zakamska, N. L. 2022, MNRAS, 512, 3383
Ida, S., & Lin, D. N. C. 2004, ApJ, 616, 567
IJspeert, L. W., Tkachenko, A., Johnston, C., et al. 2021, A&A, 652, A120
Janson, M., Durkan, S., Hippler, S., et al. 2017, A&A, 599, A70
Johnson, J. A., Aller, K. M., Howard, A. W., & Crepp, J. R. 2010, PASP, 122, 905
Kaczmarek, T., Olczak, C., & Pfalzner, S. 2011, A&A, 528, A144
Kaib, N. A., Raymond, S. N., & Duncan, M. 2013, Nature, 493, 381
Kennedy, G. M., & Kenyon, S. J. 2008, ApJ, 673, 502
Kennedy, G. M., & Wyatt, M. C. 2014, MNRAS, 444, 3164
Kerr, F. J., & Lynden-Bell, D. 1986, MNRAS, 221, 1023
Kerr, R., Kraus, A. L., Murphy, S. J., et al. 2022, ApJ, 941, 143
Kervella, P., Arenou, F., & Thévenin, F. 2022, A&A, 657, A7
Köhler, R., & Leinert, C. 1998, A&A, 331, 977
Köhler, R., Neuhäuser, R., Krämer, S., et al. 2008, A&A, 488, 997

Korzennik, S. G., Brown, T. M., Fischer, D. A., Nisenson, P., & Noyes, R. W. 2000, ApJ, 533, L147
Kratter, K., & Lodato, G. 2016, ARA&A, 54, 271
Kratter, K. M., Murray-Clay, R. A., & Youdin, A. N. 2010, ApJ, 710, 1375
Kunimoto, M., & Bryson, S. 2021, AJ, 161, 69
Lacour, S., Wang, J. J., Rodet, L., et al. 2021, A&A, 654, L2
Lada, C. J., & Lada, E. A. 2003, ARA&A, 41, 57
Lagrange, A. M., Gratadour, D., Chauvin, G., et al. 2009, A&A, 493, L21
Lagrange, A. M., Philipot, F., Rubini, P., et al. 2023, A&A, 677, A71
Lamers, H. J. G. L. M., & Gieles, M. 2006, A&A, 455, L17
Laughlin, G., Bodenheimer, P., & Adams, F. C. 2004, ApJ, 612, L73
Leinert, C., Zinnecker, H., Weitzel, N., et al. 1993, A&A, 278, 129
Li, D., Mustill, A. J., & Davies, M. B. 2019, MNRAS, 488, 1366
Li, D., Mustill, A. J., & Davies, M. B. 2020a, MNRAS, 499, 1212
Li, D., Mustill, A. J., & Davies, M. B. 2020b, MNRAS, 496, 1149
Lindegren, L., Hernández, J., Bombrun, A., et al. 2018, A&A, 616, A2
Liu, M. C., Magnier, E. A., Deacon, N. R., et al. 2013, ApJ, 777, L20
Liu, M. C., Dupuy, T. J., & Allers, K. N. 2016, ApJ, 833, 96
Luhman, K. L. 2022, AJ, 163, 24
Luyten, W. J. 1936, ApJ, 84, 85
Machida, M. N., Inutsuka, S.-i., & Matsumoto, T. 2010, ApJ, 724, 1006
Macintosh, B., Graham, J. R., Barman, T., et al. 2015, Science, 350, 64
Malo, L., Doyon, R., Feiden, G. A., et al. 2014, ApJ, 792, 37
Mann, R. K., & Williams, J. P. 2009, ApJ, 694, L36
Mann, R. K., Di Francesco, J., Johnstone, D., et al. 2014, ApJ, 784, 82
Mann, R. K., Andrews, S. M., Eisner, J. A., et al. 2015, ApJ, 802, 77
Maraboli, E., Mantegazza, F., & Lodato, G. 2023, Euro. Phys. J. Plus, 138, 152
Marcy, G. W., & Butler, R. P. 2000, PASP, 112, 137
Marois, C., Macintosh, B., Barman, T., et al. 2008, Science, 322, 1348
Marois, C., Zuckerman, B., Konopacky, Q. M., Macintosh, B., & Barman, T. 2010, Nature, 468, 1080
Martin, R. G., & Livio, M. 2012, MNRAS, 425, L6
Martin, R. G., & Livio, M. 2015, ApJ, 810, 105
Mason, B. D., Wycoff, G. L., Hartkopf, W. I., Douglass, G. G., & Worley, C. E. 2001, AJ, 122, 3466
Mayor, M., Marmier, M., Lovis, C., et al. 2011, arXiv e-prints [arXiv:1109.2497]
McCarthy, K., & Wilhelm, R. J. 2014, AJ, 148, 70
Mentuch, E., Brandeker, A., van Kerkwijk, M. H., Jayawardhana, R., & Hauschildt, P. H. 2008, ApJ, 689, 1127
Mesa, D., Marino, S., Bonavita, M., et al. 2021, MNRAS, 503, 1276
Mesa, D., Bonavita, M., Benatti, S., et al. 2022, A&A, 665, A73
Mesa, D., Gratton, R., Kervella, P., et al. 2023, A&A, 672, A93
Metchev, S. A., & Hillenbrand, L. A. 2009, ApJS, 181, 62
Miller, G. E., & Scalo, J. M. 1978, PASP, 90, 506
Miret-Roig, N. 2023, Ap&SS, 368, 17
Miret-Roig, N., Antoja, T., Romero-Gómez, M., & Figueras, F. 2018, A&A, 615, A51
Miret-Roig, N., Galli, P. A. B., Brandner, W., et al. 2020, A&A, 642, A179
Miret-Roig, N., Bouy, H., Raymond, S. N., et al. 2022, Nat. Astron., 6, 89
Moe, M., & Di Stefano, R. 2017, ApJS, 230, 15
Moór, A., Szabó, G. M., Kiss, L. L., et al. 2013, MNRAS, 435, 1376
Moranta, L., Gagné, J., Couture, D., & Faherty, J. K. 2022, ApJ, 939, 94
Mordasini, C., Alibert, Y., & Benz, W. 2009, A&A, 501, 1139
Mordasini, C., Alibert, Y., Benz, W., Klahr, H., & Henning, T. 2012, A&A, 541, A97
Mortier, A., Santos, N. C., Sozzetti, A., et al. 2012, A&A, 543, A45
Naud, M.-E., Artigau, É., Malo, L., et al. 2014, ApJ, 787, 5
Newton, E. R., Mann, A. W., Tofflemire, B. M., et al. 2019, ApJ, 880, L17
Nielsen, E. L., Liu, M. C., Wahhaj, Z., et al. 2013, ApJ, 776, 4
Nielsen, E. L., De Rosa, R. J., Macintosh, B., et al. 2019, AJ, 158, 13
Offner, S. S. R., Kratter, K. M., Matzner, C. D., Krumholz, M. R., & Klein, R. I. 2010, ApJ, 725, 1485
Offner, S. S. R., Dunham, M. M., Lee, K. I., Arce, H. G., & Fielding, D. B. 2016, ApJ, 827, L11
Otegi, J. F., Bouchy, F., & Helled, R. 2020, A&A, 634, A43
Parker, R. J. 2014, MNRAS, 445, 4037
Parker, R. J. 2020, R. Soc. Open Sci., 7, 201271
Parker, R. J., Alcock, H. L., Nicholson, R. B., Panić, O., & Goodwin, S. P. 2021, ApJ, 913, 95
Patience, J., King, R. R., De Rosa, R. J., et al. 2012, A&A, 540, A85
Pawellek, N., Wyatt, M., Matrà, L., Kennedy, G., & Yelverton, B. 2021, MNRAS, 502, 5390
Pearce, T. D., Launhardt, R., Ostermann, R., et al. 2022, A&A, 659, A135
Pecaut, M. J., & Mamajek, E. E. 2013, ApJS, 208, 9
Penoyre, Z., Belokurov, V., & Evans, W. 2021, AAS/Division of Dynamical Astron. Meeting, 53, 301.05
Perryman, M. A. C., Lindegren, L., Kovalevsky, J., et al. 1997, A&A, 323, L49

Pfalzner, S. 2013, A&A, 549, A82
Pfalzner, S., & Vincke, K. 2020, ApJ, 897, 60
Pflamm-Altenburg, J., & Kroupa, P. 2006, MNRAS, 373, 295
Podolak, M., & Zucker, S. 2004, Meteorit. Planet. Sci., 39, 1859
Poleski, R., Skowron, J., Mróz, P., et al. 2021, Acta Astron., 71, 1
Pollack, J. B., Hubickyj, O., Bodenheimer, P., et al. 1996, Icarus, 124, 62
Popinchalk, M., Faherty, J. K., Curtis, J. L., et al. 2023, ApJ, 945, 114
Pourbaix, D., Tokovinin, A. A., Batten, A. H., et al. 2004, A&A, 424, 727
Prša, A., Kochoska, A., Conroy, K. E., et al. 2022, ApJS, 258, 16
Raghavan, D., McAlister, H. A., Henry, T. J., et al. 2010, ApJS, 190, 1
Rameau, J., Chauvin, G., Lagrange, A. M., et al. 2013, A&A, 553, A60
Raymond, S. N., & Morbidelli, A. 2022, Astrophys. Space Sci. Lib., 466, 3
Raymond, S. N., Izidoro, A., & Morbidelli, A. 2020, in Planetary Astrobiology, eds. V. S. Meadows, G. N. Arney, B. E. Schmidt, & D. J. Des Marais (Tucson: University of Arizona Press), 287
Rosenthal, L. J., Knutson, H. A., Chachan, Y., et al. 2022, ApJS, 262, 1
Sahlmann, J., Ségransan, D., Queloz, D., et al. 2011, A&A, 525, A95
Salpeter, E. E. 1955, ApJ, 121, 161
Samland, M., Mollière, P., Bonnefoy, M., et al. 2017, A&A, 603, A57
Santos, N. C., Mayor, M., Bonfils, X., et al. 2011, A&A, 526, A112
Schneider, A. C., Cushing, M. C., Kirkpatrick, J. D., et al. 2014, AJ, 147, 34
Schneider, A. C., Windsor, J., Cushing, M. C., Kirkpatrick, J. D., & Shkolnik, E. L. 2017, AJ, 153, 196
Schneider, A. C., Shkolnik, E. L., Allers, K. N., et al. 2019, AJ, 157, 234
Schneider, A. C., Burgasser, A. J., Bruursema, J., et al. 2023, ApJ, 943, L16
Shkolnik, E. L., Allers, K. N., Kraus, A. L., Liu, M. C., & Flagg, L. 2017, AJ, 154, 69
Slawson, R. W., Prša, A., Welsh, W. F., et al. 2011, AJ, 142, 160
Sozzetti, A., Torres, G., Latham, D. W., et al. 2009, ApJ, 697, 544
Stahl, A. G., Johns-Krull, C. M., & Flagg, L. 2022, ApJ, 941, 101
Steinmetz, M., Matijevič, G., Enke, H., et al. 2020, AJ, 160, 82
Stevenson, A. T., Haswell, C. A., Barnes, J. R., & Barstow, J. K. 2023, MNRAS, 526, 5155
Stone, J. M., Skemer, A. J., Hinz, P. M., et al. 2018, AJ, 156, 286
Tal-Or, L., Trifonov, T., Zucker, S., Mazeh, T., & Zechmeister, M. 2019, MNRAS, 484, L8
Tohline, J. E. 2002, ARA&A, 40, 349
Tokovinin, A. 2018, ApJS, 235, 6
Tokovinin, A., & Moe, M. 2020, MNRAS, 491, 5158
Torres, C. A. O., Quast, G. R., Melo, C. H. F., & Sterzik, M. F. 2008, ASP Conf. Ser., 5, 757
Tran, Q. H., Bowler, B. P., Cochran, W. D., et al. 2021, AJ, 161, 173
Traven, G., Feltzing, S., Merle, T., et al. 2020, A&A, 638, A145
Trifonov, T., Tal-Or, L., Zechmeister, M., et al. 2020, A&A, 636, A74
Udry, S., Mayor, M., Naef, D., et al. 2000, A&A, 356, 590
Ujjwal, K., Kartha, S. S., Mathew, B., Manoj, P., & Narang, M. 2020, AJ, 159, 166
Unger, N., Ségransan, D., Barbato, D., et al. 2023, A&A, 680, A16
Uyama, T., Currie, T., Hori, Y., et al. 2020, AJ, 159, 40
van Terwisga, S. E., van Dishoeck, E. F., Mann, R. K., et al. 2020, A&A, 640, A27
Viana Almeida, P., Santos, N. C., Melo, C., et al. 2009, A&A, 501, 965
Vigan, A., Bonavita, M., Biller, B., et al. 2017, A&A, 603, A3
Vigan, A., Fontanive, C., Meyer, M., et al. 2021, A&A, 651, A72
Winter, A. J., Clarke, C. J., Rosotti, G., et al. 2018, MNRAS, 478, 2700
Winter, A. J., Haworth, T. J., Coleman, G. A. L., & Nayakshin, S. 2022, MNRAS, 515, 4287
Wittenmyer, R. A., Butler, R. P., Tinney, C. G., et al. 2016, ApJ, 819, 28
Wittenmyer, R. A., Clark, J. T., Zhao, J., et al. 2019, MNRAS, 484, 5859
Wolthoff, V., Reffert, S., Quirrenbach, A., et al. 2022, A&A, 661, A63
Wood, M., & Mann, A. 2023, Am. Astron. Soc. Meeting Abs., 55, 402.10
Wood, M. L., Mann, A. W., & Kraus, A. L. 2021, AJ, 162, 128
Wright, J. T., Marcy, G. W., Howard, A. W., et al. 2012, ApJ, 753, 160
Wright, N. J., Goodwin, S., Jeffries, R. D., Kounkel, M., & Zari, E. 2022, arXiv e-prints [arXiv:2203.10007]
Yuan, C. 1977, A&A, 58, 53
Zhang, Z., Liu, M. C., Best, W. M. J., Dupuy, T. J., & Siverd, R. J. 2021, ApJ, 911, 7
Zhou, G., Huang, C. X., Bakos, G. Á., et al. 2019, AJ, 158, 141
Zhou, G., Wirth, C. P., Huang, C. X., et al. 2022, AJ, 163, 289
Zhu, W. 2022, AJ, 164, 5
Zuckerman, B. 2019, ApJ, 870, 27
Zuckerman, B., Song, I., & Bessell, M. S. 2004, ApJ, 613, L65
Zuckerman, B., Bessell, M. S., Song, I., & Kim, S. 2006, ApJ, 649, L115
Zúñiga-Fernández, S., Bayo, A., Elliott, P., et al. 2021, A&A, 645, A30
Zurlo, A., Goździewski, K., Lazzoni, C., et al. 2022, A&A, 666, A133

Appendix A: Gaia RV jitter
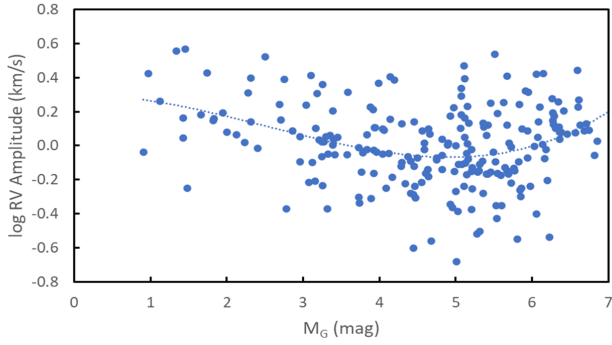
Fig. A.1. Run of the ratio between Gaia robust RV amplitude and its median value for each association with the absolute magnitude of the stars. Stars in the young associations considered in this paper and the Hyades are plotted. Only stars without any companion within 100 au are considered. The dashed line is a polynomial best fit through data.
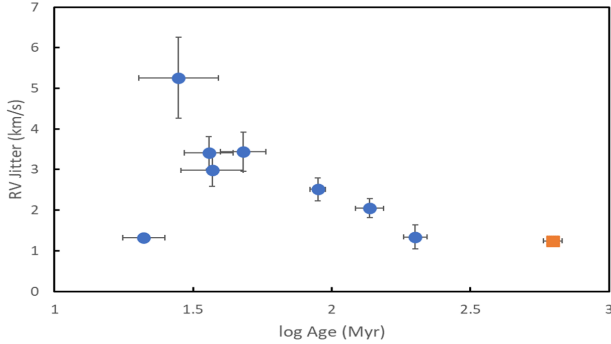
Fig. A.2. Run of the median Gaia robust RV amplitude with the age for young associations (blue filled symbols) and the Hyades (open red square). Only stars without any companion within 100 au are considered

The Gaia robust RV amplitude may signal a variation of the RV of the centre of mass of stars. However, this quantity is also influenced by activity and rotation. In order to consider it properly, these dependencies should be taken into account. In practice, we expect trends with the absolute magnitude and age of the stars. To show this, we constructed two plots. The first one (Figure A.1) shows the run of the ratio between Gaia robust RV amplitude and its median value for each association with absolute magnitude of the stars. Only stars without any companion within 100 au were considered. As expected, the faster rotation of the most luminous stars causes a higher value of the Gaia robust RV amplitude; however, also the less luminous stars considered in this paper (that is however limited to masses $> 0.8~M_\odot$) have on average a value of the Gaia robust RV amplitude higher than for stars with solar masses. Once this trend with magnitude is considered, we can derive median values of the Gaia robust RV amplitude for each different association and consider the trend with age. This is shown in Figure A.2. As expected, the median value of the Gaia robust RV amplitude decreases with age. However, the youngest association considered here, the BPMG, has a rather low value of the median Gaia robust RV amplitude.

In practice, we find that the expected value of the Gaia robust RV amplitude J (in km s^{-1}) for stars that should have constant RV may be represented by using the following relations:

$$J = 1.3 * f \tag{A.1}$$

if the age of the association t (in Myr) is higher than 300, and:

$$J = (1.7327 * \log t + 5.813) * f \tag{A.2}$$

if it is lower. The quantity f (in km s^{-1}) is given by:

$$\log f = 0.0068732 M_G^3 - 0.053288 M_G^2 + 0.028749 M_G + 0.25273 \tag{A.3}$$

where M_G is the stellar absolute magnitude in the Gaia $G-$band. The r.m.s. scatter around this relation is about 0.2 dex. We will adopt these relations as estimate of the jitter in Gaia RVs. We may consider as SBs those star deviating more than 2.5 σ from the mean value; that is, those stars with robust RV amplitude larger than 3.16J, that is roughly 11.3 and 5.8 km s^{-1} for solar type stars of 20 and 200 Myr, respectively.

Appendix B: About *RUWE*

In general, as discussed in Appendix D of Gratton et al. (2023b) there is a range of possible solutions compatible with any observed value of *RUWE*, defining a V-shaped area in the $\log a$ vs. $\log q$ plane. The projected semimajor axis corresponding to the maximum sensitivity of *RUWE* (that is the minimum mass of a secondary producing a given value of *RUWE*) is at about 2-3 au (depending on the primary mass), a value set by the length of the Gaia astrometric DR3 astrometric sequence (34 months); this is because a growing fraction of the astrometric trend is absorbed by the proper motion estimate for longer periods, producing smaller residuals around the best fit line (for this same reason we would expect even shorter periods in the case of Gaia DR2, as used by Wood et al. (2021)). Hence we expect that most binaries detected using *RUWE* have periods of a few years and separation of a few au, with a peak-to-valley range of about one order of magnitude around this value. Stars with *RUWE* > 1.4 should have periods that are systematically shorter than the stars with significant PMa (that typically have periods of decades corresponding to the time separation between Hipparcos and Gaia epochs), though there is some overlap between the two groups (that is, objects with both *RUWE* > 1.4 and S/N(PMa)> 3). This partial but not full overlap is indeed observed (see Gratton et al. 2023b), but there are several objects with large *RUWE* and low PMa and viz. There is also overlap with SB, that typically have shorter periods than those with significant *RUWE*. The plots of Figure 3 fully confirm our expectations. Rather, Wood et al. (2021) considered an empirical calibration of the *RUWE* values against high contrast and interferometric measurements of companions; this calibration (A. L. Kraus et al. 2021, in preparation) is still unpublished so we cannot use it. Typical separations for binaries with significant *RUWE* signals considered by Wood et al. (2021) are tens of au and then periods of several decades to a century. However, it is not fully clear that their empirical calibration provides an unbiased estimate of the appropriate parameters for binaries with significant *RUWE* signals because only companions far enough to be visually detected can be considered in a similar calibration. As a consequence, the separation of the companions may be systematically overestimated. This bias is for instance present when we consider the stars in our sample and in the Hyades. Over a whole sample of about 350 stars, 79 have *RUWE* > 1.4 and G > 5; a visual companion has been detected only for 30 of these stars. We can attribute the lack of detections for 49 of the high *RUWE* stars at least in part as due to companions that are closer than the sensitivity limit of visual observations. The median separation of the

30 visually detected companions among stars with high *RUWE* is 0.10 arcsec, that corresponds to a semi-major axis of 5 au for a typical distance of 50 pc. While still likely biased towards high separation, this is substantially less than the median value estimated by Wood et al. (2021) (see their Figure 6, that suggests a value around 0.2 arcsec for a sample of stars that often are more distant than the stars considered in our paper).

Appendix C: Companions of stars in young associations

This Appendix contains tables giving the relevant data about companions around the programme stars. Tables C.1 - C.8 contain the basic data for the members of the various moving groups (a table for each moving group). The first four columns contain the Hipparcos, HD, and 2MASS numbers as well as alternative names for each star. Column 5 gives the membership probability obtained using the Banyan-Σ code (Gagné et al. 2018c). Columns 6 and 7 give the coordinates. Column 8 the parallax. Whenever possible this was from Gaia DR3 Gaia Collaboration (2023b); else it was taken from Gaia DR2 or alternatively from the Hipparcos catalogue (ESA Publications Division 1997). Columns 9 and 10 give the Gaia G magnitude of the primary G_A and if existing of the secondary G_B, respectively. Column 11 gives the 2MASS K magnitude (Cutri et al. 2003). Columns 12 and 13 give the the absolute M_G magnitude of the primary and secondary (M_{GB}). Column 14 gives the absolute M_K magnitude of the primary.

Tables C.9 - C.16 explains if relevant information about binarity are available and Tables C.17 - C.24 give the data relevant (a table for each moving group). In these second group of tables, the first four columns are as described above. Column 5 gives the Gaia *RUWE* parameter; columns 6-10 give the Gaia mean RV, its error, the number of epochs considered in its derivation, the probability that variation around the mean value is due to random noise, and the robust RV amplitude. Columns 11 and 12 give the separation and position angle of visual companions. Column 13 gives the signal-to-noise ratio (S/N) of the Proper Motion anomaly (PMa) as given by Kervella et al. (2022).

Tables C.25 - C.32 give the derived values for the stars and their companions (a table for each moving group). The first four columns are as described above. Column 5 and 6 gives the mass of the primary and of companions. Here, mass of the primary is the mass of all components within the semimajor axis of the companion considered. Column 7 gives the semi-major axis a. Column 8 gives the mass ratio q. Column 9 gives the detection method: either visual binary VIS if the secondary was detected with some imaging mode and a separate magnitude could be obtained; or dynamical binary DYN if the secondary is only detected from the dynamical impact on the primary. Finally, Column 10 gives a reference appropriate for each object. In many cases this is a reference to a paper describing the detection and characterisation of the companions. In addition: Gaia means that the companion was detected as a separate entry in the Gaia catalogue; RUWE/RV/PMa and RUWE/RV means that the companion was detected from a high RUWE value (> 1.4), a high scatter in RV (> 10 km s^{-1}) or from a high S/N PMa (> 3). All available data were used to derive a consistent solution, using the method described in Gratton et al. (2023b).

Table C.1. Photometry of stars in the AB Dor moving group

HIP	HD	2MASS	Others/WDS	Prob	RA degree	Dec degree	π mas	G_A mag	G_B mag	K_A mag	M_G mag	M_{GB} mag	M_K mag
	1405	J00182085+3057224	PW And	99.0	4.5870	30.95615	35.43	8.512		6.387	6.259		4.134
3589	4277	J00455088+5458402	BD+54 144	99.3	11.46204	54.97783	20.61	7.627	9.927	6.361	4.197	6.497	2.931
5191	6569	J01062614-1417468		99.0	16.60897	-14.29642	21.99	9.226	13.714	7.340	5.938	10.426	4.052
6276		J01203226-1128035	BD-12 243	99.7	20.13445	-11.46770	28.33	8.234		6.549	5.495		3.810
	236717	J01242709+5751062		9.8	21.11297	57.85171	25.8598	8.384		6.754	5.447		3.817
		J02051802+5217027	TYC 3293-1912-1	63.3	31.32513	52.28408	12.9464	10.826		8.67	6.387		4.231
10272	13482	J02121535+2357298	J02123+2357AB	97.5	33.06421	23.95820	27.30	7.764	9.092	5.727	4.945	6.273	2.908
		J02223387+5033369	BD+49 646	98.6	35.64120	50.56026	19.0571	9.350		7.495	5.750		3.895
11696	15407A	J02305064+5532543		99.1	37.71107	55.54840	20.2679	6.855		5.835	3.389		2.369
							20.2679		9.55346			6.088	
12635	16760B	J02422094+3837212		97.8	40.58729	38.62254	20.27	9.924		7.762	6.458		4.296
12638	16760	J02422130+3837073	BD+37 604	88.6	40.58881	38.61868	17.57	8.565		7.033	4.789		3.257
							17.57		9.924			6.148	
13027	17332		J02475+1922AB	99.8	41.86426	19.37182	30.19	7.192	7.880		4.591	5.279	
13209	17573	J02495902+2715381	41 Ari	99.1	42.49597	27.26051	21.162	3.633		3.864	0.261		0.492
14684	19668	J03094227-0934463	IS Eri	98.8	47.42620	-9.57961	25.82	8.299		6.701	5.359		3.761
14809		J03111383+2224571	J03112+2225A	98.4	47.80767	22.41586	19.72	8.349	10.186	6.968	4.824	6.661	3.443
15353	20888	J03175907-6655367	J03180-6656A	98.9	49.49614	-66.92685	16.65	6.016	12.710	5.691	2.123	8.817	1.798
16563	21845	J03331347+4615269	V577 Per	99.7	53.30621	46.25737	27.48	8.016	10.496	6.368	5.211	7.691	3.563
			GD50		57.20912	-0.97556	32.22						
	24681	J03552040-0143451	TYC4718-894-1	99.3	58.83502	-1.72922	17.94	8.804		7.253	5.074		3.523
18859	25457	J04023675-0016078	HR 1249	99.8	60.65310	-0.26892	53.46	5.247		4.181	3.887		2.821
19183	25953	J04064153+0141020		99.1	61.67305	1.68391	17.52	7.707		6.582	3.925		2.800
19422	25665	J04093502+6932292		60.4	62.39600	69.54139	53.26	7.429		5.457	6.061		4.089
		J04213348-2543091	CD-26 1643	98	65.38946	-25.71925	18.3264	8.125		6.873	4.440		3.188
	28982	J04330622-2400477	EB	91.5	68.27587	-24.01330	18.3483	8.937		7.274	5.255		3.592
							18.3483		16.906187			13.224	
	31652	J04572232-0907595		35.1	74.34302	-9.13322	10.99	9.944		8.352	5.149		3.557
		J05023042-3959129	CD-40 1701	97.5	75.62678	-39.98695	18.11	10.339		8.050	6.629		4.340
		J05044132+4024003	TYC2899-1744-1	92.8	76.17217	40.40004	16.38	10.645		8.278	6.717		4.350
									14.810			10.882	
	32981	J05062769-1549303		68.9	76.61537	-15.82511	11.76	8.933		7.743	4.285		3.095
25647	36705	J05284484-6526551	AB Dor	99.5	82.18705	-65.44869	65.32	6.690		4.686	5.765		3.761
							65.32		11.354			10.429	
		J05350411-3417519	CD-34 2331	46.9	83.76713	-34.29777	11.62	11.511	16.293	9.122	6.838	11.620	4.449
26373	37572	J05365685-4757528	J05369-4758A	99.9	84.23689	-47.96469	40.66	7.550	9.294	5.811	5.596	7.339	3.857
26401	37551	J05372-4243AB	WX Col	87.5	84.30383	-42.71547	12.43	9.453	10.348		4.925	5.820	
							12.43		14.576			10.048	
			CP-19 878	34.9	84.84646	-19.55813	14.30	10.289			6.065		
		J06083386-3402549	CD-34 2676	10.3	92.14112	-34.04860	11.55	10.009		8.195	5.322		3.508
							11.55						
							11.55		12.456			7.769	
30314	45270	J06223097-6013072		99.9	95.62892	-60.21865	41.89	6.365		5.045	4.475		3.155
31711	48189	J06380036-6132001	HR 2468	0.1	99.50147	-61.53336	45.71	6.142		4.544	4.442		2.844
		J07305952-8419275	CD-84 80	96.8	112.74768	-84.32436	14.46	9.701	13.501	7.906	5.502	9.302	3.707
37855	64982	J07453559-7940080		67.3	116.39809	-79.66893	11.46	8.842		7.586	4.138		2.882
							11.46		11.695			6.991	
55746	99827	J11251773-8457164		29.3	171.32392	-84.95454	11.25	7.548		6.492	2.804		1.748
							11.25						
							11.25		19.894			15.150	
		J12361640-7931344	TYC 9420-68-1	89.2	189.06839	-79.52624	13.1547	10.788	11.262	8.708	6.383	6.790	4.303
		J12361110-7931384	TYC 9420-112-1	92.2	189.04626	-79.52732	12.75						
63742	113449	J13034967-0509423	J13038-0510AB	2.6	195.95689	-5.16181	48.88	7.431	12.472	5.509	5.877	10.918	3.955
80218	147512	J16223272-0414571		92.1	245.63634	-4.24925	37.16	7.162		5.622	5.012		3.472
82688	152555	J16540815-0420248		95.6	253.53393	-4.34018	22.13	7.685	13.924	6.363	4.410	10.649	3.088
	317617	J17285563-3243568		47.6	262.23172	-32.73245	17.57	9.350		7.669	5.574		3.893
									12.472			8.696	
93375	176367	J19010604-2842502		61.0	285.27518	-28.71401	15.28	8.374		7.151	4.295		3.072
94235	178085	J19105782-6016202		97.2	287.74104	-60.27220	17.06	8.173	13.773	6.881	4.333	9.933	3.041
95347	201919	J19235315-4036571	Alpha Sgr	80.5	290.97156	-40.61594	17.94	3.950		4.200	0.219		0.469
		J19330374+0345397	TYC0486-4943	20.6	293.26563	3.76103	14.23	10.805	12.649	8.656	6.572	8.416	4.423
		J20044935-0239203	BD-03 4778	36.4	301.20567	-2.65566	14.88	9.808	14.015	7.921	5.671	9.878	3.784
109268	209952	J22081397-4657393	Alpha Gru	99.4	332.05827	-46.96097	32.29	1.773		2.090	-0.682		-0.365
113579	217343	J23001929-2609135	J23005-2619C	93.1	345.08036	-26.15375	31.47	7.322		5.943	4.811		3.432
113597	217379	J23002791-2618431	J23005-2619AB	59.5	345.11647	-26.31189	32.74	9.556		6.267	7.131		3.842
									10.059			7.634	
114530	218860	J23115205-4508106		98.7	347.96689	-45.13629	20.93	8.606	12.472	7.032	5.210	9.076	3.636
115162		J23193955+4215098		94.9	349.91484	42.25273	19.49	8.767		7.224	5.216		3.673
115738	220825	J23265595+0115201	kap Psc	98.4	351.73315	1.25560	20.32	4.915		4.960	1.454		1.499
116910	222575	J23415428-3558397		64.7	355.47622	-35.97772	15.44	9.278		7.624	5.221		3.567
117452	223352	J23485554-2807490	delta Scl	98.3	357.23144	-28.13027	22.73	4.554		4.532	1.337		1.315
							22.73		8.835			5.618	
118008	224228	J23561067-3903086		99.9	359.04447	-39.05234	45.47	7.941		5.907	6.230		4.196

Table C.2. Photometry of stars in the Argus moving group

HIP	HD	2MASS	Others/WDS	Prob	RA	Dec	π	G_A	G_B	K_A	M_G	M_{GB}	M_K
					degree	degree	mas	mag	mag	mag	mag	mag	mag
7345	9672	J01343776-1540348	49 Cet	96.6	23.6574	-15.6764	16.84	5.611		5.458	1.743		1.590
		J05345923-2954041	CD-29 2360	99.3	83.7468	-29.9011	17.42	10.253		7.994	6.458		4.199
		J07015339-4227561	CD-42 2906	99.7	105.4725	-42.4656	11.37	10.412	14.28	8.648	5.691	9.559	3.927
		J07282203-4908377	CD-48 2972	99.9	112.0918	-49.1438	11.47	9.639		8.058	4.936		3.355
36312	59659	J07283006-4908589		99.9	112.1253	-49.1497	11.42	8.678	9.64	7.585	3.966	4.927	2.873
		J07311991-5447027	CPD-54 1295	98.1	112.8330	-54.7841	9.33	10.311	15.82	8.749	5.160	10.665	3.598
36948	61005	J07354747-3212141		99.9	113.9478	-32.2039	27.41	8.016		6.458	5.205		3.647
		J07472597-4902511	CD-48 3199	99.8	116.8582	-49.0475	8.75	10.401		8.840	5.112		3.551
		J07484982-4327055	CD-43 3604	98.5	117.2076	-43.4516	10.62	10.776	11.376	8.189	5.906	6.506	3.319
		J07541770-5711131	TYC8561-1051-1	97.8	118.5738	-57.1870	6.43	10.521	10.934	9.211	4.562	4.975	3.252
							6.43						
		J07535548-5710073	TYC 8561-0970-1	98.1	118.4812	-57.1687	6.43	11.466	15.798	9.670	5.507	9.839	3.741
							6.43	10.521	12.492		4.562	6.533	
		J08391155-5834281	CD-58 2194	98.9	129.7981	-58.5745	8.73	10.028		8.368	4.732		3.072
									18.337			13.041	
		J08500812-5745593	CD-57 2315	99.9	132.5338	-57.7665	10.27	10.211	10.511	7.960	5.268	5.568	3.017
		J09020394-5808497	TYC 8594-0058-1	99.1	135.5164	-58.1472	6.73	11.158		9.387	5.297		3.526
	CPD-62 1197	J09133027-6259092	GSC 08944-01516	98.5	138.3761	-62.9859	8.42	10.35		8.323	4.977		2.950
47135	84075	J09361783-7820417		99.9	144.0743	-78.3449	15.60	8.445		7.160	4.411		3.126
		J09395143-2134175	BD-20 2977	97.3	144.9643	-21.5715	11.27	10.11		8.376	5.370		3.636
		J09424742-7239499	TYC 9217-0641-1	81.0	145.6976	-72.6639	6.42	12.034		9.824	6.070		3.860
									18.24			12.276	
		J09471986-4003098	CD-39 5833	99.8	146.8327	-40.0527	9.71	10.522		8.881	5.457		3.816
	85151			99.7	147.1799	-44.9021	9.42	9.442	10.13		4.312	5.000	
	309851	J09555832-6721218		99.9	148.9930	-67.3561	9.28	9.617		8.312	4.454		3.149
50191	88955	J10144416-4207189	q Vel	98.7	153.6840	-42.1219	32.18	3.846		3.740	1.384		1.278
51194	90874	J10272528-6542167	HR 4115	99.5	156.8553	-65.7047	14.70	5.99		5.788	1.827		1.625
57013	101615	J11411978-4305442	HR4502	92.0	175.3325	-43.0957	15.61	5.53		5.442	1.501		1.409
									13.197			9.164	
57632	102647	J11490366+1434197	beta Leo	87.1	177.2649	14.5721	90.91	2.06		1.900	1.853		1.693
		J12063292-4247508	CD-42 7422	84.4	181.6372	-42.7975	8.98	10.49		8.579	5.254		3.347
	CD-74 673	J12203437-7539286	TYC 9412-1370-1	38.5	185.1432	-75.6580	16.03	10.15		7.927	6.176		3.952
	CD-75 652	J13491293-7549475	TYC 9426-682-1	99.9	207.3039	-75.8298	12.09	9.52	16.236	8.015	4.930	11.649	3.428
68994	123058	J14072929-6133441		99.7	211.8720	-61.5623	13.99	7.66		6.715	3.390		2.444
	129496	J14462144-6746158		99.6	221.5892	-67.7710	12.13	8.73		7.429	4.151		2.849
74405	133813	J15122343-7515156	NY Aps	99.9	228.0977	-75.2543	19.09	9.27		7.377	5.675		3.781
76736	138965	J15401155-7013403	HR5792	99.4	235.0481	-70.2279	12.72	6.43		6.268	1.949		1.791
79797	145689	J16170540-6756285	HR6037	99.9	244.2725	-67.9413	18.19	5.93		5.657	2.232		1.956
							18.19						
89925	168913	J18205694+2951317	HR6876, 108 Her	99.0	275.2374	29.8589	17.92	5.56		4.994	1.828		1.261
98103	188728	J19561425+1125254	phi Aql	90.3	299.0594	11.4237	14.75	5.27	13.59	5.257	1.116		1.101
												9.434	
							14.75		15.725			11.569	
98495	188228	J20003558-7254380	eps Pav	99.8	300.1481	-72.9105	31.04	3.96		3.800	1.423		1.260
99770	192640	J20143203+3648225	b03 Cyg	99.7	303.6335	36.8063	24.93	4.89		4.422	1.873		1.405

Table C.3. Photometry of stars in the BPMG

HIP	HD	2MASS	Others/WDS	Prob	RA degree	Dec degree	π mas	G_A mag	G_B mag	K_A mag	M_G mag	M_{GB} mag	M_K mag
560	203	J00065008-2306271		95.7	1.7087	-23.1075	25.16	6.094		5.240	3.098		2.244
		J01373940+1835332	TYC1208-468-1	76.6	24.4141	18.5924	18.95	10.032	10.181		6.420	6.569	
10679	14082B	J02172472+2844305		98.7	34.3531	28.7418	25.23	7.623		6.262	4.633		3.272
10680	14082	J02172527+2844423		99.3	34.3554	28.7450	25.28	6.904	7.623	5.787	3.918	4.637	2.801
11437		J02272924+3058246	AG Tri	99.4	36.8719	30.9735	24.42	9.744	11.434	7.080	6.683	8.373	4.019
21547	29391	J04373613-0228248	51 Eri	9.1	69.4006	-2.4735	33.44	5.141		4.537	2.762		2.158
							33.44	5.141	9.801	4.537	2.762	7.422	2.158
	286264	J05004928+1527006	V1841 Ori	99.7	75.2054	15.4502	18.83	10.362		7.637	6.736		4.011
25486	35850	J05270477-1154033	AF Lep	99.9	81.7698	-11.9010	37.25	6.210		4.926	4.066		2.782
27321	39060	J05471708-5103594	beta Pic	99.9	86.8212	-51.0665	51.44	3.823		3.480	2.380		2.040
							51.44	3.823		3.480	2.380		2.037
29964	45081	J06182824-7202416	AO Men	99.4	94.6175	-72.0448	25.57	9.273		6.814	6.312		3.853
76629		J15385757-5742273	V343 Nor	99.3	234.7398	-57.7076	25.83	7.677		5.852	4.738		2.913
							25.83		13.208			10.269	
		J17150362-2749397	TYC6820-0223-1	33.1	258.7650	-27.8277	12.00	10.092		8.054	5.488		3.450
84586	155555	J17172550-6657039		99.8	259.3563	-66.9510	32.95	6.461		4.702	4.050		2.291
							32.95	6.461	11.470	4.702	4.050	9.059	2.291
		J17295506-5415487	TYC8728-2262-1	97.4	262.4795	-54.2635	14.79	9.324		7.364	5.174		3.214
86598	160305	J17414903-5043279		99.0	265.4543	-50.7245	15.20	8.195		6.992	4.104		2.901
	161460	J17483374-5306433		85.6	267.1406	-53.1120	13.05	8.864		6.776	4.442		2.354
88399	164249	J18030341-5138564		99.8	270.7642	-51.6490	20.29	6.912		5.913	3.448		2.449
							20.29	6.912	12.313	5.913	3.448	8.849	2.449
88726	165189	J18064990-4325297	HR6749	95.5	271.7079	-43.4252	22.74	5.615	5.687	5.140	2.399	2.471	1.924
89829	168210	J18195221-2916327		93.2	274.9675	-29.2758	12.43	8.671		7.053	4.142		2.524
92024	172555	J18452691-6452165	HR7012	99.8	281.3621	-64.8713	32.95	4.725	8.887	4.298	2.314	6.476	1.887
		J18453704-6451460	CD-64 1208	72.0	281.4044	-64.8628	35.16	8.877	11.877	6.096	6.607		3.826
	173167	J18480637-6213470		99.5	282.0265	-62.2297	19.77	7.175		6.136	3.655		2.616
							19.77	7.175	11.125	6.136	3.655	7.605	2.616
92680	174429	J18530587-5010499	PZ Tel	97.4	283.2745	-50.1805	21.16	8.102		6.366	4.730		2.994
		"J19114467-2604085 "	TYC6878-195-1	92.4	287.9361	-26.0690	14.77	9.877		7.750	5.724		3.597
95261	181296	J19225122-5425263	eta Tel	99.5	290.7134	-54.4239	20.60	5.012	6.936	5.010	1.581		1.579
							20.60	5.012	6.936	5.010	1.581	3.505	1.579
95270	181327	J19225894-5432170		99.7	290.7456	-54.5380	20.93	6.936		5.910	3.540		2.514
98839	190102	J20041810-2619461		46.6	301.0754	-26.3295	21.11	8.023	13.691	6.627	4.645	10.295	3.249
99273	191089	"J20090521-2613265 "		99.2	302.2717	-26.2240	19.96	7.076		6.076	3.577		2.577
103311	199143	J20554767-1706509		97.1	313.9486	-17.1142	21.78	7.131		5.811	3.821		2.501
							21.78	7.131	9.911	5.811	3.821	6.601	2.501
							21.78	7.131	12.741	5.811	3.821	9.431	2.501
107620	207043	J21475527-5255502		97.5	326.9804	-52.9306	30.08	7.431		6.050	4.822		3.441

Table C.4. Photometry of stars in the Carina moving group

HIP	HD	2MASS	Others/WDS	Prob	RA degree	Dec degree	π mas	G_A mag	G_B mag	K_A mag	M_G mag	M_{GB} mag	M_K mag
15201	21024	J03155768-7723184	iot Hyi	58.5	48.9903	-77.3885	34.26	5.405		4.470	3.079		2.144
									13.855			11.529	
26144	37402	J05342614-6006151		99.6	83.6089	-60.1042	14.06	8.266		7.088	4.006		2.828
									14.132			9.872	
	42270	J05532917-8156532		97.4	88.3722	-81.9481	17.00	8.915	11.971	6.944	5.067	8.123	3.096
29314	43199	J06105289-6129594		96.4	92.7205	-61.4997	13.10	7.370		6.554	2.956		2.140
30034	44627	J06191291-5803156	AB Pic	99.6	94.8038	-58.0543	19.95	8.838		6.981	5.338		3.481
32235	49855	J06434625-7158356		99.9	100.9427	-71.9765	18.05	8.994		7.278	5.277		3.561
33737	55279	J07003046-7941459		99.9	105.1270	-79.6961	15.76	9.777		7.652	5.765		3.640
40916	70703	J08210046-5213406		99.0	125.2519	-52.2280	13.75	6.618		6.276	2.310		1.968
41081	71043	J08225514-5207254	HR 3300	99.8	125.7298	-52.1237	14.28	5.888		5.873	1.662		1.647
45585	80950	J09172755-7444045	HR 3721	97.5	139.3649	-74.7346	13.09	5.862		5.865	1.447		1.450
46063	81544	J09233498-6111359	V479 Car	99.8	140.8957	-61.1933	10.37	9.746		7.964	4.825		3.043
		J09303148-7041479	TYC 9200-446-1	72.2	142.6312	-70.6967	9.97	10.076		8.565	5.069		3.558
46720	83096	J09312500-7344496		98.7	142.8537	-73.7470	12.81	7.412	9.192	6.172	2.950	4.730	1.710
									13.904			9.442	
47391	83944	J09392101-6119410	m Car	68.4	144.8375	-61.3280	14.48	4.481		4.647	0.285		0.451
		J09534760-5453540	TYC 8602-718-1	42.7	148.4483	-54.8983	11.77	10.583		8.578	5.937		3.932
	298936	J10131476-5230540	TWA-21	99.8	153.3116	-52.5150	18.84	9.476		7.194	5.851		3.569
		J10300355-7432320	CD-73 584	96.5	157.5148	-74.5423	13.41	10.084		8.186	5.722		3.824

Table C.5. Photometry of stars in the Carina-Near moving group

HIP	HD	2MASS	Others/WDS	Prob	RA degree	Dec degree	π mas	G_A mag	G_B mag	K_A mag	M_G mag	M_{GB} mag	M_K mag
35564	57852	HIP35564	HR 2814	99.9	110.08926	-52.31152	28.63	5.899			3.183		
									6.464			3.748	
	57853								6.464		3.748		
36414	59704	J07293141-3807217		98.7	112.38089	-38.12266	18.87	7.613		6.442	3.991		2.820
37563	62850	J07423606-5917507		99.9	115.65025	-59.29742	30.44	7.041		5.701	4.458		3.118
37635	62848	J07432149-5209508		94.8	115.83953	-52.16401	33.67	6.552		5.321	4.188		2.957
37918	63581	J07461480-5948506		71.0	116.56183	-59.81411	29.13	7.94		6.275	5.262		3.597
									8.067			5.389	
37923	63608	J07461694-5948341		99.9	116.57066	-59.80949	29.62	8.067		6.411	5.425		3.769
40188	69051	J08123271-5408473		59.3	123.13620	-54.14631	11.93	6.893	15.662	6.105	2.276	11.045	1.488
40774		J08191905+0120198	V0397 Hya	93.7	124.82938	1.33886	44.68	8.09		6.106	6.340		4.356
42074	72760	J08343166-0043339		82.8	128.63107	-0.72599	47.40	7.111	15.662	5.423	5.491	14.042	3.802
58240	103742	J11564232-3216053		89.7	179.17629	-32.26815	28.16	7.503	7.653	6.131	4.751	4.901	3.379
58241	103743	J11564379-3216026		99.8	179.18241	-32.26741	28.21	7.653		6.240	4.905		3.492
60831	108574	J12280445+4447394		96.5	187.01852	44.79431	22.06	7.298		6.117	4.016		2.835
									7.878			4.596	
60832	108575	J12280480+4447305		91.8	187.01999	44.79180	22.09	7.878		6.495	4.599		3.216
60994	108799	J12300479-1323350	HR 4758	98.3	187.51989	-13.39318	40.57	6.293	8.922	4.832	4.334	6.963	2.873
68030	121560	J13554999+1403234		94.1	208.95830	14.05650	40.80	6.034		4.843	4.087		2.896

Table C.6. Photometry of stars in the Columba moving group

HIP	HD	2MASS	Others/WDS	Prob	RA degree	Dec degree	π mas	G_A mag	G_B mag	K_A mag	M_G mag	M_{GB} mag	M_K mag
3210	3888	J00405159-5312357		25.7	10.2149	-53.2099	22.57	7.249		6.113	4.017		2.881
6165	8077	J01190560-5351020		2.2	19.7734	-53.8505	11.50	8.753		7.615	4.056		2.918
7805	10472	J01402406-6059566		77.8	25.1003	-60.9991	14.05	7.530		6.632	3.269		2.371
	TYC 8047-232-1	J01521461-5219332	CD-52 381	45.8	28.0609	-52.3259	11.59	10.614		8.405	5.934		3.725
11029	14691	J02220152-1046390	HR692	99.5	35.5064	-10.7775	33.51	5.335		4.522	2.961		2.148
12413	16754	J02394796-4253300	HR789	73.1	39.9499	-42.8918	24.71	4.685		4.460	1.649		1.424
							24.71		12.378			9.342	
14551	19545	J03075083-2749520	HR 943	74.8	46.9619	-27.8312	18.85	6.155		5.772	2.531		2.148
							18.85		14.111			10.487	
14913	20121	J03122575-4425111	HR 968	97.1	48.1073	-44.4197	22.74	6.003	6.943	4.827	2.787	3.727	1.611
							22.74		8.697			5.481	
16449	21997	J03315364-2536509	HR1082	99.5	52.9735	-25.6141	14.36	6.371		6.100	2.157		1.886
17675	23384	J03471061+5142230		96.4	56.7943	51.7064	17.11	6.830		6.064	2.996		2.230
17782	23524	J03482301+5202163		79.5	57.0958	52.0379	19.35	8.616		6.747	5.799	5.799	3.180
19775	26980	J04142257-3819016		99.9	63.5940	-38.3171	12.61	8.946		7.620	4.449		3.123
	27679	J04211032-2432211		98.7	65.2930	-24.5392	11.82	9.223		7.810	4.586		3.173
		J04345077-3547211	CD-36 1785	99.8	68.7116	-35.7892	11.43	10.626		8.592	5.915		3.881
		J04411573-3513582	CPD-35 525	99.9	70.3157	-35.2328	12.80	9.865		8.188	5.401		3.724
22152	29329	J04460056+7636399	HR1468	95.5	71.5024	76.6110	30.69	6.351		5.284	3.786		2.719
22226	30447	J04464950-2618087		99.5	71.7064	-26.3025	12.45	7.768		6.894	3.244		2.370
	31242	J04515354-4647134	CD-46 1587	99.7	72.9733	-46.7870	11.88	9.745	12.141	8.160	5.118	7.514	3.533
		J04515303-4647309	GSC8077-1788	97.5	72.9710	-46.7919	11.96	12.141		8.888	7.530		4.277
	272836	J04530520-4844386		99.7	73.2717	-48.7441	11.90	10.330	14.698	8.238	5.707	10.075	3.615
23171	32476	J04590561-6325297		79.8	74.7740	-63.4248	11.59	10.233	10.513		5.552	5.832	
23179	31647	J04591543+3753251	Omega Aur	99.5	74.8142	37.8902	20.24	4.980	7.684		1.511	4.215	1.453
23316	32372	J05005186-4101065		99.9	75.2161	-41.0185	12.88	9.200		7.756	4.750		3.306
23362	32309	J05012558-2003067	HR1621	99.9	75.3566	-20.0519	16.57	4.871		4.974	0.967		1.070
24947	35114	J05203803-3945179	AS Col	99.4	80.1585	-39.7549	21.12	7.261		6.144	3.885		2.768
25436	35996	J05262401-4322325	CD-43 1847	99.2	81.6001	-43.3758	10.86	8.133	8.953	7.207	3.312	4.132	2.386
25434		J05262296-4322360	CD-43 1846	67.4	81.5957	-43.3767	10.83	8.953		7.760	4.126		2.933
	35841	J05263658-2229238	BD-22 1109	52.0	81.6524	-22.4899	9.65	8.810	16.815	7.826	3.732	11.737	2.748
	274561	J05285509-4534584	CD-45 2003	40.7	82.2296	-45.5829	9.78	11.105		8.994	6.056		3.945
25709	36329	J05292409-3430554	CD-34 2279	99.9	82.3504	-34.5154	13.87	8.332		6.949	4.042		2.659
		J05301907-1916318	AG Lep	1.4	82.5795	-19.2755	8.84	9.404	11.105	7.925	4.137		2.658
										5.838			
	36869	J05340914-1517031	AH Lep	99.9	83.5383	-15.2843	17.35	8.215	14.039	6.852	4.412	10.236	3.049
26309	37286	J05361029-2842289	HR1915	99.9	84.0429	-28.7080	17.10	6.240		5.864	2.405		2.029
26395	37306	J05370877-1146317		99.5	84.2866	-11.7756	14.38	6.092		5.971	1.880		1.759
26453	37484	J05373962-2837346		99.9	84.4151	-28.6263	17.00	7.167		6.277	3.319		2.429
	TYC 5346-132-1	J05383500-0856405	BD-08 1195	75.9	84.6459	-8.9446	12.21	9.638		7.970	5.071		3.403
	TYC 5925-1221-1	J05402073-1940108	AI Lep	99.9	85.0864	-19.6697	13.67	8.954		7.466	4.633		3.145
	38207	J05432094-2011214	BD-20 1162	4.1	85.8373	-20.1893	9.09	8.370		7.495	3.164		2.289
26966	38206	J05432166-1833268	HR1975	99.9	85.8403	-18.5575	14.15	5.729		5.783	1.482		1.536
26990	38397	J05433580-3955246		99.7	85.8992	-39.9235	18.66	7.998		6.756	4.352		3.110
	TYC 6502-1188-1	J05502142-2915206	CD-29 2531	27.7	87.5893	-29.2557	8.80	10.946	20.867	9.071	5.668	15.589	3.793
	TYC 8520-32-1	J05510116-5238126	CD-52 1363	16.8	87.7548	-52.6369	7.54	10.307		8.660	4.693		2.986
28036	40216	J05554314-3806162	CD-38 2296	99.9	88.9298	-38.1045	18.95	7.353	13.187	6.206	3.741	9.575	2.594
28474	41071	J06004130-4453500	RT Pic	98.5	90.1721	-44.8973	18.48	8.895		7.321	5.228	7.500	3.654
	TYC 5944-411-1	J06050784-2143305		94.7	91.2827	-21.7252	12.97	9.737		8.179	5.302		3.743
30030	43989	J06190805-0326203	V1358 Ori	99.9	94.7836	-3.4390	19.35	7.707		6.552	4.141		2.986
	TYC 7617-549-1	J06260690-4102538	CD-40 2458	98.2	96.5288	-41.0483	10.12	9.867		8.020	4.894		3.047
	295290	J06402236-0331591	TYC 4803-1418-1	99.6	100.0932	-3.5331	16.52	8.806		6.955	4.896		3.045
32104	48097	J06422431+1738430	26 Gem	7.7	100.6013	17.6453	21.07	5.185		5.011	1.803		1.629
	48370	J06430102-0253192	BD-02 1732	21.6	100.7543	-2.8887	27.72	7.746		6.268	4.960		3.482
	TYC 7100-2112-1	J06524674-3636169	CD-36 3202	95.9	103.1948	-36.6047	11.03	10.838		8.738	6.051		3.951
	51797	J06562354-4646549	CD-46 2777	77.1	104.0981	-46.7820	10.59	9.432		7.803	4.557		2.928
114189	218396	J23072869+2108033	HR8799	55.0	346.8696	21.1343	24.76	5.910		5.240	2.879		2.209
116805	222439	J23402449+4420021	kap And	15.3	355.1021	44.3339	19.37	4.052		4.340	0.488		0.776

Table C.7. Photometry of stars in the Tucana-Horologium moving group

HIP	HD	2MASS	Others/WDS	Prob	RA degree	Dec degree	π mas	G_A mag	G_B mag	K_A mag	M_G mag	M_{GB} mag	M_K mag
490	105	J00055255-4145109		99.9	1.4689	-41.7531	25.75	7.395		6.464	4.449		3.171
1113	987	J00135300-7441178		99.9	3.4709	-74.6883	21.80	8.654		7.406	5.347		3.655
1481	1466	J00182612-6328389		99.9	4.6088	-63.4775	23.36	7.339		6.462	4.181		2.991
2484	2884	J00313267-6257297	bet1 Tuc	93.4	7.8861	-62.9582	22.84	4.329		4.664	1.122		1.274
2487	2885	J00313347-6257560	bet2 Tuc	0.0	7.8893	-62.9656	22.84	4.329	4.564	4.320	1.122	1.357	0.901
2578	3003	J00324391-6301533	bet3 Tuc	99.9	8.1829	-63.0315	22.84	4.329	4.529	5.061	1.122	1.322	1.778
							22.84		5.055			1.848	
2729	3221	J00345120-6154583		99.9	11.3673	-51.6261	22.51	9.113		7.337	6.625		3.295
	TYC 9351-1110-1	J00422033-7747397	CD-78 24	99.9	10.5846	-77.7944	20.08	9.830		8.220	6.344		4.043
	TYC 7002-2219-1	J01220441-3337036	CD-34 521	99.9	20.5185	-33.6177	25.90	10.392		8.307	7.459		4.514
6485	8558	J01232126-5728507		99.9	20.8386	-57.4807	22.09	8.389		7.241	5.110		3.568
6856	9054	J01280868-5238191	CC Phe	99.9	22.0361	-52.6387	25.11	8.975		7.405	5.974		3.833
7699	10269	J01390761-5625459		99.9	24.7825	-56.4295	21.31	6.980		6.335	3.623		2.632
8233	10863	J01460105-2720556	HR517	97.0	26.5049	-27.3490	22.28	6.299		5.723	3.038		2.195
9141	12039	J01574896-2154052	DK Cet	99.9	29.4541	-21.9015	24.21	7.914		6.856	4.834	4.834	3.392
9892	13183	J02071805-5311565		99.8	31.8253	-53.1990	20.16	8.516		7.347	5.039		3.417
9902	13246	J02073220-5940459		3.0	31.8589	-59.6794	22.03	7.384	9.886	6.534	4.099	6.601	2.919
	TYC 8489-1155-1	J02073220-5940210	CD-60 416	99.9	31.8842	-59.6725	22.00	9.886		8.328	6.598		4.249
10602	14228	J02163059-5130437	phi Eri	99.9	34.1274	-51.5122	21.22	3.556		3.780	0.190		0.494
11360	15115	J02261625+0617331		98.8	36.5677	6.2926	20.41	6.694		6.028	3.243		2.371
12394	16978	J02393538-6816008	eps Hyi	99.9	39.8973	-68.2669	21.48	4.112		4.443	0.772		0.914
	TYC 8060-1673-1	J03304909-4555573	CD-46 1064	99.9	52.7046	-45.9326	22.78	9.380		7.772	6.168		3.891
	22213	J03341633-1204073		98.9	53.5681	-12.0687	19.46	8.572	12.330	7.338	5.018	8.776	3.236
15247	20385	J03164066-0331489		98.8	49.1694	-3.5303	20.51	7.349		6.457	3.908		2.658
16853	22705	J03365341-4957288		99.9	54.2225	-49.9580	23.66	7.491		6.492	4.361		3.007
									13.551			10.421	
17764	24636	J03481148-7441388		99.9	57.0478	-74.6941	17.51	7.037		6.367	3.253		2.352
17797			f Eri	99.9	57.1495	-37.6202	18.81	4.748			1.120		1.196
							18.81	4.748	12.245		1.120	8.617	
	24071	J03483548-3737190			57.1478	-37.6220	18.81	4.748	5.347		1.120	1.719	
18714	25402	J04003198-4144544		22.0	60.1333	-41.7484	19.27	8.234	12.278	7.203	4.658		3.299
												8.702	
	TYC 5882-1169-1	J04021648-1521297	BD-15 705	99.9	60.5687	-15.3583	18.28	9.766		8.228	6.076		3.883
	TYC 5324-1293-1	J04364709-1209207	BD-12 943	99.4	69.1963	-12.1557	14.59	9.537	14.171	8.315	5.357	9.992	3.585
20042	27376	J04175366-3347540	ups04 Eri	99.9	64.4739	-33.7984	18.33	3.552		3.864	0.618		0.271
							18.33		13.968			10.283	
21632	29615	J04384393-2702018		99.9	69.6831	-27.0338	18.40	8.333	14.453	7.273	4.657	10.777	3.190
21965	30051	J04431720-2337419		90.8	70.8217	-23.6283	14.47	7.001		6.288	2.804		1.826
22295	32195	J04480518-8046452		48.4	72.0216	-80.7792	16.01	8.016		7.170	4.038		2.890
	TYC 5908-230-1	J04593202-1917416	BD-19 1062	97.6	74.8835	-19.2949	15.04	10.255		8.766	6.142		3.953
	TYC 5335-312-1	J05153652-0930512	BD-09 1108	14.6	78.9022	-9.5143	12.20	9.542	14.818	8.522	4.973	10.249	3.515
							12.20	9.542	14.082	8.522	4.973	9.513	3.515
32435	53842	J06461348-8359294		99.4	101.5564	-83.9915	17.34	7.368	12.920	6.553	3.564	9.116	2.495
100751	193924	J20253886-5644062	alpha Pav	94.1	306.4119	-56.7351	18.24	1.910		2.304	-1.785		-1.216
105388	202917	J21204994-5302030		99.9	320.2082	-53.0342	21.41	8.492		7.386	5.145		3.561
107947	207575	J21520973-6203085		99.9	328.0405	-62.0524	21.39	7.110		6.358	3.761		2.678
108422	208233	J21575146-6812501		98.7	329.4650	-68.2143	19.06	8.648		7.310	5.049		3.145
							19.06		13.322			9.722	
	TYC 5242-324-1	J23093711-0225551	BD-03 5579	66.1	347.4047	-2.4320	19.22	10.404		8.567	6.823		4.237
	TYC 9529-0340-1	J23274943-8613187	CD-86 147	99.7	351.9558	-86.2219	15.78	9.184		7.950	5.175		3.491
	222259B	J23393929-6911396	DS Tuc B	99.9	354.9136	-69.1943	22.65	9.406		7.630	6.182		3.808
116748	222259A	J23393949-6911448	DS Tuc A	99.9	354.9145	-69.1958	22.64	8.341	9.406	7.122	5.115	6.180	3.454

Table C.8. Photometry of stars in the Volans/Crius 221 moving group

HIP	HD	2MASS	Others/WDS	Prob	RA degree	Dec degree	π mas	G_A mag	G_B mag	K_A mag	M_G mag	M_{GB} mag	M_K mag
		J00301560-8613552	TYC 9494-799-1	0.0	7.5722	-86.2321	18.31	9.460		7.685	5.77		4.00
	67928	J08075272-5135016	TYC 8148-343-1	0.0	121.9696	-51.5836	9.36	9.857	12.357	8.232	4.71	7.21	3.09
	69406	J08134777-5837139	CPD-58 1080B	0.0	123.4489	-58.6204	9.18	8.364		7.488	3.18		2.30
									11.716		6.53		
		J08363202-6024116	TYC 8926-337-1	0.0	129.1333	-60.4030	9.29	11.113		9.269	5.95		4.11
45096	299896	J09111005-5501535	TYC 8587-323-1	0.0	137.7915	-55.0312	24.54	9.248		7.167	6.20		4.12
	79648	J09134337-4642014	TYC 8166-809-1	0.0	138.4305	-46.7003	14.25	9.545		7.971	5.31		3.74
45478	80157	J09160129-5533297	TYC 8587-1754-1	21.7	139.0051	-55.5581	11.48	8.035		7.14	3.33		2.44
		J09231316-4520256	TYC 8167-1155-1	0.0	140.8047	-45.3404	9.59	11.236		9.26	6.15		4.17
47351	83946	J09385410-6459267	TYC 8949-116-1	99.9	144.7251	-64.9906	11.05	8.728		7.662	3.94		2.88
		J09430884-6313043	TYC 8946-1225-1	0.0	145.7866	-63.2177	8.89	10.212		8.596	4.96		3.34
							8.89		17.370			12.11	
		J10111554-6530330	TYC 8951-622-1	2.3	152.8144	-65.5091	10.14	9.967	15.969	8.539	5.00	11.00	3.57
		J10295615-6451235	TYC 8964-396-1	0.0	157.4836	-64.8564	9.01	10.861		9.164	5.63		3.94
52462	92945	J10432828-2903513	TYC 6645-338-1	0.0	160.8667	-29.0645	46.49	7.485		5.66	5.82		4.00
52787	93528	J10473117-2220528	TYC 6081-65-1	0.0	161.8792	-22.3482	29.83	8.166	9.50	6.505	5.54	6.88	3.88
54155	96064	J11044148-0413159	TYC 4924-1114-1	0.0	166.1720	-4.2216	38.01	7.414		5.801	5.31		3.70
		J11110405-7824116	TYC 9414-379-1	0.2	167.7661	-78.4028	13.34	10.659	11.153	8.079	6.28	6.78	3.70
58029	103381	J11540534-2958570	TYC 6678-1031-1	0.0	178.5216	-29.9827	23.69	8.271		6.775	5.14		3.65
	104315	J12003839-7200251	TYC 9235-1497-1	1.0	180.1590	-72.0069	12.18	9.992		8.367	5.42		3.80
		J12170220-5546112	TYC 8637-2580-1	0.0	184.2585	-55.7698	14.52	10.549		8.403	6.36		4.21
61284	109138	J12332981-7523112	TYC 9412-190-1	0.0	188.3725	-75.3864	15.66	9.316		7.756	5.29		3.73
		J12543443-4558310	TYC 8245-2246-1	0.0	193.6435	-45.9757	14.74	9.676	12.798	7.829	5.52	8.64	3.67
							14.74		14.954			10.80	
		J13193133-7036309	TYC 9246-361-1	0.0	199.8795	-70.6086	14.53	10.535		8.434	6.35		4.25
73052	130943	J14554612-7309599	TYC 9270-1659-1	0.0	223.9407	-73.1668	16.25	7.680		6.649	3.73		2.70
	153555	J17041857-6233182	TYC 9043-817-1	0.0	256.0771	-62.5553	10.24	9.067	16.845	7.902	4.12	11.90	2.95
84642	155915	J17181464-6027275	TYC 9052-1117-1	0.0	259.5605	-60.4581	16.74	9.143		7.527	5.26		3.65
		J17244456-5153425	TYC 8353-292-1	0.0	261.1854	-51.8955	12.54	10.587		8.669	6.08		4.16
	321224	J18025629-3643280	TYC 7403-6190-1	0.0	270.7342	-36.7250	19.86	9.324		7.519	5.81		4.01
96334	183414	J19350972-6958321	TYC 9309-599-1	0.0	293.7904	-69.9764	26.2	7.733		6.298	4.82		3.39
96880	184587	J19413575-7226457	TYC 9314-767-1	0.0	295.3988	-72.4468	23.99	8.956		7.068	5.86		3.97
		J08264964-6346369	TYC 8933-327-1	36.9	126.7068	-63.7769	12.22	10.538		8.655	5.974		4.09
	73129	J08324622-6508272		51.0	128.1926	-65.1409	12.16	9.221	14.899	7.851	4.645	10.32	3.28
43783	76728	J08550282-6038406	HR3571	56.5	133.7619	-60.6446	11.19	3.728		4.098	-1.027		-0.66
							11.19		12.800			8.04	
45594	80563	J09173415-6323145		99.9	139.3923	-63.3874	10.98	8.215		7.280	3.418		2.48
46460	82406	J09283051-6642067	HR 3783	99.1	142.1272	-66.7019	11.99	5.883		5.714	1.278		1.11
47017	83359	J09345645-6459579		99.8	143.7352	-64.9995	11.51	7.912		6.813	3.217		2.12
							11.51		12.282			7.59	
47115	83253	J09360518-6457011		98.6	144.0216	-64.9502	11.86	6.565		6.261	1.935		1.63
							11.86						
47335	83948	J09384522-6651326		99.9	144.6880	-66.8589	11.70	7.345	10.730	6.729	2.686	6.07	2.07
		J09391046-6646155	TYC 8953-1289-1	99.9	144.7936	-66.7710	11.88	10.723		8.796	6.098		4.17
47351	83946	J09385410-6459267		99.9	144.7254	-64.9908	11.05	8.719		7.662	3.935		2.88
		J09481924-6403217	TYC 8950-1447-1	99.9	147.0802	-64.0561	13.00	11.034		8.845	6.603		4.41
		J10082200-6756402	TYC 9210-1818-1	99.8	152.0916	-67.9445	11.55	11.300	16.132	9.070	6.612	11.44	4.38
	CD-67 852	J10122991-6752334	TYC 9210-1730-1	99.9	153.1246	-67.8759	12.28	9.767		8.239	5.213		3.68
50567	89928	J10194613-7133173		4.5	154.9417	-71.5546	11.78	9.341		7.927	4.696		3.28

Table C.9. Information about multiplicity for stars in the AB Dor moving group.

2MASS	Age Myr	TESS	RV	HCI	RUWE	PMA
J00182085+3057224	137	1	1	0	1	0
J00455088+5458402	137	1	1	0	1	1
J01062614-1417468	137	1	2	1	1	1
J01203226-1128035	137	1	2	1	1	1
J01242709+5751062	137	1	1	0	1	0
J02051802+5217027	137	1	1	0	1	0
J02121535+2357298	137	1	0	0	1	1
J02223387+5033369	137	1	1	0	1	0
J02305064+5532543	137	1	1	1	1	1
J02422094+3837212	137	1	2	0	1	1
J02422130+3837073	137	1	2	0	1	1
J02495902+2715381	137	1	0	1	0	0
J03094227-0934463	137	1	2	1	1	1
J03111383+2224571	137	1	1	1	1	1
J03175907-6655367	137	1	1	1	1	1
J03331347+4615269	137	1	1	0	1	1
J03552040-0143451	137	1	1	1	1	0
J04023675-0016078	137	1	2	1	1	1
J04064153+0141020	137	1	2	1	1	1
J04093502+6932292	137	1	2	0	1	1
J04213348-2543091	137	1	0	0	1	0
J04330622-2400477	137	1	1	0	1	0
J04572232-0907595	137	1	1	0	1	0
J05023042-3959129	137	1	1	0	1	0
J05044132+4024003	137	2	1	0	1	0
J05062769-1549303	137	1	1	1	1	0
J05284484-6526551	137	1	1	1	1	1
J05350411-3417519	137	1	1	0	1	0
J05365685-4757528	137	1	2	1	1	1
J05372-4243AB	137	1	0	0	1	1
J06083386-3402549	137	1	1	1	1	0
J06223097-6013072	137	1	2	1	1	1
J06380036-6132001	137	1	0	1	1	1
J07305952-8419275	137	1	1	0	1	0
J07453559-7940080	137	1	1	0	1	1
J11251773-8457164	137	1	1	0	1	1
J12361640-7931344	137	1	1	0	1	0
J12361110-7931384	137	1	1	0	1	0
J13034967-0509423	137	1	2	1	0	0
J16223272-0414571	137	1	2	0	1	1
J16540815-0420248	137	1	2	1	1	1
J17285563-3243568	137	1	1	1	1	0
J19010604-2842502	137	1	1	1	1	1
J19105782-6016202	137	1	1	1	1	1
J19235315-4036571	137	1	0	1	1	1
J19330374+0345397	137	1	1	1	1	0
J20044935-0239203	137	1	1	1	1	0
J22081397-4657393	137	1	1	1	1	0
J23001929-2609135	137	1	2	1	1	1
J23002791-2618431	137	1	1	1	1	1
J23115205-4508106	137	1	2	1	1	1
J23193955+4215098	137	1	1	0	1	1
J23265595+0115201	137	1	1	1	1	1
J23415428-3558397	137	1	1	1	1	1
J23485554-2807490	137	1	2	1	1	1
J23561067-3903086	137	1	2	1	1	1

Notes. TESS=1 means that there is TESS data, 0 that there is not. RV=1 means that there is Gaia RV data; RV=2 means that there is high precision RV data; RV=0 means that there is no RV data. HCI=1 means that there is HCI data, 0 that there is not. RUWE=1 means that there is RUWE data, 0 that there is not. PMA=1 means that there is PMA data, 0 that there is not.

Table C.10. Information about multiplicity for stars in the Argus moving group.

2MASS	Age Myr	TESS	RV	HCI	RUWE	PMA
J01343776-1540348	48	1	2	1	1	1
J05345923-2954041	48	1	1	0	1	0
J07015339-4227561	48	1	1	1	1	0
J07282203-4908377	48	1	1	1	1	0
J07283006-4908589	48	1	1	1	1	1
J07311991-5447027	48	1	1	0	1	0
J07354747-3212141	48	1	2	1	1	1
J07472597-4902511	48	2	1	0	1	0
J07484982-4327055	48	2	1	1	1	0
J07541770-5711131	48	2	1	1	1	0
J07535548-5710073	48	1	1	1	1	0
J08391155-5834281	48	1	1	0	1	0
J08500812-5745593	48	1	1	1	1	0
J09020394-5808497	48	1	1	0	1	0
J09133027-6259092	48	1	1	1	1	0
J09361783-7820417	48	1	2	1	1	1
J09395143-2134175	48	1	1	0	1	0
J09424742-7239499	48	1	1	0	1	0
J09471986-4003098	48	2	2	1	1	0
HD85151	48	1	0	0	1	0
J09555832-6721218	48	1	1	0	1	0
J10144416-4207189	48	1	2	1	1	1
J10272528-6542167	48	1	1	1	1	1
J11411978-4305442	48	1	2	1	1	1
J11490366+1434197	48	1	2	1	1	0
J12063292-4247508	48	1	1	0	1	0
J12203437-7539286	48	1	1	1	1	0
J13491293-7549475	48	1	1	0	1	0
J14072929-6133441	48	1	1	1	1	1
J14462144-6746158	48	1	1	0	1	0
J15122343-7515156	48	1	2	1	1	1
J15401155-7013403	48	1	1	1	1	1
J16170540-6756285	48	1	2	1	1	1
J18205694+2951317	48	1	0	0	1	1
J19561425+1125254	48	1	1	0	1	1
J20003558-7254380	48	1	2	1	1	1
J20143203+3648225	48	1	1	0	1	1

Notes. TESS=1 means that there is TESS data, 0 that there is not. RV=1 means that there is Gaia RV data; RV=2 means that there is high precision RV data; RV=0 means that there is no RV data. HCI=1 means that there is HCI data, 0 that there is not. RUWE=1 means that there is RUWE data, 0 that there is not. PMA=1 means that there is PMA data, 0 that there is not.

Table C.11. Information about multiplicity for stars in the BPMG.

2MASS	Age Myr	TESS	RV	HCI	RUWE	PMA
J00065008-2306271	21	1	1	1	1	1
J01373940+1835332	21	1	1	1	1	0
J02172472+2844305	21	1	1	1	1	1
J02172527+2844423	21	1	1	1	1	1
J02272924+3058246	21	1	2	1	1	1
J04373613-0228248	21	1	2	1	1	1
J05004928+1527006	21	1	1	1	1	0
J05270477-1154033	21	1	2	1	1	1
J05471708-5103594	21	1	2	1	1	1
J06182824-7202416	21	1	2	1	1	1
J15385757-5742273	21	1	1	1	1	1
J17150362-2749397	21	0	0	1	0	0
J17172550-6657039	21	1	1	1	1	1
J17295506-5415487	21	1	1	1	1	0
J17414903-5043279	21	1	1	1	1	1
J17483374-5306433	21	1	1	1	1	0
J18030341-5138564	21	1	2	1	1	1
J18064990-4325297	21	1	0	1	1	1
J18195221-2916327	21	0	0	1	1	1
J18452691-6452165	21	1	2	1	1	1
J18453704-6451460	21	1	1	1	1	0
J18480637-6213470	21	1	0	0	0	0
J18530587-5010499	21	1	2	1	1	1
J19114467-2604085	21	0	0	1	1	0
J19225122-5425263	21	1	2	1	1	1
J19225894-5432170	21	1	2	1	1	1
J20041810-2619461	21	0	1	0	1	1
J20090521-2613265	21	0	2	1	1	1
J20554767-1706509	21	0	0	1	1	1
J21475527-5255502	21	1	1	0	1	1

Notes. TESS=1 means that there is TESS data, 0 that there is not. RV=1 means that there is Gaia RV data; RV=2 means that there is high precision RV data; RV=0 means that there is no RV data. HCI=1 means that there is HCI data, 0 that there is not. RUWE=1 means that there is RUWE data, 0 that there is not. PMA=1 means that there is PMA data, 0 that there is not.

Table C.12. Information about multiplicity for stars in the Carina moving group.

2MASS	Age Myr	TESS	RV	HCI	RUWE	PMA
J03155768-7723184	28	1	1	1	1	1
J05342614-6006151	28	1	1	0	1	1
J05532917-8156532	28	1	2	1	1	0
J06105289-6129594	28	1	1	0	1	1
J06191291-5803156	28	1	2	1	1	1
J06434625-7158356	28	1	2	1	1	1
J07003046-7941459	28	1	2	1	1	1
J08210046-5213406	28	1	1	0	1	1
J08225514-5207254	28	1	2	1	1	1
J09172755-7444045	28	1	2	1	1	1
J09233498-6111359	28	1	1	1	1	1
J09303148-7041479	28	2	1	0	1	0
J09312500-7344496	28	1	0	1	1	1
J09392101-6119410	28	1	1	0	1	1
J09534760-5453540	28	1	1	0	1	0
J10131476-5230540	28	1	2	1	1	0
J10300355-7432320	28	1	1	0	1	0

Notes. TESS=1 means that there is TESS data, 0 that there is not. RV=1 means that there is Gaia RV data; RV=2 means that there is high precision RV data; RV=0 means that there is no RV data. HCI=1 means that there is HCI data, 0 that there is not. RUWE=1 means that there is RUWE data, 0 that there is not. PMA=1 means that there is PMA data, 0 that there is not.

Table C.13. Information about multiplicity for stars in the Carina Near moving group.

2MASS	Age Myr	TESS	RV	HCI	RUWE	PMA
HIP35564	200	1	1	1	1	1
J07293141-3807217	200	1	1	1	1	1
J07423606-5917507	200	1	1	1	1	1
J07432149-5209508	200	1	1	1	1	1
J07461480-5948506	200	1	1	1	1	1
J07461694-5948341	200	2	2	1	1	1
J08123271-5408473	200	1	1	0	1	1
J08191905+0120198	200	1	2	1	1	1
J08343166-0043339	200	1	1	1	1	1
J11564232-3216053	200	1	1	1	1	1
J11564379-3216026	200	1	2	1	1	1
J12280445+4447394	200	1	2	0	1	1
J12280480+4447305	200	1	2	0	1	1
J12300479-1323350	200	1	1	0	1	1
J13554999+1403234	200	1	1	1	1	1

Notes. TESS=1 means that there is TESS data, 0 that there is not. RV=1 means that there is Gaia RV data; RV=2 means that there is high precision RV data; RV=0 means that there is no RV data. HCI=1 means that there is HCI data, 0 that there is not. RUWE=1 means that there is RUWE data, 0 that there is not. PMA=1 means that there is PMA data, 0 that there is not.

Table C.14. Information about multiplicity for stars in the Columba moving group.

2MASS	Age Myr	TESS	RV	HCI	RUWE	PMA
J00405159-5312357	36	1	1	0	1	1
J01190560-5351020	36	1	1	1	1	1
J01402406-6059566	36	1	2	1	1	1
J01521461-5219332	36	1	2	1	1	0
J02220152-1046390	36	1	1	0	1	1
J02394796-4253300	36	1	0	1	1	1
J03075083-2749520	36	1	2	1	1	1
J03122575-4425111	36	1	0	0	1	0
J03315364-2536509	36	1	1	1	1	1
J03471061+5142230	36	2	1	0	1	1
J03482301+5202163	36	1	0	0	0	0
J04142257-3819016	36	1	1	1	1	1
J04211032-2432211	36	1	1	1	1	0
J04345077-3547211	36	1	1	1	1	0
J04411573-3513582	36	1	1	0	1	0
J04460056+7636399	36	1	2	0	1	1
J04464950-2618087	36	1	1	1	1	1
J04515354-4647134	36	1	1	1	1	0
J04515303-4647309	36	1	1	1	1	0
J04530520-4844386	36	1	1	1	1	0
J04590561-6325297	36	1	0	0	1	1
J04591543+3753251	36	1	0	0	1	1
J05005186-4101065	36	1	1	1	1	1
J05012558-2003067	36	1	1	0	1	1
J05203803-3945179	36	1	1	1	1	1
J05262401-4322325	36	1	1	1	1	1
J05262296-4322360	36	1	1	1	1	1
J05263658-2229238	36	1	1	1	1	0
J05285509-4534584	36	1	1	0	1	0
J05292409-3430554	36	1	0	1	1	1
J05301907-1916318	36	1	1	0	1	0
J05340914-1517031	36	1	0	1	1	0
J05361029-2842289	36	1	1	1	1	1
J05370877-1146317	36	1	0	1	1	1
J05373962-2837346	36	1	2	1	1	1
J05383500-0856405	36	1	1	1	1	0
J05402073-1940108	36	1	0	1	1	0
J05432094-2011214	36	1	2	1	1	0
J05432166-1833268	36	1	1	1	1	1
J05433580-3955246	36	1	1	1	1	1
J05502142-2915206	36	1	1	0	1	0
J05510116-5238126	36	1	1	0	1	0
J05554314-3806162	36	1	1	1	1	1
J06004130-4453500	36	1	2	1	1	1
J06050784-2143305	36	1	1	0	1	0
J06190805-0326203	36	1	2	1	1	1
J06260690-4102538	36	1	1	1	1	0
J06402236-0331591	36	1	0	0	1	0
J06422431+1738430	36	1	1	1	1	1
J06430102-0253192	36	1	1	1	1	0
J06524674-3636169	36	1	1	0	1	0
J06562354-4646549	36	1	2	1	1	0
J23072869+2108033	36	1	2	1	1	1
J23402449+4420021	36	1	0	1	1	1

Notes. TESS=1 means that there is TESS data, 0 that there is not. RV=1 means that there is Gaia RV data; RV=2 means that there is high precision RV data; RV=0 means that there is no RV data. HCI=1 means that there is HCI data, 0 that there is not. RUWE=1 means that there is RUWE data, 0 that there is not. PMA=1 means that there is PMA data, 0 that there is not.

Table C.15. Information about multiplicity for stars in the Tuc-Hor moving group.

2MASS	Age Myr	TESS	RV	HCI	RUWE	PMA
J00055255-4145109	37	1	2	1	1	1
J00135300-7441178	37	1	2	1	1	1
J00182612-6328389	37	1	2	1	1	1
J00313267-6257297	37	1	1	1	1	1
J00313347-6257560	37	1	0	1	0	0
J00324391-6301533	37	1	2	1	1	1
J00345120-6154583	37	1	2	1	1	1
J00422033-7747397	37	1	1	1	1	0
J01220441-3337036	37	1	1	1	1	0
J01232126-5728507	37	1	2	1	1	1
J01280868-5238191	37	1	1	1	1	1
J01390761-5625459	37	1	1	1	1	1
J01460105-2720556	37	1	1	0	1	1
J01574896-2154052	37	1	2	1	1	1
J02071805-5311565	37	1	2	1	1	1
J02072611-5940459	37	1	1	1	1	1
J02072320-5940210	37	1	1	1	1	0
J02163059-5130437	37	1	0	1	1	1
J02261625+0617331	37	1	2	1	1	1
J02393538-6816008	37	1	0	1	1	1
J03304909-4555573	37	1	2	1	0	0
J03341633-1204073	37	1	0	1	0	0
J03164066-0331489	37	1	1	1	1	1
J03365341-4957288	37	1	1	1	1	1
J03481148-7441388	37	1	1	1	1	1
HIP 17797	37	1	0	1	1	1
J03483548-3737190	37	1	0	1	1	0
J04003198-4144544	37	1	1	1	1	1
J04021648-1521297	37	1	2	1	1	0
J04364709-1209207	37	1	1	1	1	0
J04175366-3347540	37	1	0	1	1	1
J04384393-2702018	37	1	1	1	1	1
J04431720-2337419	37	1	1	1	1	1
J04480518-8046452	37	1	1	1	1	1
J04593202-1917416	37	1	1	1	1	0
J05153652-0930512	37	1	1	1	1	0
J06461348-8359294	37	1	1	1	1	1
J20253886-5644062	37	1	0	1	0	0
J21204994-5302030	37	1	2	1	1	1
J21520973-6203085	37	1	2	1	1	1
J21575146-6812501	37	1	1	1	1	1
J23093711-0225551	37	1	1	1	1	0
J23274943-8613187	37	1	1	1	1	0
J23393929-6911396	37	1	1	1	1	0
J23393949-6911448	37	1	2	1	1	1

Notes. TESS=1 means that there is TESS data, 0 that there is not. RV=1 means that there is Gaia RV data; RV=2 means that there is high precision RV data; RV=0 means that there is no RV data. HCI=1 means that there is HCI data, 0 that there is not. RUWE=1 means that there is RUWE data, 0 that there is not. PMA=1 means that there is PMA data, 0 that there is not.

Table C.16. Information about multiplicity for stars in the Volans/Crius 221 moving group.

2MASS	Age Myr	TESS	RV	HCI	RUWE	PMA
J00301560-8613552	89	1	1	0	1	0
J08075272-5135016	89	2	0	0	1	0
J08134777-5837139	89	2	1	0	1	0
J08363202-6024116	89	1	1	0	1	0
J09111005-5501535	89	1	2	0	1	1
J09134337-4642014	89	1	1	0	1	0
J09160129-5533297	89	1	0	0	1	1
J09231316-4520256	89	2	1	0	1	0
J09385410-6459267	89	1	1	1	1	1
J09430884-6313043	89	1	1	1	1	0
J10111554-6530330	89	2	1	0	1	0
J10295615-6451235	89	1	1	0	1	0
J10432828-2903513	89	1	2	1	1	1
J10473117-2220528	89	1	1	1	1	1
J11044148-0413159	89	1	2	1	1	1
J11110405-7824116	89	1	1	0	1	0
J11540534-2958570	89	1	1	1	1	1
J12003839-7200251	89	2	1	0	1	0
J12170220-5546112	89	1	1	0	1	0
J12332981-7523112	89	2	2	1	1	1
J12543443-4558310	89	1	1	0	1	0
J13193133-7036309	89	2	1	0	1	0
J14554612-7309599	89	1	1	0	1	1
J17041857-6233182	89	2	1	0	1	0
J17181464-6027275	89	1	1	1	1	1
J17244456-5153425	89	1	1	0	1	0
J18025629-3643280	89	2	1	0	1	0
J19350972-6958321	89	1	2	1	1	1
J19413575-7226457	89	1	1	0	1	1
J08264964-6346369	89	1	1	0	1	0
J08324622-6508272	89	2	1	0	1	0
J08550282-6038406	89	1	1	0	1	1
J09173415-6323145	89	1	1	0	1	1
J09283051-6642067	89	1	1	1	1	1
J09345645-6459579	89	1	1	0	1	1
J09360518-6457011	89	1	0	1	1	1
J09384522-6651326	89	1	1	0	1	1
J09391046-6646155	89	2	1	0	1	0
J09385410-6459267	89	1	1	0	1	1
J09481924-6403217	89	2	1	0	1	0
J10082200-6756402	89	2	1	0	1	0
J10122991-6752334	89	1	1	0	1	0
J10194613-7133173	89	1	1	0	1	1

Notes. TESS=1 means that there is TESS data, 0 that there is not. RV=1 means that there is Gaia RV data; RV=2 means that there is high precision RV data; RV=0 means that there is no RV data. HCI=1 means that there is HCI data, 0 that there is not. RUWE=1 means that there is RUWE data, 0 that there is not. PMA=1 means that there is PMA data, 0 that there is not.

Table C.17. Binary data for stars in the AB Dor moving group

HIP	HD	2MASS	Others/WDS	RUWE	RV km s⁻¹	RV err km s⁻¹	Nb	pvalue	RV ampl km s⁻¹	sep arcsec	PA degree	S/N PMA
	1405	J00182085+3057224	PW And	0.989	-11.91	0.33	17	7.00678E-06	3.87			
3589	4277	J00455088+5458402	BD+54 144	0.959	-16.99	0.17	71	0	4.99	2.72	68.9	3.00
5191	6569	J01062614-1417468		0.956	7.87	0.21	15	0.016022373	1.73	22.56	331.12	1.03
6276		J01203226-1128035	BD-12 243	0.984	10.21	0.14	37	7.83559E-06	1.87			2.06
	236717	J01242709+5751062		0.965	-11.94	0.13	29	0.36065376	0.91			
		J02051802+5217027	TYC 3293-1912-1	0.872	-10.52	0.48	14	0.005912767	4.38			
10272	13482	J02121535+2357298	J02123+2357AB	1.003	-0.64					1.73	231.84	0.23
		J02223387+5033369	BD+49 646	1.000	-11.50	0.56	7	0.004280141	3.17			
11696	15407A	J02305064+5532543		1.061	-8.17	1.04	21	0	16.12			4.18
										21.27	304.88	
12635	16760B	J02422094+3837212		26.545	-3.95	0.38	8	1.68E-12	2.36			12.39
12638	16760	J02422130+3837073	BD+37 604	1.120	-3.99	0.38	10	0.02058884	3.27	0.026		3.11
										14.51	343.50	
13027	17332		J02475+1922AB	1.011	4.34	0.25	11	2.54E-08	1.93	3.64	307.19	17.97
13209	17573	J02495902+2715381	41 Ari							0.20		
14684	19668	J03094227-0934463	IS Eri	0.951	14.23	0.17	14	3.55E-03	1.07			1.74
14809		J03111383+2224571	J03112+2225A	0.965	4.93	0.20	10	0.41239625	1.48	33.22	320.93	0.22
15353	20888	J03175907-6655367	J03180-6656A	1.067	25.66	0.40	7	0.03524709	2.37	5.01	17.42	0.87
16563	21845	J03331347+4615269	V577 Per	1.006	-5.92	0.15	25	0.003924302	1.44	9.50	142.34	2.48
			GD50									
	24681	J03552040-0143451	TYC4718-894-1	1.102	17.34	0.44	12	1.0088139e-7	4.02			
18859	25457	J04023675-0016078	HR1249	0.988	17.62	0.15	14	0.000832118	1.00			0.37
19183	25953	J04064153+0141020		1.016	17.38	0.20	19	9.81175E-05	1.92	4.194	205.86	1.62
19422	25665	J04093502+6932292		1.004	-13.66	0.12	28	0.025971709	0.81			1.84
		J04213348-2543091	CD-261643	1.077								
	28982	J04330622-2400477	EB	4.131	25.82	0.32	37	0	5.69			
										1.99	250.76	
	31652	J04572232-0907595		1.051	23.08	0.22	25	0.21613929	3.48			
		J05023042-3959129	CD-40 1701	1.086	28.34	0.26	17	0.08361041	2.71			
		J05044132+4024003	TYC2899-1744-1	2.245	17.30	4.64	10	0	25.32			
										2.75	27.71	
	32981	J05062769-1549303		0.992	25.71	0.16	24	0.2152785	1.54			
25647	36705	J05284484-6526551	AB Dor	25.130	31.48	1.34	17	0	15.28	0.304		24.33
										8.86	347.24	
		J05350411-3417519	CD-34 2331	0.952	23.25	3.00	31	0	57.11	370.73	43.79	
26373	37572	J05365685-4757528	J05369-4758A	1.003	32.23	0.13	25	0.006159556	1.37	18.25	285.91	2.07
26401	37551	J05372-4243AB	WX Col	0.974						4.00	114.99	1.13
										157.51	335.53	
			CP-19 878	12.564	24.82	1.12	34	0	21.77			
		J06083386-3402549	CD-34 2676	2.316	29.38	0.46	16	0.005138393	5.30	0.088	265.8	
										0.56	154.60	
										186.69	235.45	
30314	45270	J06223097-6013072		0.874	31.45	0.15	16	0.001827182	1.01			3.57
31711	48189	J06380036-6132001	HR 2468	24.094						0.924	96	9.11
		J07305952-8419275	CD-84 80	1.629	23.89	0.37	10	0.08881974	3.00	0.6	134	
37855	64982	J07453559-7940080		7.633	26.35	0.36	9	0.5708684	1.28			2.49
										5.75	189.87	
55746	99827	J11251773-8457164		3.538	19.42	0.26	18	8.457457e-12	2.73	0.061		10.54
										3.628		
										296.10	254.99	
		J12361640-7931344	TYC 9420-68-1	0.840	21.95	0.28	17	0.08770331	2.45	15.01	254.88	
		J12361110-7931384	TYC 9420-112-1	0.925	22.88	0.33	19	0.55711365	5.06			
63742	113449	J13034967-0509423	J13038-0510AB						13.03	0.034		
80218	147512	J16223272-0414571		0.952	-20.28	0.12	14	0.80386555	0.42			1.07
82688	152555	J16540815-0420248		0.878	-16.49	0.15	22	0.001051901	1.66	3.80	58.36	2.87
	317617	J17285563-3243568		0.791	-9.97	0.29	6	0.4362791	1.41	0.418	318.6	
										2.39	109.96	
93375	176367	J19010604-2842502		0.895	-5.45	0.39	9	1.319708e-7	2.76			0.76
94235	178085	J19105782-6016202		1.070	9.47	0.25	20	5.0157234e-10	3.55	0.55	156.00	5.82
95347	201919	J19235315-4036571	Alpha Sgr	2.863								0.56
		J19330374+0345397	TYC0486-4943	1.000	-20.53	0.68	4	0.35042986	2.43	28.05	288.05	
		J20044935-0239203	BD-03 4778	0.928	-16.08	0.31	21	0.008049527	2.71	2.67	208.08	
109268	209952	J22081397-4657393	Alpha Gru	1.211	8.71	1.77	22					
113579	217343	J23001929-2609135	J23005-2619C	1.728								2.56
113597	217379	J23002791-2618431	J23005-2619AB	1.465	-21.88	0.52	18	0.49186167	6.68			2.87
										2.28	239.35	
114530	218860	J23115205-4508106		1.011	9.52	0.15	34	6.27488E-05	1.93	19.45	58.41	0.81
115162		J23193955+4215098		1.011	-19.77	0.14	32	0.3173372	1.14			0.76
115738	220825	J23265595+0115201	kap Psc	0.850	-1.79	1.12	10	1.56E-08	7.59			1.15
116910	222575	J23415428-3558397		1.079	9.70	1.30	10	0	9.58			0.08
117452	223352	J23485554-2807490	delta Scl	1.251	10.48	0.88	10	0.00347646	7.37	3.675	237.9	1.69
										74.71	296.49	
118008	224228	J23561067-3903086		1.020	12.84	0.13	16	0.6326387	0.60			0.59

Table C.18. Binary data for stars in the Argus moving group

HIP	HD	2MASS	Others/WDS	RUWE	RV km s^{-1}	RV err km s^{-1}	Nb	pvalue	RV ampl km s^{-1}	sep arcsec	PA degree	S/N PMA
7345	9672	J01343776-1540348	49 Cet	0.782	8.76	0.50	23	1.61E-01	9.18			1.69
		J05345923-2954041	CD-29 2360	1.912	25.45	0.38	28	3.87717E-05	5.91			
		J07015339-4227561	CD-42 2906	0.833	23.51	0.31	13	1.92E-01	2.35	6.25	109.97	
		J07282203-4908377	CD-48 2972	0.817	19.46	0.96	20	1.11E-16	14.58			
36312	59659	J07283006-4908589		0.982	18.38	0.36	15	6.88E-08	3.15	81.64	285.06	0.55
		J07311991-5447027	CPD-54 1295	0.977	19.46	0.37	9	0.5561346	2.86	3.45	9.55	
36948	61005	J07354747-3212141		0.940	22.35	0.14	29	3.73325E-05	1.45			1.27
		J07472597-4902511	CD-48 3199	1.045	16.94	0.95	17	0.002867112	10.15			
		J07484982-4327055	CD-43 3604	9.324	16.51	2.39	15	0	26.27	0.10	35.00	
		J07541770-5711131	TYC8561-1051-1	1.134	15.50	0.32	17	0.5484566	4.21	18.72	251.16	
										192.32	290.04	
		J07535548-5710073	TYC 8561-0970-1	1.014	15.27	0.84	16	0.006417626	11.87	3.54	174.30	
										479.77	35.38	
		J08391155-5834281	CD-58 2194	2.527	15.48	1.84	22	0	29.38			
										540.33	114.37	
		J08500812-5745593	CD-57 2315	6.460	8.54	1.93	9	0	12.70	0.10	197.00	
		J09020394-5808497	TYC 8594-0058-1	0.752	14.71	2.08	14	0	21.86			
	CPD-62 1197	J09133027-6259092	GSC08944-01516	3.794	7.08	2.09	26	0	23.85	0.04	55.69	
47135	84075	J09361783-7820417		0.968	5.26	0.19	19	0.002867148	1.81			1.78
		J09395143-2134175	BD-20 2977	0.984	18.52	0.51	12	0.006290988	4.44			
		J09424742-7239499	TYC 9217-0641-1	1.009	7.26	2.20	17	2.20787E-06	28.08	41.15	104.71	
		J09471986-4003098	CD-39 5833	0.955	15.14	0.36	30	0.004634501	6.13			
	85151			0.962						2.39	115.75	
	309851	J09555832-6721218		1.170	7.86	0.53	12	2.53547E-05	4.75			
50191	88955	J10144416-4207189	q Vel	2.873								0.97
51194	90874	J10272528-6542167	HR 4115	0.762	6.88	0.36	16	0.000724321	4.94			2.87
57013	101615	J11411978-4305442	HR4502	0.993	13.82	3.51	22	0	39.24			1.27
										8.35	182.48	
57632	102647	J11490366+1434197	beta Leo	1.125	11.49	0.14	12	0.68566024	0.79			
		J12063292-4247508	CD-42 7422	4.253	0.44	1.61	17	1.79E-12	22.38			
	CD-74 673	J12203437-7539286	TYC9412-1370-1	26.350	5.15	1.70	16	0	16.39			
	CD-75 652	J13491293-7549475	TYC9426-682-1	0.939	-2.18	0.92	6	2.2861E-06	5.16	21.33	256.95	
68994	123058	J14072929-6133441		0.886	-4.07	0.16	73	1.91E-07	3.48			1.49
	129496	J14462144-6746158		0.942	-3.11	1.22	14	0	12.92			
74405	133813	J15122343-7515156	NY Aps	1.008	-3.68	0.23	20	0.039328106	2.45			1.28
76736	138965	J15401155-7013403	HR5792	0.901	-9.38	0.30	28	0.17358921	5.35			1.21
79797	145689	J16170540-6756285	HR6037	0.890	-9.77	0.24	31	0.2854766	3.59	6.67	2.94	1.39
										6.67		
89925	168913	J18205694+2951317	HR6876, 108 Her	1.118								0.66
98103	188728	J19561425+1125254	phi Aql	0.787	-26.95	6.18	19	0	69.25	0.000878		2.28
										2.89	184.62	
										244.17	256.93	
98495	188228	J20003558-7254380	eps Pav	3.006	-8.13	0.52	19	0.022858383	5.00			2.11
99770	192640	J20143203+3648225	b03 Cyg	1.062	-20.52	0.40	19	1.86E-11	5.92			2.01

Table C.19. Binary data for stars in the BPMG

HIP	HD	2MASS	Others/WDS	RUWE	RV km s^{-1}	RV err km s^{-1}	Nb	pvalue	RV ampl km s^{-1}	sep arcsec	PA degree	S/N PMA
560	203	J00065008-2306271		0.933	6.06	0.49	18	7.13E-03	3.42			3.02
		J01373940+1835332	TYC1208-468-1	1.371	-2.15	1.74	7	6.08E-05	9.62	1.635	22.805	
10679	14082B	J02172472+2844305		0.919	5.00	0.16	12	3.93E-02	0.95			5.21
10680	14082	J02172527+2844423		1.008	5.54	0.27	12	8.29E-10	2.15			2.04
11437		J02272924+3058246	AG Tri	0.892	5.55	0.23	10	8.89E-01	1.62	22.002	315.683	0.57
21547	29391	J04373613-0228248	51 Eri	1.145								2.08
				22.864						66.963	162.627	
	286264	J05004928+1527006	V1841 Ori	1.025	14.92	3.18	14	0.00E+00	35.36			
25486	35850	J05270477-1154033	AF Lep	0.918	21.10	0.37	45	0.00E+00	8.82			8.99
27321	39060	J05471708-5103594	beta Pic	3.072	16.84	0.34	13	2.38E-12	3.17			0.86
29964	45081	J06182824-7202416	AO Men	0.843								1.52
76629		J15385757-5742273	V343 Nor	0.997	3.85	0.21	35	0.00E+00	3.22			22.87
				8.614	1.66	2.08	14	9.27E-08	20.04	10.316	323.344	
		J17150362-2749397	TYC 6820-0223-1									
84586	155555	J17172550-6657039		1.061	2.96	34.36	33	2.60E-01	7.03			4.87
				1.472						34.118	93.137	
		J17295506-5415487	TYC 8728-2262-1	0.897	-1.58	1.50	11	0.00E+00	12.22			
86598	160305	J17414903-5043279		0.993	1.28	0.43	19	2.05E-11	6.24			2.51
	161460	J17483374-5306433		1.067	2.91	2.31	14	8.48E-04	25.17			
88399	164249	J18030341-5138564		1.090	0.36	0.14	17	4.83E-02	1.05			3.98
				1.226	-0.63	1.25	14	5.60E-02	14.33	6.494	89.123	
88726	165189	J18064990-4325297	HR6749	1.137						1.777	1.489	3.83
89829	168210	J18195221-2916327		0.728								0.45
92024	172555	J18452691-6452165	HR7012	1.069	2.80	0.24	26	5.27E-13	3.29	71.331	64.622	2.46
		J18453704-6451460	CD-64 1208	10.937	6.18	1.91	16	0.00E+00	21.35			
	173167	J18480637-6213470								549.840	290.259	
92680	174429	J18530587-5010499	PZ Tel	0.949	-3.59	1.55	14	0.00E+00	11.76			4.40
		J19114467-2604085	TYC6878-195-1	11.992								
95261	181296	J19225122-5425263	eta Tel	1.013						416.326	170.669	2.16
95270	181327	J19225894-5432170		0.961								2.33
98839	190102	J20041810-2619461		0.928	-9.78	0.14	18	3.05E-01	0.87	3.082	110.558	5.10
99273	191089	J20090521-2613265		0.878	-6.13	0.15	17	6.00E-02	1.16			2.65
103311	199143	J20554767-1706509		1.033						324.924	138.353	56.68
										327.105	138.367	
107620	207043	J21475527-5255502		0.863	-0.01	0.12	32	8.11E-02	1.16			2.34

Table C.20. Binary data for stars in the Carina moving group

HIP	HD	2MASS	Others/WDS	RUWE	RV km s^{-1}	RV err km s^{-1}	Nb	pvalue	RV ampl km s^{-1}	sep arcsec	PA degree	S/N PMA
15201	21024	J03155768-7723184	iot Hyi	1.000	14.16	0.13	9	0.8163255	0.42			6.74
										275.57	77.14	
26144	37402	J05342614-6006151		8.692	21.79	1.22	16	0	11.45	0.01	166.00	1.61
										291.84		
	42270	J05532917-8156532		0.990	17.03	0.90	8	1.75E-14	6.66	2.08	285.32	
29314	43199	J06105289-6129594		0.978	14.47	0.53	20	8.48E-05	5.94			0.85
30034	44627	J06191291-5803156	AB Pic	0.923	22.02	0.19	21	2.47E-02	1.96	5.39	175.26	6.26
32235	49855	J06434625-7158356		1.019	20.45	0.22	11	3.45E-01	1.59			1.82
33737	55279	J07003046-7941459		1.120	17.08	0.38	14	1.15E-05	3.88			1.18
40916	70703	J08210046-5213406		0.837	22.32	0.74	15	2.23E-10	7.22			1.66
41081	71043	J08225514-5207254	HR 3300	0.762	24.82	0.70	16	1.14E-01	7.96			1.89
45585	80950	J09172755-7444045	HR 3721	1.070	17.22	0.20	12	9.57E-01	1.59			5.37
46063	81544	J09233498-6111359	V479 Car	0.975	19.54	0.51	18	8.27E-09	5.73			0.83
		J09303148-7041479	TYC 9200-446-1	0.762	24.82	0.70	16	1.14E-01	7.96			
46720	83096	J09312500-7344496		1.105						1.94	132.52	2.7
										55.02	105.85	
47391	83944	J09392101-6119410	m Car	0.790	23.45	0.78	20	5.32E-10	11.61	0.12		45.8
		J09534760-5453540	TYC 8602-718-1	4.861	24.14	0.78	9	2.82E-04	6.41			
	298936	J10131476-5230540	TWA-21	0.902	17.59	0.32	12	5.31E-02	2.65			
		J10300355-7432320	CD-73 584	0.894	16.92	0.33	13	3.60E-01	3.16			

Table C.21. Binary data for stars in the Carina Near moving group

HIP	HD	2MASS	Others/WDS	RUWE	RV km s^{-1}	RV err km s^{-1}	Nb	pvalue	RV ampl km s^{-1}	sep arcsec	PA degree	S/N PMA
35564	57852	HIP35564	HR2814	8.691	22.89	2.14	10	0.00E+00	16.96			0.88
	57853			22.137						9.05	26.72	
36414	59704	J07293141-3807217		0.941	26.65	0.23	24	0.00E+00	3.13			1.25
37563	62850	J07423606-5917507		0.960	17.48	0.14	16	1.17E-01	1.01			1.41
37635	62848	J07432149-5209508		17.534	18.33	0.30	15	0.00E+00	2.91			45.54
37918	63581	J07461480-5948506		17.199	17.73	0.27	18	0.00E+00	3.20	0.065	282.1	25.39
										23.15	44.63	
37923	63608	J07461694-5948341		1.176	17.43	0.14	17	1.46E-02	0.91			0.18
40188	69051	J08123271-5408473		0.894	28.76	0.28	18	6.31E-05	2.74	2.59	299.85	0.9
40774		J08191905+0120198	V0397 Hya	1.053			10		0.05			0.88
42074	72760	J08343166-0043339		0.992	35.00	0.12	25	0.985	0.44			78.51
58240	103742	J11564232-3216053		1.058	6.35	0.13	29	6.59E-02	1.13	18.70	81.71	0.89
58241	103743	J11564379-3216026		1.027	6.98	0.13	30	3.01E-01	1.38			2.1
60831	108574	J12280445+4447394		0.905	-2.31	0.13	27	1.98E-02	1.02			3.12
										9.71	156.98	
60832	108575	J12280480+4447305		1.067	-2.05	0.17	4	5.33E-01	0.48			5.94
60994	108799	J12300479-1323350	HR4758	0.927	1.30	0.14	21	1.57E-04	1.00	2.12	346.77	84.19
68030	121560	J13554999+1403234		0.926	-10.27	0.12	20	6.88E-01	0.75			1.89

Table C.22. Binary data for stars in the Columba moving group

HIP	HD	2MASS	Others/WDS	RUWE	RV km s^{-1}	RV err km s^{-1}	Nb	pvalue	RV ampl km s^{-1}	sep arcsec	PA degree	S/N PMA
3210	3888	J00405159-5312357		1.081	9.08	0.18	32	2.41E-10	2.62	0.05		1.55
6165	8077	J01190560-5351020		0.951	12.16	0.43	13	3.35E-09	4.19			1.22
7805	10472	J01402406-6059566		0.945	14.29	0.25	24	3.08E-06	3.58			2.21
	TYC8047-232-1	J01521461-5219332	CD-52 381	0.869	13.35	1.25	27	3.39E-10	11.47	3.27	358.84	
11029	14691	J02220152-1046390	HR692	0.893	12.79	0.25	18	6.11E-09	2.75			2.87
12413	16754	J02394796-4253300	HR789	5.363						0.11		45.58
										25.32	8.19	
14551	19545	J03075083-2749520	HR943	4.176	16.86	0.75	30	0.00E+00	11.76	0.044		7.18
										59.30	203.07	
14913	20121	J03122575-4425111	HR968	0.996						0.30	135.00	
										3.57	190.20	
16449	21997	J03315364-2536509	HR1082	1.079	16.04	0.17	51	0.7131891	3.94			3.48
17675	23384	J03471061+5142230		0.995	-1.68	0.24	21	4.44E-16	2.56			3.15
17782	23524	J03482301+5202163								0.25		
19775	26980	J04142257-3819016		0.946	15.65	0.12	23	0.19978106	0.86			1.18
	27679	J04211032-2432211		1.016	21.52	0.21	34	2.05676E-05	3.52			
		J04345077-3547211	CD-36 1785	0.975	21.61	0.56	22	0.003181187	7.18			
		J04411573-3513582	CPD-35 525	0.941	23.14	0.18	26	0.03661233	2.33			
22152	29329	J04460056+7636399	HR1468	0.900	-9.80	0.28	17	0	3.10			3.09
22226	30447	J04464950-2618087		1.042	23.62	0.23	28	0.051032983	3.59			1.94
	31242	J04515354-4647134	CD-46 1587	0.976	20.86	0.39	18	0.013338176	4.95	18.38	196.50	
		J04515303-4647309	GSC8077-1788	2.529	24.32	4.70	22	0	59.53			
	272836	J04530520-4844386		1.018	22.90	0.37	8	0.21698473	2.24	1.52	358.71	
23171	32476	J04590561-6325297		1.096						1.52	289.97	2.71
23179	31647	J04591543+3753251	Omega Aur	1.086						4.74	4.30	0.85
23316	32372	J05005186-4101065		0.877	22.46	0.27	15	0.007667075	2.80			1.64
23362	32309	J05012558-2003067	HR1621	1.123	26.62	0.63	29	0.049831875	9.05			1.95
24947	35114	J05203803-3945179	AS Col	0.956	24.72	0.45	19	0	5.76			2.18
25436	35996	J05262401-4322325	CD-43 1847	1.065	24.37	0.71	18	0	8.58	12.01	252.58	1.46
25434		J05262296-4322360	CD-43 1846	0.852	25.83	0.76	13	0	8.26	0.0576	302	6.13
	35841	J05263658-2229238	BD-22 1109	0.983	23.95	0.25	27	6.27941E-05	3.31	164.63	147.19	
	274561	J05285509-4534584	CD-45 2003	0.842	22.97	0.61	24	1.87E-08	8.96			
25709	36329	J05292409-3430554	CD-34 2279	1.050								1.7
		J05301907-1916318	AG Lep	1.575	24.62	0.57	20	0	8.67			
				16.36	16.21							
	36869	J05340914-1517031	AH Lep	1.013						8.31	152.20	
26309	37286	J05361029-2842289	HR1915	0.992	24.77	0.23	25	0.15054144	3.29			0.7
26395	37306	J05370877-1146317		1.031								1.29
26453	37484	J05373962-2837346		1.032	25.66	0.15	26	0.26487374	1.45			0.67
	TYC 5346-132-1	J05383500-0856405	BD-08 1195	1.046	23.87	0.73	18	0	7.38			
	TYC 5925-1221-1	J05402073-1940108	AI Lep	0.990								
	38207	J05432094-2011214	BD-20 1162	0.905	26.12	0.28	25	0.11601605	4.31			
26966	38206	J05432166-1833268	HR1975	0.982	25.49	0.35	20	0.9752228	1.91			1.11
26990	38397	J05433580-3955246		1.061	24.20	0.17	18	0.009607261	1.40			1.74
	TYC 6502-1188-1	J05502142-2915206	CD-29 2531	1.243	26.65	1.12	13	0.13073398	8.71	519.43	134.40	
	TYC 8520-32-1	J05510116-5238126	CD-52 1363	0.932	21.56	1.47	12	1.58E-11	11.05			
28036	40216	J05554314-3806162	CD-38 2296	0.966	25.50	0.17	23	1.49797E-06	1.58	2.17	246.10	10.51
28474	41071	J06004130-4453500	RT Pic	1.012	24.24	0.18	17	0.015156002	1.71	0.696	75.42	20.37
	TYC 5944-411-1	J06050784-2143305		0.918	25.96	0.14	42	0.10430364	2.44			
30030	43989	J06190805-0326203	V1358 Ori	0.930	20.36	0.38	17	7.44E-15	4.88			1.78
	TYC 7617-549-1	J06260690-4102538	CD-40 2458	0.942	25.66	0.34	15	6.34809E-05	3.44			
	295290	J06402236-0331591	TYC4803-1418-1	1.095								
32104	48097	J06422431+1738430	26 Gem	8.173	13.17	1.52	7	0	7.29	0.036		0.58
	48370	J06430102-0253192	BD-02 1732	1.112	23.63	0.18	18	0.000511343	1.48			
	TYC 7100-2112-1	J06524674-3636169	CD-36 3202	0.921	21.56	5.21	29	0	97.59			
	51797	J06562354-4646549	CD-46 2777	0.971	24.75	0.32	10	0.04290542	2.08			
114189	218396	J23072869+2108033	HR8799	1.474	-10.41	0.23	19	6.10E-09	2.50			4.68
116805	222439	J23402449+4420021	kap And	1.908						1.06		1.62

Table C.23. Binary data for stars in the Tuc-Hor moving group

HIP	HD	2MASS	Others/WDS	RUWE	RV km s⁻¹	RV err km s⁻¹	Nb	pvalue	RV ampl km s⁻¹	sep arcsec	PA degree	S/N PMA
490	105	J00055255-4145109		0.912	2.05	0.16	19	5.44E-04	1.54			2.85
1113	987	J00135300-7441178		0.834	9.09	0.19	19	1.11E-02	2.41			0.70
1481	1466	J00182612-6328389		0.994	6.53	0.16	27	4.86E-06	1.57			3.46
2484	2884	J00313267-6257297	bet1 Tuc	0.839	10.77	0.45	17	3.28E-01	5.44	2.4		1.63
2487	2885	J00313347-6257560	bet2 Tuc							27.02	168.28	
2578	3003	J00324391-6301533	bet3 Tuc	1.025	3.60	0.25	20	8.65E-01	3.08	0.1	172	0.47
										552.82	118.50	
2729	3221	J00345120-6154583		2.080	5.19	1.00	26	0.00E+00	15.65	0.02	250.00	2.07
	TYC 9351-1110-1	J00422033-7747397	CD-78 24	0.976	10.92	0.45	17	3.16E-06	5.40			
	TYC 7002-2219-1	J01220441-3337036	CD-34 521	1.138	4.50	0.21	29	2.50E-01	3.26			
6485	8558	J01232126-5728507		1.070	8.68	0.17	23	2.46E-02	1.72			1.62
6856	9054	J01280868-5238191	CC Phe	0.872	7.93	0.18	20	5.45E-01	1.73			0.90
7699	10269	J01390761-5625459		1.027	9.42	0.16	29	1.54E-01	2.15			0.92
8233	10863	J01460105-2720556	HR517	1.071	8.98	0.36	28	1.51E-04	5.15			3.01
9141	12039	J01574896-2154052	DK Cet	0.966	5.99	0.18	22	1.06E-06	2.01	0.20	324.00	2.24
9892	13183	J02071805-5311565		0.982								1.09
9902	13246	J02072611-5940459		0.996	10.80	0.21	27	0.00E+00	3.01	101.48	346.89	1.75
	TYC 8489-1155-1	J02073220-5940210	CD-60 416	0.920	9.39	0.49	23	8.07E-11	8.30			
10602	14228	J02163059-5130437	phi Eri	2.390								0.74
11360	15115	J02261625+0617331		1.127	6.91	0.27	15	3.96E-06	2.57			1.73
12394	16978	J02393538-6816008	eps Hyi	2.626								0.44
	TYC 8060-1673-1	J03304909-4555573	CD-46 1064	0.921	14.44	0.23	18	4.06E-04	2.51			
	22213	J03341633-1204073		0.983							1.69	279.68	
15247	20385	J03164066-0331489		1.332	10.21	0.48	8	1.28E-04	2.89	0.84	120.55	66.00
16853	22705	J03365341-4957288		9.442	15.73	1.76	16	0.00E+00	16.01			5.21
										2.71	89.11	
17764	24636	J03481148-7441388		0.929	14.49	0.15	27	5.00E-05	1.74			2.41
17797		HIP 17797	f Eri	1.966						0.13	7.81	11.48
				1.371						8.37	36.62	
	24071	J03483548-3737190		0.961						86.21	-38.62	
18714	25402	J04003198-4144544		1.47	15.22	0.53	21	0.00E+00	6.79	0.0442	351.6	71.88
										8.76	159.60	
	TYC 5882-1169-1	J04021648-1521297	BD-15 705	1.041	14.51	0.27	23	5.37E-05	3.34			
	TYC 5324-1293-1	J04364709-1209207	BD-12 943	0.957	17.20	0.28	24	6.63E-03	4.03	13.54	233.67	
20042	27376	J04175366-3347540	ups04 Eri	2.960						5.45	162.89	
												1.32
21632	29615	J04384393-2702018		1.027	18.24	0.30	23	0.00E+00	3.48	23.03	90.48	0.81
21965	30051	J04431720-2337419		26.654	20.93	0.54	43	0.00E+00	4.78			5.11
22295	32195	J04480518-8046452		0.957	14.30	0.30	18	1.59E-06	3.73			1.54
	TYC 5908-230-1	J04593202-1917416	BD-19 1062	1.102	19.46	0.20	28	5.95E-01	3.03			
	TYC 5335-312-1	J05153652-0930512	BD-09 1108	1.077	20.66	0.33	28	1.96E-09	5.00	11.23	250.37	
										10.83	245.87	
32435	53842	J06461348-8359294		1.031	13.75	0.18	23	3.90E-08	1.71	1.44	313.28	4.30
100751	193924	J20253886-5644062	alpha Pav									
105388	202917	J21204994-5302030		0.900	-1.95	0.23	17	3.55E-02	2.68			2.61
107947	207575	J21520973-6203085		0.852	2.59	0.15	44	4.11E-15	2.09			2.37
108422	208233	J21575146-6812501		10.369	5.95	4.66	8	0.00E+00	35.72			2.72
										1.63	192.41	
	TYC 5242-324-1	J23093711-0225551	BD-03 5579	1.080	-12.69	0.31	13	1.91E-01	2.61			
	TYC 9529-0340-1	J23274943-8613187	CD-86 147	1.039	9.45	1.76	10	0.00E+00	12.64			
	222259B	J23393929-6911396	DS Tuc B	0.954	5.17	0.42	10	1.13E-02	2.84			
116748	222259A	J23393949-6911448	DS Tuc A	0.912	7.13	0.28	17	1.00E-05	3.34	5.37	347.65	4.65

Table C.24. Binary data for stars in the Volans/Crius 221 moving group

HIP	HD	2MASS	Others/WDS	RUWE	RV km s^{-1}	RV err km s^{-1}	Nb	pvalue	RV ampl km s^{-1}	sep arcsec	PA degree	S/N PMA
		J00301560-8613552	TYC 9494-799-1	0.929	14.21	0.21	15	0.00314	1.79			
	67928	J08075272-5135016	TYC 8148-343-1	2.251						0.70	183.00	
	69406	J08134777-5837139	CPD-58 1080B	1.661	27.87	0.33	22	0.00002	5.08			
										6.95	172.40	
		J08363202-6024116	TYC 8926-337-1	0.996	25.96	0.30	25	0.79582	5.16			
45096	299896	J09111005-5501535	TYC 8587-323-1	0.801	26.85	0.25	8	0.06292	1.57			0.92
	79648	J09134337-4642014	TYC 8166-809-1	0.915	26.59	0.17	18	0.30521	1.94			
45478	80157	J09160129-5533297	TYC 8587-1754-1	0.904	26.37	0.17	29	0.01570	2.25			2.43
		J09231316-4520256	TYC 8167-1155-1	0.920	26.95	0.43	22	0.01823	6.65			
47351	83946	J09385410-6459267	TYC 8949-116-1	0.768	22.21	0.46	10	0.00003	3.22			2.17
		J09430884-6313043	TYC 8946-1225-1	1.892	19.93	2.64	12	0.00000	22.67	0.15	324.00	
										48.23	141.45	
		J10111554-6530330	TYC 8951-622-1	0.946	21.53	0.18	13	0.96463	1.35	3.55	145.81	
		J10295615-6451235	TYC 8964-396-1	0.891	21.30	0.39	16	0.17815	4.52			
52462	92945	J10432828-2903513	TYC 6645-338-1	0.980	22.57	0.13	28	0.00485	1.07			3.38
52787	93528	J10473117-2220528	TYC 6081-65-1	0.968	23.76	0.15	12	0.15481	0.94	234.77	340.08	0.63
54155	96064	J11044148-0413159	TYC 4924-1114-1	0.977	18.50	0.13	19	0.72239	0.79	11.72	222.00	3.64
		J11110405-7824116	TYC 9414-379-1	1.229	15.34	0.34	12	0.04961	3.36	1.74	24.72	
58029	103381	J11540534-2958570	TYC 6678-1031-1	1.007	15.71	0.16	18	0.00028	1.70			1.91
	104315	J12003839-7200251	TYC 9235-1497-1	0.845	16.31	0.31	16	0.01791	3.30			
		J12170220-5546112	TYC 8637-2580-1	0.997	16.05	0.21	21	0.14589	2.74			
61284	109138	J12332981-7523112	TYC 9412-190-1	0.978	16.18	0.28	9	0.12018	1.75			1.64
		J12543443-4558310	TYC 8245-2246-1	0.937	12.20	0.34	8	0.03156	2.02	2.22	125.33	
										53.68	183.22	
		J13193133-7036309	TYC 9246-361-1	0.989	12.95	0.31	16	0.02818	3.22			
73052	130943	J14554612-7309599	TYC 9270-1659-1	0.914	10.50	0.13	26	0.72946	1.25			2
	153555	J17041857-6233182	TYC 9043-817-1	0.827	0.80	0.33	9	0.00118	2.27	61.86	229.75	
84642	155915	J17181464-6027275	TYC 9052-1117-1	1.457	2.93	0.27	16	0.01420	3.19	0.22	191.30	70
		J17244456-5153425	TYC 8353-292-1	0.854	-4.07	0.29	19	0.05813	3.45			
	321224	J18025629-3643280	TYC 7403-6190-1	0.630	-11.51	0.19	5	0.66403	0.71			
96334	183414	J19350972-6958321	TYC 9309-599-1	0.995	3.22	0.13	25	0.07587	1.25			4.63
96880	184587	J19413575-7226457	TYC 9314-767-1	0.872	4.60	0.14	24	0.32864	1.41			1.36
		J08264964-6346369	TYC 8933-327-1	11.87	29.59	1.31	28	0	16.57			
	73129	J08324622-6508272		0.914	5.27	0.35	14	0.00028	3.14	387.84	122.44	
43783	76728	J08550282-6038406	HR3571	3.731	22.65	0.46	22	0.0022	7.25			9.86
										17.90	317.00	
45594	80563	J09173415-6323145		1.067	24.22	0.20	20	0.044	2.21			1.87
46460	82406	J09283051-6642067	HR3783	3.192	16.94	11.82	9	0	72.02			1.69
47017	83359	J09345645-6459579		0.971	42.82	11.93	18	0	122.37			1.46
										10.67	203.98	
47115	83253	J09360518-6457011		0.773							1.05	169.30	5.98
										471.03	247.91	
47335	83948	J09384522-6651326		1.011	25.47	0.30	26	0.0194	4.40	350.30	25.13	1.93
		J09391046-6646155	TYC 8953-1289-1	0.821	22.29	0.27	22	0.265	4.22			
47351	83946	J09385410-6459267		0.768	22.21	0.46	10	2.91E-05	3.21			2.17
		J09481924-6403217	TYC 8950-1447-1	0.902	22.37	0.30	19	0.322	4.23			
		J10082200-6756402	TYC 9210-1818-1	0.948	20.81	0.35	18	0.550	4.67	23.84	179.32	
	CD-67 852	J10122991-6752334	TYC 9210-1730-1	0.959	21.32	0.19	17	0.410	1.87			
50567	89928	J10194613-7133173		44.080	17.10	0.46	17	0	5.0			12.73

Table C.25. Mass and separation of companions in the AB Dor moving group

HIP	HD	2MASS	Others/WDS	M_A $M_\odot$	M_B $M_\odot$	a au	q	Method	Source
	1405	J00182085+3057224	PW And	0.877					
3589	4277	J00455088+5458402		1.106	0.848	131.996	0.767	VIS	Cvetković (2011)
5191	6569	J01062614-1417468		0.911	0.204	1025.517	0.224	VIS	Gaia
6276		J01203226-1128035	BD-12 243	0.952					
	236717	J01242709+5751062		0.956					
		J02051802+5217027	TYC 3293-1912-1	0.862					
10272	13482	J02121535+2357298	J02123+2357AB	1.001	0.875	63.303	0.874	VIS	Gaia
		J02223387+5033369	BD+49 646	0.929					
11696	15407A	J02305064+5532543		1.385	0.0048	7.7	0.0035	DYN	Mesa, 2024, in preparation
				1.389	0.896	1049.30	0.65	VIS	Gaia
12635	16760B	J02422094+3837212		0.853	0.267	2.16	0.31	DYN	Pma+RUWE+RV
12638	16760	J02422130+3837073		1.018	0.367	1.310	0.36	DYN	Tokovinin (2018)
				1.388	0.889	825.767	0.641	VIS	Gaia
13027	17332		J02475+1922AB	1.041	0.971	120.644	0.932	VIS	Gaia
13209	17573	J02495902+2715381	41 Ari	2.960	1.470	9.451	0.497	DYN	Speckle inteferometry
14684	19668	J03094227-0934463	IS Eri	0.964					
14809/14807		J03111383+2224571	J03112+2225A	1.014	0.826	1684.042	0.81	VIS	Gaia
15353	20888	J03175907-6655367	J03180-6656A	1.733	0.439	300.615	0.253	VIS	Gaia
16563	21845	J03331347+4615269	J03332+4615A	0.976	0.654	345.747	0.669	VIS	Gaia
			GD50	7.800					Gagné et al. (2018b)
	24681	J03552040-0143451	TYC4718-894-1	0.989					
18859	25457	J04023675-0016078	HR1249	1.182					
19183	25953	J04064153+0141020		1.171	0.360	239.399	0.307	VIS	Bonavita et al. (2022a)
19422	25665	J04093502+6932292		0.899					
		J04213348-2543091	CD-26 1643	1.063					
	28982	J04330622-2400477	EB	0.973	0.800	11	0.82	DYN	Prša et al. (2022)
				1.773	0.085	108.29	0.05	VIS	Gaia
	31652	J04572232-0907595		0.982					
		J05023042-3959129	CD-40 1701	0.830					
		J05044132+4024003	TYC2899-1744-1	0.818	0.203	2.726	0.25	DYN	RUWE+RV
				1.021	0.250	167.681	0.24	VIS	Gaia
	32981	J05062769-1549303		1.089					
25647	36705	J05284484-6526551	AB Dor	0.928	0.090	4.654	0.097	VIS	Tokovinin (2018)
				1.018	0.660	135.655	0.648	VIS	Gaia (sec is a binary: Tokovinin (2018))
		J05350411-3417519	CD-34 2331	0.810	0.800	31893.086	0.988	VIS	Gaia (sec is a binary: Tokovinin (2018))
26373	37572	J05365685-4757528	J05369-4758A	0.943	0.810	448.987	0.859	VIS	Gaia (sec is a binary: Tokovinin (2018))
26401	37551		J05372-4243AB	1.003	0.923	321.971	0.920	VIS	Gaia
				1.926	0.248	12672.838	0.129	VIS	Gaia
			CP-19 878	0.898					
		J06083386-3402549	CD-34 2676	0.967	0.210	7.619	0.217	VIS	Bonavita et al. (2022a)
				1.177	0.490	48.655	0.416	VIS	Bonavita et al. (2022a)
				1.667	0.810	16162.348	0.486	VIS	Gaia (sec is a binary: Tokovinin (2018))
30314	45270	J06223097-6013072		1.058	0.0011	13.28	0.0010	DYN	Mesa et al. (2022)
31711	48189	J06380036-6132001	HR 2468	1.063	0.720	20.217	0.678	VIS	Tokovinin (2018)
		J07305952-8419275	CD-84 80	0.951	0.720	41.496	0.757	VIS	Mason et al. (2001)
37855	64982	J07453559-7940080		1.118	0.205	1.94	0.18	DYN	Pma+RUWE+RV
				1.323	0.810	502.094	0.614	VIS	Gaia. Sec is a binary (Tokovinin 2018)
55746	99827	J11251773-8457164		1.350	1.050	5.422	0.778	VIS	Tokovinin (2018)
				2.400	0.670	322.489	0.280	VIS	Tokovinin (2018)
				3.320	0.050	26319.732	0.016	VIS	Gaia
		J12361640-7931344	TYC 9420-68-1	0.862	0.807	1140.93	0.94	VIS	Gaia
		J12361110-7931384	TYC 9420-112-1						
63742	113449	J13034967-0509423	J13038-0510AB	0.917	0.510	0.696	0.556	DYN	Pourbaix et al. (2004); Bonavita et al. (2016)
80218	147512	J16223272-0414571	LTT 6534	0.995					
82688	152555	J16540815-0420248		1.068	0.182	171.679	0.170	VIS	Gaia, Bonavita et al. (2022a)
	317617	J17285563-3243568		0.945	0.240	23.791	0.254	VIS	Bonavita et al. (2022a)
				1.185	0.461	136.193	0.389	VIS	Gaia, Bonavita et al. (2022a)
93375	176367	J19010604-2842502		1.087					
94235	178085	J19105782-6016202		1.080	0.262	32.30	0.243	VIS	Zhou et al. (2022)
				1.082	0.262	32.296	0.243	VIS	
95347	201919	J19235315-4036571	Alpha Sgr	3.079					
		J19330374+0345397	TYC0486-4943	0.838	0.514	1970.402	0.614	VIS	
		J20044935-0239203	BD-03 4778	0.936	0.270	179.273	0.288	VIS	
109268	209952	J22081397-4657393	Alpha Gru	4.367					
113579	217343	J23001929-2609135	J23005-2619C	1.015					
113597	217379	J23002791-2618431	J23005-2619AB	0.610	0.570	0.154	0.93	DYN	Tokovinin (2018)
				1.180	0.664	69.78	1.09	VIS	Gaia
114530	218860	J23115205-4508106		0.977	0.393	929.169	0.402	VIS	Gaia
115162		J23193955+4215098		0.976					
115738	220825	J23265595+0115201	kap Psc	2.068					
116910	222575	J23415428-3558397		0.976					
117452	223352	J23485554-2807490	delta Scl	2.139	1.240	161.683	0.580	VIS	Tokovinin (2018)
				3.379	1.250	3286.926	0.584	VIS	Gaia, Tokovinin (2018)
118008	224228	J23561067-3903086		0.880					

Table C.26. Mass and separation of companions in the Argus moving group

HIP	HD	2MASS	Others/WDS	M_A $M_\odot$	M_B $M_\odot$	a au	q	Method	Source
7345	9672	J01343776-1540348	49 Cet	1.910					
		J05345923-2954041	CD-29 2360	0.853	0.144	0.313	0.169	DYN	RUWE-Pma-RV
		J07015339-4227561	CD-42 2906	0.935	0.315	549.947	0.337	VIS	Gaia
		J07282203-4908377	CD-48 2972	1.002					
36312	59659	J07283006-4908589		1.160	1.002	7150.207	0.864	VIS	Gaia
		J07311991-5447027	CPD-54 1295	0.981	0.180	369.863	0.184	VIS	Gaia
36948	61005	J07354747-3212141		0.977					
		J07472597-4902511	CD-48 3199	0.985					
		J07484982-4327055	CD-43 3604	0.770	0.720	9.420	0.926	VIS	Mason et al. (2001)
		J07541770-5711131	TYC8651-1051-1	1.045	0.998	2911.876	0.955	VIS	Gaia
				2.044	1.226	29917.323	0.600	VIS	Gaia
		J07535548-5710073	TYC 8561-0970-1	0.951	0.275	550.241	0.289	VIS	Gaia
				3.269	0.843	74631.764	0.258	VIS	Gaia
		J08391155-5834281	CD-58 2194	1.024	0.658	0.253	0.643	DYN	RUWE-Pma-RV
				1.682	0.069	61913.853	0.041	VIS	Gaia
		J08500812-5745593	CD-57 2315	0.804	0.787	9.740	0.973	VIS	Mason et al. (2001)
		J09020394-5808497	TYC 8594-0058-1	0.969					
	CPD-62 1197	J09133027-6259092	GSC08944-01516	0.905	0.706	4.155	0.782	VIS	Bonavita et al. (2022a)
47135	84075	J09361783-7820417		1.068					
		J09395143-2134175	BD-20 2977	0.963					
		J09424742-7239499	TYC 9217-0641-1	0.898	0.230	0.051	0.256	DYN	RUWE-Pma-RV
				1.128	0.100	6414.589	0.088	VIS	Gaia
		J09471986-4003098	CD-39 5833	0.955					
	85151			1.084	0.996	254.039	0.919	VIS	Gaia
	309851	J09555832-6721218		1.061					
50191	88955	J10144416-4207189	q Vel	2.110	0.559	0.285	0.265	DYN	RUWE-Pma-RV
51194	90874	J10272528-6542167	HR 4115	1.868					
57013	101615	J11411978-4305442	HR4502	2.040	0.482	0.045	0.236	DYN	RUWE-Pma-RV, Prša et al. (2022)
				2.522	0.378	534.698	0.150	VIS	Gaia
57632	102647	J11490366+1434197	beta Leo	1.855					
		J12063292-4247508	CD-42 7422	0.973	0.635	0.47	0.653	DYN	RUWE-Pma-RV
	CD-74 673	J12203437-7539286	TYC9412-1370-1	0.886	0.564	1.60	0.636	DYN	RUWE-Pma-RV
	CD-75 652	J13491293-7549475	TYC9426-682-1	1.003	0.109	1763.665	0.109	VIS	Gaia
68994	123058	J14072929-6133441		1.385					
	129496	J14462144-6746158		1.115					
74405	133813	J15122343-7515156	NY Aps	0.936					
76736	138965	J15401155-7013403	HR5792	1.810					
79797	145689	J16170540-6756285	HR6037	1.689	0.058	366.768	0.067	VIS	Huélamo et al. (2010)
				1.747	0.055	366.768	0.947	VIS	Nielsen et al. (2013)
89925	168913	J18205694+2951317	HR6876, 108 Her	1.867	1.600	0.092	0.857	DYN	Fekel et al. (2009)
98103	188728	J19561425+1125254	phi Aql	2.285	0.520	0.060	0.228	DYN	Tokovinin (2018)
				2.805	0.334	195.989	0.146	VIS	Gaia
				3.139	0.113	16556.750	0.036	VIS	Gaia
98495	188228	J20003558-7254380	eps Pav	2.086					
99770	192640	J20143203+3648225	b03 Cyg	1.845	0.0161	16.90	0.0087	VIS	Currie et al. (2023)

Table C.27. Mass and separation of companions in the BPMG

HIP	HD	2MASS	Others/WDS	M_A $M_\odot$	M_B $M_\odot$	a au	q	Method	Source
560	203	J00065008-2306271		1.342	0.0017	16.6	0.0013	DYN	
	TYC1208-468-1			0.884	0.738	86.3	0.835	VIS	Gaia DR3
10679	14082B	J02172472+2844305		1.103					Gaia DR3
10680	14082	J02172527+2844423		1.169	1.016	544.0	0.869	VIS	Gaia DR3
		J02272924+3058470	AG Tri	0.820	0.490	900.860	0.598	VIS	
21547	29391	J04373613-0228248	51 Eri	1.486	0.005	11.1	0.0031	VIS	De Rosa et al. (2020); Samland et al. (2017)
				1.491	0.645	2002.468	0.433	VIS	Gaia DR3
	286264	J05004928+1527006	1841 Ori	0.810					
25486	35850	J05270477-1154033	AF Lep	1.152	0.005	9.0	0.0047	VIS	Gratton et al. (2023c)
27321	39060	J05471708-5103594	beta Pic	1.629	0.007	2.7	0.0042	VIS	Lacour et al. (2021)
				1.635	0.011	9.930	0.0068	VIS	Lacour et al. (2021)
29964	45081	J06182824-7202416	AO Men	0.880					
76029	138029	J15314272-5158333	V343 Nor	1.180	0.290	2.9	0.246	VIS	VIS
				1.470	0.430	399.400	0.293	VIS	
		J17150362-2749397	TYC6820-0223-1	0.980	0.930	10.3	0.949	VIS	Bonavita et al. (2022a)
84586	155555	J17172550-6657039	V824 Ara	1.156	1.080	0.036	0.936	DYN	Tokovinin (2018)
				2.236	0.0038	7.3	0.0017	DYN	Gratton et al. (2023a)
				2.238	0.490	1035.435	0.219	VIS	Gaia DR3
		J17295506-5415487	TYC8728-2262-1	0.980	0.140	0.060	0.143	DYN	SB
86598	160305	J17414903-5043279		1.148					
	161460	J17483374-5306433		1.110	1.030	8.4	0.928	VIS	
88399	164249	J18030341-5138564		1.246	0.0043	7.0	0.0035	DYN	Mesa et al. (2022)
				1.246	0.509	320.062	0.408	VIS	Gaia DR3
88726	165189	J18064990-4325297	HR6749	1.621	1.593	78.161	0.983	VIS	Gaia DR3; Hagelberg et al. (2020)
89829	168210	J18195221-2916327		1.145					
92024	172555	J18452691-6452165	HR7012	1.655	0.749	2164.834	0.453	VIS	Tokovinin (2018)
		J18453704-6451460	CD-64 1208	0.848	0.280	7.160	0.330	VIS	VIS
	173167	J18480637-6213470		1.207	0.603	1.530	0.500	VIS	Tokovinin (2018)
				1.810	0.627	27811.819	0.346	VIS	Gaia DR3
92680	174429	J18530587-5010499	PZ Tel	1.095	0.056	20.000	0.051	VIS	Vigan et al. (2021)
95261	181296	J19225122-5425263	eta Tel	2.010	0.048	197.070	0.024	VIS	Bonavita et al. (2022a)
				2.058	1.263	20210.017	0.614	VIS	Rameau et al. (2013); Vigan et al. (2021)
95270	181327	J19225894-5432170		1.228					Gaia DR3
98839	190102	J20041810-2619461		1.102	0.005	7.500	0.0044	DYN	Gaia DR3
99273	191089	J20090521-2613265		1.221					
103311	199143	J20554767-1706509		1.182	0.720	50.505	0.609	VIS	Tokovinin (2018)
				1.902	1.182	14918.460	0.627	VIS	Gaia DR3
107620	207043	J21475527-5255502		1.080					

Table C.28. Mass and separation of companions in the Carina moving group

HIP	HD	2MASS	Others/WDS	M_A $M_\odot$	M_B $M_\odot$	a au	q	Method	Source
15201	21024	J03155768-7723184	iot Hyi	1.413	0.0135	17.8	0.0096	DYN	PMa+RUWE+RV
				1.422	0.116	8042.698	0.082	VIS	Gaia
26144	37402	J05342614-6006151		1.149	0.473	0.915	0.412	VIS	SB
				1.622	0.270	20754.354	0.167	VIS	Gaia
	42270	J05532917-8156532		0.989	0.571	122.322	0.577	VIS	Gaia
29314	43199	J06105289-6129594		1.446					
30034	44627	J06191291-5803156	AB Pic	0.965	0.0080	3.570	0.0071	DYN	PMa+RUWE+RV
				1.140	0.022	270.247	0.019	VIS	Vigan et al. (2021)
32235	49855	J06434625-7158356		0.971					
33737	55279	J07003046-7941459		0.928					
40916	70703	J08210046-5213406		1.658					
41081	71043	J08225514-5207254	HR 3300	1.952					
45585	80950	J09172755-7444045	HR 3721	2.072	0.00176	6.8	0.0085	DYN	PMa+RUWE+RV
46063	81544	J09233498-6111359	V479 Car	1.014					Elliott et al. (2015) is background using Gaia data
	TYC 9200-446-1	J09303148-7041479		0.989					
46720	83096	J09312500-7344496		1.448	1.024	151.807	0.707	VIS	Gaia
				2.472	0.333	4294.486	0.135	VIS	Gaia
47391	83944	J09392101-6119410	m Car	3.007	0.353	8.440	0.117	DYN	PMa+RUWE+RV
	TYC 8602-718-1	J09534760-5453540		0.911	0.237	2.53	0.260	DYN	PMa+RUWE+RV
	298936	J10131476-5230540	TWA-21	0.920					
		J10300355-7432320	CD-73 584	0.932					

Table C.29. Mass and separation of companions in the Carina-Near moving group

HIP	HD	2MASS	Others/WDS	M_A $M_\odot$	M_B $M_\odot$	a au	q	Method	Source
35564		J070202142-5218413	HR2814	1.387	0.683	1.046	0.492	DYN	RUWE+Pma+RV
				2.070	1.626	316.003	0.785	VIS	Gaia
	57853			1.226	0.400	0.567	0.326	VIS	Tokovinin (2018)
36414	59704	J07293141-3807217		1.153					
37563	62850	J07423606-5917507		1.060					
37635	62848	J07432149-5209508		1.108	0.180	3.84	0.163	DYN	RUWE+Pma+RV
37918	63581	J07461480-5948506		0.972	0.280	1.931	0.253	VIS	Bonavita et al. (2022a)
				1.252	0.961	794.662	0.989	VIS	Gaia
37923	63608	J07461694-5948341		0.958					
40188	69051	J08123271-5408473		1.671	0.148	217.40	0.089	VIS	Gaia
40774		J08191905+0120198	V0397 Hya	0.867					
42074	72760	J08343166-0043339		0.952	0.130	31.95	0.137	VIS	Hirsch et al. (2021)
58240	103742	J11564232-3216053		1.022	1.006	664.037	0.984	VIS	Gaia
58241	103743	J11564379-3216026		1.005					
60831	108574	J12280445+4447394		1.147	0.0034	9.5	0.0030	DYN	RUWE+Pma+RV
				1.156	1.041	440.072	0.908	VIS	Gaia
60832	108575	J12280480+4447305		1.040	0.01074	9.3	0.0071	DYN	RUWE+Pma+RV
60994	108799	J12300479-1323350	HR 4758	1.080	0.781	52.309	0.723	VIS	Gaia
68030	121560	J13554999+1403234		1.129					

Table C.30. Mass and separation of companions in the Columba moving group

HIP	HD	2MASS	Others/WDS	M_A $M_\odot$	M_B $M_\odot$	a au	q	Method	Source
3210	3888	J00405159-5312357		1.146	0.400	2.245	0.349	VIS	Bonavita et al. (2016)
6165	8077	J01190560-5351020		1.137					
7805	10472	J01402406-6059566		1.457					
	TYC8047-232-1	J01521461-5219332	CD-52 381	0.912	0.020	282.193	0.022	VIS	Chauvin et al. (2010)
11029	14691	J02220152-1046390	HR692	1.445					
12413	16754	J02394796-4253300	HR789	1.958	0.600	4.490	0.306	VIS	Bonavita et al. (2016)
				2.558	0.348	1024.673	0.136	VIS	Gaia, Bonavita et al. (2016)
14551	19545	J03075083-2749520	HR943	1.578	0.091	2.390	0.058	DYN	PMa/RUWE/RV
				1.669	0.198	3146.170	0.118	VIS	Gaia
14913	20121	J03122575-4425111	HR968	1.336	1.096	13.193	0.825	VIS	Mason et al. (2001)
				2.432	0.953	156.875	0.392	VIS	Gaia
16449	21997	J03315364-2536509	HR1082	1.719	0.0056	12.5	0.0033	DYN	PMa/RUWE/RV
17675	23384	J03471061+5142230		1.436	0.0097	24.1	0.0068	DYN	PMa/RUWE/RV
17782	23524	J03482301+5202163		0.755	0.755	12.920	1.000	VIS	Mason et al. (2001)
19775	26980	J04142257-3819016		1.062					
	27679	J04211032-2432211		1.042					
		J04345077-3547211	CD-36 1785	0.914					
		J04411573-3513582	CPD-35 525	0.960					
22152	29329	J04460056+7636399	HR1468	1.213	0.0012	17.1	0.0010	DYN	PMa/RUWE/RV
22226	30447	J04464950-2618087		1.473					
	31242	J04515354-4647134	CD-46 1587	0.985	0.687	1547.969	0.697	VIS	Gaia
	272836	J04530520-4844386		0.933	0.244	127.841	0.262	VIS	Elliott et al. (2015), Gaia
23171	32476	J04590561-6325297		0.947	0.921	131.224	0.973	VIS	Gaia
23179	31647	J04591543+3753251	Omega Aur	2.035	1.102	234.223	0.542	VIS	Gaia, De Rosa et al. (2014)
23316	32372	J05005186-4101065		1.022					
23362	32309	J05012558-2003067	HR1621	2.392					
24947	35114	J05203803-3945179	AS Col	1.182					
25436	35996	J05262401-4322325	CD-43 1847	1.430	1.120	1105.820	0.783	VIS	Gaia
25434		J05262296-4322360	CD-43 1846	1.121	0.360	5.318	0.321	VIS	Bonavita et al. (2022a)
	35841	J05263658-2229238	BD-22 1109	1.232	0.104	17068.242	0.085	VIS	Gaia
	274561	J05285509-4534584	CD-45 2003	0.899					
25709	36329	J05292409-3430554	CD-34 2279	1.140					
		J05301907-1916318	AG Lep	1.118	0.228	2.346	0.204	DYN	PMa/RUWE/RV
				1.346	0.921	1849.979	0.684	VIS	Gaia
	36869	J05340914-1517031	AH Lep	1.067	0.225	479.072	0.211	VIS	Gaia
26309	37286	J05361029-2842289	HR1915	1.623					
26395	37306	J05370877-1146317		1.842					
26453	37484	J05373962-2837346		1.426					
	TYC 5346-132-1	J05383500-0856405	BD-08 1195	0.989					
	TYC 5925-1221-1	J05402073-1940108	AI Lep	1.036					
	38207	J05432094-2011214	BD-20 1162	1.392					
26966	38206	J05432166-1833268	HR1975	2.051					
26990	38397	J05433580-3955246		1.077					
	TYC6502-1188-1	J05502142-2915206	CD-29 2531	0.937	0.049	59024.980	0.052	VIS	Gaia
	TYC8520-32-1	J05510116-5238126	CD-52 1363	1.029	0.130	5.130	0.126	DYN	RUWE-RV
28036	40216	J05554314-3806162	CD-38 2296	1.228	0.312	114.703	0.254	VIS	Gaia, Galicher et al. (2016); Bonavita et al. (2022a)
28474	41071	J06004130-4453500	RT Pic	0.975	0.139	37.663	0.143	VIS	Bonavita et al. (2022b)
	TYC5944-411-1	J06050784-2143305		0.969					
30030	43989	J06190805-0326203	V1358 Ori	1.118					
	TYC7617-549-1	J06260690-4102538	CD-40 2458	1.006					
	295290	J06402236-0331591	TYC 4803-1418-1	1.006					
32104	48097	J06422431+1738430	26 Gem	1.879	0.510	1.696	0.271	VIS	Brandt et al. (2014)
	48370	J06430102-0253192	BD-02 1732	1.000					
	TYC7100-2112-1	J06524674-3636169	CD-36 3202	0.900	0.590	0.023	0.656	DYN	RUWE-RV
	51797	J06562354-4646549	CD-46 2777	1.046					
114189	218396	J23072869+2108033	HR8799	1.468	0.008	16.100	0.0052	VIS	Zurlo et al. (2022)
				1.476	0.009	26.460	0.0063	VIS	Zurlo et al. (2022)
				1.485	0.008	40.970	0.0052	VIS	Zurlo et al. (2022)
				1.493	0.006	71.140	0.0039	VIS	Zurlo et al. (2022)
116805	222439	J23402449+4420021	kap And	2.801	0.014	54.724	0.0050	VIS	Carson et al. (2013); Uyama et al. (2020)

[1]This star is classified as an EB apparently from Gaposchkin (1932) with a period of about seven days and dm=3.1 mag. However HARPS RV is constant with 150 ms (PtV) over 80 days (Trifonov et al. 2020). In addition, it is very difficult to produce the light curve required to produce such a deep eclipse.

Table C.31. Mass and separation of companions in the Tuc-Hor moving group

HIP	HD	2MASS	Others/WDS	M_A $M_\odot$	M_B $M_\odot$	a au	q	Method	Source
490	105	J00055255-4145109		1.062					
1113	987	J00135300-7441178		0.965					
1481	1466	J00182612-6328389		1.109	0.0016	14.2	0.0014	DYN	Mesa et al. (2022)
2484	2884	J00313267-6257297	bet1 Tuc	2.280	0.480	105.275	0.211	VIS	Tokovinin (2018)
2487	2885	J00313347-6257560	bet2 Tuc	2.760	2.126	1192.927	0.770	VIS	Gaia
2578	3003	J00324391-6301533	bet3 Tuc	2.280	2.148	4.379	0.942	VIS	Mason et al. (2001)
				3.730	1.857	24205.795	0.498	VIS	Gaia
2729	3221	J00345120-6154583		0.831	0.831	0.951	1.000	VIS	Bonavita et al. (2022a)
	TYC 9351-1110-1	J00422033-7747397	CD-78 24	0.867					
	TYC 7002-2219-1	J01220441-3337036	CD-34 521	0.697					
6485	8558	J01232126-5728507		0.986					
6856	9054	J01280868-5238191	CC Phe	0.908					
7699	10269	J01390761-5625459		1.273					
8233	10863	J01460105-2720556	HR517	1.424	0.0052	22.1	0.0037	DYN	RUWE/RV/Pma
9141	12039	J01574896-2154052	DK Cet	0.927	0.927	8.263	1.000	VIS	Biller et al. (2007); Bonavita et al. (2022a)
9892	13183	J02071805-5311565		0.992					
9902	13246	J02072611-5940459		1.127	0.834	4607.402	0.740	VIS	Gaia
	TYC 8489-1155-1	J02073220-5940210	CD-60 416	0.835					
10602	14228	J02163059-5130437	phi Eri	3.112					Multiple system WDS; Should be in Gaia
11360	15115	J02261625+0617331		1.474					
12394	16978	J02393538-6816008	eps Hyi	2.546					
	TYC 8060-1673-1	J03304909-4555573	CD-46 1064	0.887					
	22213	J03341633-1204073		0.994	0.446	86.676	0.449	VIS	Elliott et al. (2015), Gaia
15247	20385	J03164066-0331489		1.175	0.676	40.80	0.575	VIS	Gaia+PMa
16853	22705	J03365341-4957288		1.076	0.330	2.060	0.307	DYN	Bonavita et al. (2016)
				1.406	0.205	114.545	0.146	VIS	Elliott et al. (2015), Gaia
17764	24636	J03481148-7441388		1.467					
17797			f Eri	2.282	0.550	6.646	0.241	VIS	Bonavita et al. (2022a)
				2.832	0.476	445.000	0.168	VIS	Gaia
	24071	J03483548-3737190		3.308	1.922	4583.445	0.581	VIS	Gaia
18714	25402	J04003198-4144544		1.033	0.250	2.350	0.242	VIS	Bonavita et al. (2022a)
				1.283	0.460	454.909	0.445	VIS	Gaia
	TYC 5882-1169-1	J04021648-1521297	BD-15 705	0.897					
	TYC 5324-1293-1	J04364709-1209207	BD-12 943	0.964	0.255	928.148	0.264	VIS	Gaia
20042	27376	J04175366-3347540	ups04 Eri	2.680	2.305	0.098	0.860	DYN	Pourbaix et al. (2004)
				4.985	0.220	297.599	0.044	VIS	Gaia
21632	29615	J04384393-2702018		1.033	0.170	1251.693	0.165	VIS	Gaia
21965	30051	J04431720-2337419		1.490	0.630	1.999	0.423	DYN	Goldin & Makarov (2007)
22295	32195	J04480518-8046452		1.141					
	TYC 5908-230-1	J04593202-1917416	BD-19 1062	0.890					
	TYC 5335-312-1	J05153652-0930512	BD-09 1108	0.998	0.540	921.011	0.863	VIS	Gaia
				1.538	0.322	887.873	0.322	VIS	Gaia
32435	53842	J06461348-8359294		1.298	0.386	82.743	0.297	VIS	Bonavita et al. (2022a)
100751	193924	J20253886-5644062	alpha Pav	5.310	4.450	0.216	0.838	DYN	Luyten (1936)
105388	202917	J21204994-5302030		0.982					
107947	207575	J21520973-6203085		1.222					
108422	208233	J21575146-6812501		0.991	0.421	1.26	0.425	DYN	RUWE/RV/Pma
				1.412	0.291	85.367	0.206	VIS	Gaia
	TYC 5242-324-1	J23093711-0225551	BD-03 5579	0.802					
	TYC 9529-0340-1	J23274943-8613187	CD-86 147	0.980	0.115	0.082	0.117	DYN	RUWE/RV
	222259B	J23393929-6911396	DS Tuc B	0.886					
116748	222259A	J23393949-6911448	DS Tuc A	0.985	0.0000453	0.0795	0.00005	DYN	TESS
					0.886	237.030	0.899	VIS	Gaia

Table C.32. Mass and separation of companions in the Volans/Crius 221 moving group

HIP	HD	2MASS	Others/WDS	M_A $M_\odot$	M_B $M_\odot$	a au	q	Method	Source
		J08264964-6346369	TYC 8933-327-1	0.908	0.557	1.45	0.614	DYN	RUWE/Pma/RV
	73129	J08324622-6508272		1.034	0.307	31730.892	0.297	VIS	Gaia
43783	76728	J08550282-6038406	HR3571	5.061	0.911	3.742	0.180	DYN	RUWE/Pma/RV
				5.972	0.586	1472.161	0.098	VIS	Mason et al. (2001)
45594	80563	J09173415-6323145		1.369					
46460	82406	J09283051-6642067	HR3783	2.176	0.851	0.82	0.391	DYN	RUWE/Pma/RV
47017	83359	J09345645-6459579		0.971	0.883	0.043	0.909	DYN	Ellipsoidal variable: solution with TESS period
									+ Gaia RV amplitude; consistent with position on the cmd
				1.854	0.673	971.810	0.363	VIS	Gaia
47115	83253	J09360518-6457011		1.816	0.97	88.30	0.535	VIS	This paper
				2.786	2.352	40940.092	0.844	VIS	Gaia
47335	83948	J09384522-6651326		1.527	0.898	29535.947	0.588	VIS	Gaia
		J09391046-6646155	TYC 8953-1289-1						
47351	83946	J09385410-6459267		1.168					
		J09481924-6403217	TYC 8950-1447-1	0.834					
		J10082200-6756402	TYC 9210-1818-1	0.833	0.175	1834.241	0.210	VIS	Gaia
	CD-67 852	J10122991-6752334	TYC 9210-1730-1	0.976					
50567	89928	J10194613-7133173		1.028	0.488	2.45	0.475	DYN	Gaia, RUWE/Pma/RV
		00301560-8613552	TYC 9494-799-1	0.927					
	67928	08075272-5135016	TYC 8148-343-1	1.026	0.740	74.786	0.721	VIS	(Mason et al. 2001)
	69406	08134777-5837139	CPD-58 1080B	1.388	0.275	1.58	0.198	VIS	RUWE/Pma/RV
				1.663	0.844	756.57	0.507	VIS	Gaia
		08363202-6024116	TYC 8926-337-1	0.910					
45096	299896	09111005-5501535	TYC 8587-323-1	0.884					
	79648	09134337-4642014	TYC 8166-809-1	0.967					
45478	80157	09160129-5533297	TYC 8587-1754-1	1.416					
		09231316-4520256	TYC 8167-1155-1	0.890					
47351	83946	09385410-6459267	TYC 8949-116-1	1.165					
		09430884-6313043	TYC 8946-1225-1	1.000	0.515	16.873	0.515	VIS	(Mason et al. 2001)
				1.515	0.117	5425.159	0.077	VIS	Gaia
		10111554-6530330	TYC 8951-622-1	0.996	0.152	350.436	0.152	VIS	Gaia
		10295615-6451235	TYC 8964-396-1	0.940					
52462	92945	10432828-2903513	TYC 6645-338-1	0.922	0.0007	14.6	0.0008	DYN	Mesa et al. (2021)
52787	93528	10473117-2220528	TYC 6081-65-1	0.948	0.794	7870.202	0.838	VIS	Gaia
54155	96064	11044148-0413159	TYC 4924-1114-1	0.968	1.230	308.314	1.271	VIS	Tokovinin (2018)
		11110405-7824116	TYC 9414-379-1	0.874	0.809	130.086	0.926	VIS	Gaia
58029	103381	11540534-2958570	TYC 6678-1031-1	0.982					
	104315	12003839-7200251	TYC 9235-1497-1	0.958					
		12170220-5546112	TYC 8637-2580-1	0.865					
61284	109138	12332981-7523112	TYC 9412-190-1	0.970					
		12543443-4558310	TYC 8245-2246-1	0.950	0.471	150.356	0.496	VIS	Gaia
				1.421	0.390	3641.534	0.270	VIS	Gaia. Wide companion is a a binary
		13193133-7036309	TYC 9246-361-1	0.867					
73052	130943	14554612-7309599	TYC 9270-1659-1	1.231					
	153555	17041857-6233182	TYC 9043-817-1	1.122	0.107	6040.787	0.095	VIS	Gaia
84642	155915	17181464-6027275	TYC 9052-1117-1	0.972	0.290	13.142	0.298	VIS	Bonavita et al. (2022a)
		17244456-5153425	TYC 8353-292-1	0.897					
	321224	18025629-3643280	TYC 7403-6190-1	0.923					
96334	183414	19350972-6958321	TYC 9309-599-1	1.014	0.0037	6.2	0.0037	DYN	Mesa et al. (2022)
96880	184587	19413575-7226457	TYC 9314-767-1	0.919					